# THE EFFECT OF THERMAL ENERGY TRANSPORT ON THE PERFORMANCE OF (SEMI) FLOATING RING BEARING SYSTEMS FOR TURBOCHARGERS

A Thesis

by

FENG YU

Submitted to the Office of Graduate Studies of
Texas A&M University
in partial fulfillment of the requirements for the degree of

MASTER OF SCIENCE

| | |
|---|---|
| Chair of Committee, | Luis San Andrés |
| Committee Members, | Yong-Joe Kim |
| | Hamn-Ching Chen |
| Head of Department, | Andreas A. Polycarpou |

August 2013

Major Subject: Mechanical Engineering

# ABSTRACT

The thesis studies the effect of thermal energy flows on the performance of an oil lubricated (semi) floating ring bearing used in a passenger vehicle turbocharger. The model of the inner and outer fluid film flows in the floating bearing fully considers the thermal energy flows in the bearing system with a source from the hot shaft and drag power dissipation in both films. Implementation of the finite element method and the control volume method gives the solution of the heat conduction equation for the ring and the thermal energy transport equations for both films, respectively.

The developed numerical tool (XLBRG_TH®) is validated by comparison of predictions for the inner film pressure and temperature distributions against archival test data for a journal bearing with two supply grooves. The tool is next used to analyze the performance characteristics of a (semi) floating ring bearing in a turbocharger application, as well as the effects of some physical and operating parameters on the performance.

The results show that the inner film flow carries the largest fraction of thermal energy produced by shear drag power losses and heat flowing from the hot shaft. Lower oil supply temperature results in a larger heat flowing from the shaft but slightly influences the drag power loss. Either higher supply pressure or a larger film clearance promotes flow rate through the film region and then raises the heat flow from the hot journal and the drag power loss. Since the thermal energy from the hot shaft into the film is overwhelming, a higher shaft temperature raises the peak and average temperatures of the inner film and thus causes the oil viscosity to increase which reduces the drag power

loss. Either additional or larger axial grooves on the inner side of the FRB can increase the flow rate and increase the heat flow from shaft. However, the drag power loss decreases with a wider groove because of the reduction in film area but increase with a deeper groove for a larger oil viscosity.

## ACKNOWLEDGEMENTS

I gratefully acknowledge Honeywell Turbo Technologies, for their support for this project. In particular, I acknowledge Vince Barbarie, Kostanding Gjika, and Avijit Bhattacharya, who have closely followed the progress of the research and offered their valuable suggestions. Also, I sincerely acknowledge Dr. Luis San Andrés, my advisor, for his extreme patience and careful scrutiny of my work. He has guided my research and taken every opportunity to share his knowledge and experience. Finally, I acknowledge my friends and the colleagues at the Turbomachinery Laboratory: Thomas Abraham, Qing Liu, Alain Anderson, Yujiao Tao, José Bernabé Hernández and Sunghwa Jeung. Their continuous encouragement and sincere help are highly appreciated.

NOMENCLATURE

| | |
|---|---|
| $C_v$ | Lubricant specific heat [J/(kg K)] |
| $C_P$ | Ring specific heat [J/(kg K)] |
| $C_{i,o}$ | Inner and outer film clearances [m] |
| $D_C$,$D_S$ | Casing inner diameter and shaft outer diameter [m] |
| $E_i$,$E_o$ | Total heat convected to lubricant in inner and outer films [W] |
| $e_{Jx}$,$e_{Jy}$ | Texas Department of Transportation |
| $H$ | Heat convection coefficients [W/(m$^2$ K)] |
| $h_i$, $h_o$ | Film thickness of inner and outer film [m] |
| $L_i$, $L_o$ | Axial length of the inner and outer film [m] |
| $\dot{m}_\theta$ | Circumferential mass flow rate per unit length [kg/(m s)] |
| $\dot{m}_{\theta_c}$ | Circumferential mass flow rate per unit length in the oil cavitation zone [kg/(m s)] |
| $\dot{m}$ | Axial mass flow rate per unit length [kg/(m s)] |
| $P_A$ | Ambient pressure [bar] |
| $P_{SUP}$,$P_{cav}$ | Lubricant supply pressure and cavitation pressure [bar] |
| $Q$ | Heat flow [W] |
| $Q^{i\to R}$ ,$Q^{R\to o}$ | Heat flow from inner film to ring and from ring to outer film [W] |
| $Q^{S\to i}$ ,$Q^{o\to C}$ | Heat flow from shaft to inner film and from outer film to casing [W] |
| $R_J$, $R_C$ | Radii of journal and bearing casing [m] |

| | |
|---|---|
| $R_{R_i}$, $R_{R_o}$ | Radii of ring inner and outer surfaces [m] |
| ($r$, $\theta$, $z$) | Radial, circumferential and axial direction coordinates [m] |
| $T_E$ | Exit temperature of mixed lubricants [$^o$C] |
| $T_i$,$T_o$ | Temperatures of inner and outer films [$^o$C] |
| $\overline{T}_i$ , $\overline{T}_o$ | Average temperatures of inner and outer films [$^o$C] |
| $T_{R_i}$ , $T_{R_o}$ | Ring inner and outer surface temperatures [$^o$C] |
| $T_s$ , $T_c$ | Temperatures of shaft and casing [$^o$C] |
| $T_{SUP}$ | Lubricant supply temperature [$^o$C] |
| $U_i$, $U_o$ | Velocity of the inner and outer film flow in the circumferential direction [m/s] |
| $U_m$ | Average of shaft and ring velocities, ½($U_S$+$U_R$) [m/s] |
| $\alpha$ | Material thermal expansion coefficient [1/$^o$C] |
| $\varepsilon$ | *e/c*. Journal or rig eccentricity ratio |
| $\rho$, $\mu$, $\kappa$ | Density [kg/m$^3$], viscosity [Pa s], and thermal conductivity [W/(m $^o$C)] |
| $\mu_*$, $\mu_\infty$ | Viscosity with null and infinite shear rate [Pa s] |
| $\Phi$ | Mechanical dissipated power/unit area [W/m$^2$] |
| $\wp_i$, $\wp_o$ | Total mechanical power converted into heat [W] |
| $\Delta T_E$ | Lubricant exit temperature rise [$^o$C] |
| $\Omega$ | Journal speeds [rad/s] |
| $\Omega_R$ | Ring speeds [rad/s] |

Subscripts

| | |
|---|---|
| *C* | Casing (center housing) |
| *C* | Cavitation |
| *J* | Journal |
| *i,o* | Inner, outer films |
| *R* | Ring |
| *S* | Shaft |
| *SUP* | Supply condition |
| * | Reference condition |

TABLE OF CONTENTS

Page

LIST OF FIGURES

LIST OF TABLES

# 1. INTRODUCTION

Turbocharging is currently the most commonly used method to make an automotive engine of a given size produce more power. Past research mainly focused on turbochargers (TCs) performance and their matching to engines, but few efforts have been placed into the details of the thermal energy transport in the TCs bearing system. Typical engine-oil lubricated TCs operate with component temperatures well above ambient and must withstand large temperature gradients that result in severe thermo-mechanical stresses [1]. Hence, an insight into the thermal energy flows and an effective thermal management strategy are paramount to ensure reliable TC operation.

Figure 1 depicts the main components of a turbocharger (TC), including a turbine that recovers the energy from the exhaust gases, a slender shaft connecting the turbine to the compressor, a compressor that forces air into the engine intake manifold, and the radial and thrust bearing system supporting the rotating shaft.

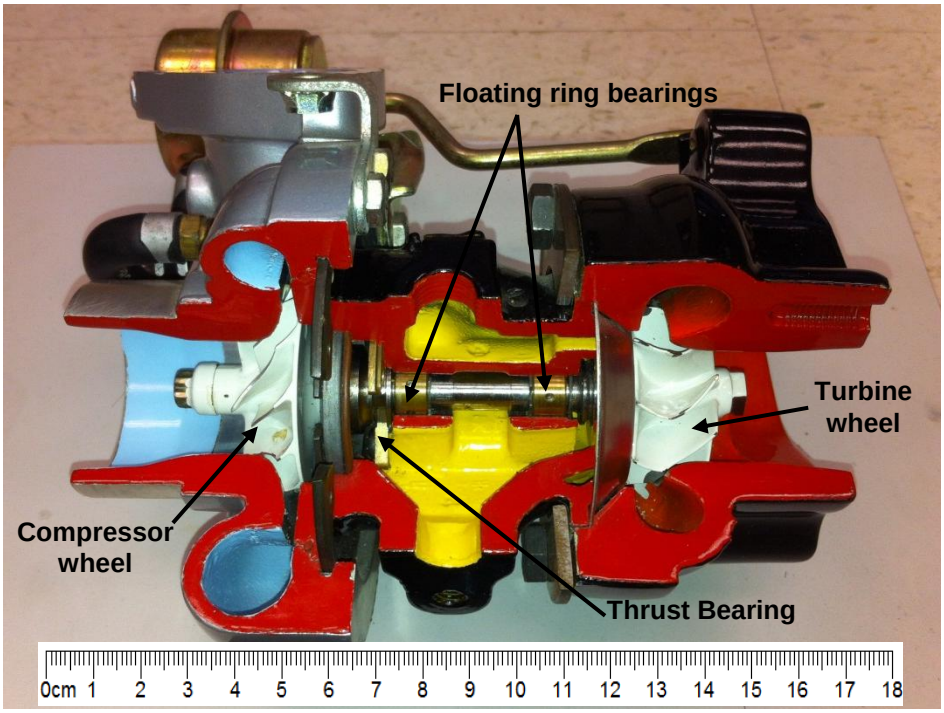


**Figure 1. Cross-section view of a small turbocharger**[1]

Figure 2 presents two typical radial bearing configurations for an engine-oil lubricated TC. For the floating ring bearing (FRB), a loosely fitted ring separates the shaft and bearing housing, so that the lubricating oil flows through the inner and outer oil films. The inner film is the gap between the shaft and the inner surface of the ring, and the outer film is the gap between the outer surface of the rotating ring and the TC casing. The drag torque from the inner film rotates the floating ring. In a semi-floating ring, a pin or button is installed in the bearing casing to prevent the ring rotation. The outer film servers as a squeeze film without lubricant shear induced by ring spinning [1].

[1] Photograph of Garrett GT25 turbocharger demonstrative model at the Turbomachinery Laboratory.

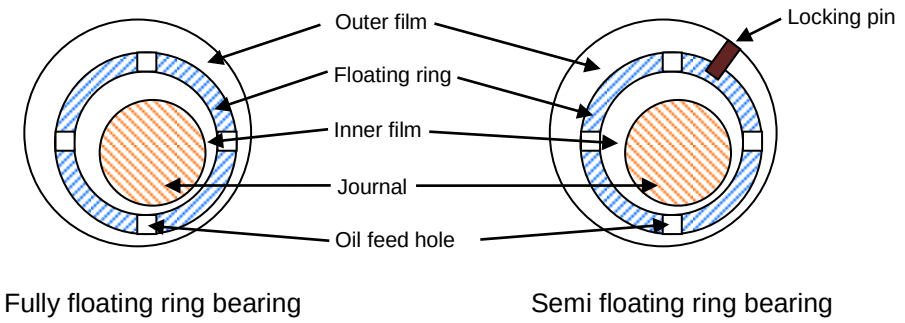


**Figure 2. Schematic view of two engine-oil lubricated bearing systems for TCs.**

The analysis of thermal energy flows is complicated because of the many possible flow paths, as Figure 3 shows. Briefly, the energy transfer processes in a conventional TC include the flows of energy associated with gas entering and leaving the TC, the work transfer along the shaft from turbine to compressor, the work converted into heat in the bearings because of drag power loss, and the internal and external heat transfers that apply to each major component of the TC. Among these heat flow paths, to model the internal heat flows is most challenging. This is probably due to the difficulty to experiment and model heat transfer occurring in a small turbine with variable inlet conditions [2]. Note that the interaction between the components and the surrounding fluid flows creates difficulties in modeling a precise thermal behavior. Heat convection coefficients are strong functions of the flow conditions. Similarly, the flow conditions in the lubricated inner and outer films are largely determined by the operating lubricant viscosity as well as by the operating film clearances that are also strong functions of the lubricant temperature and the bounding solids.

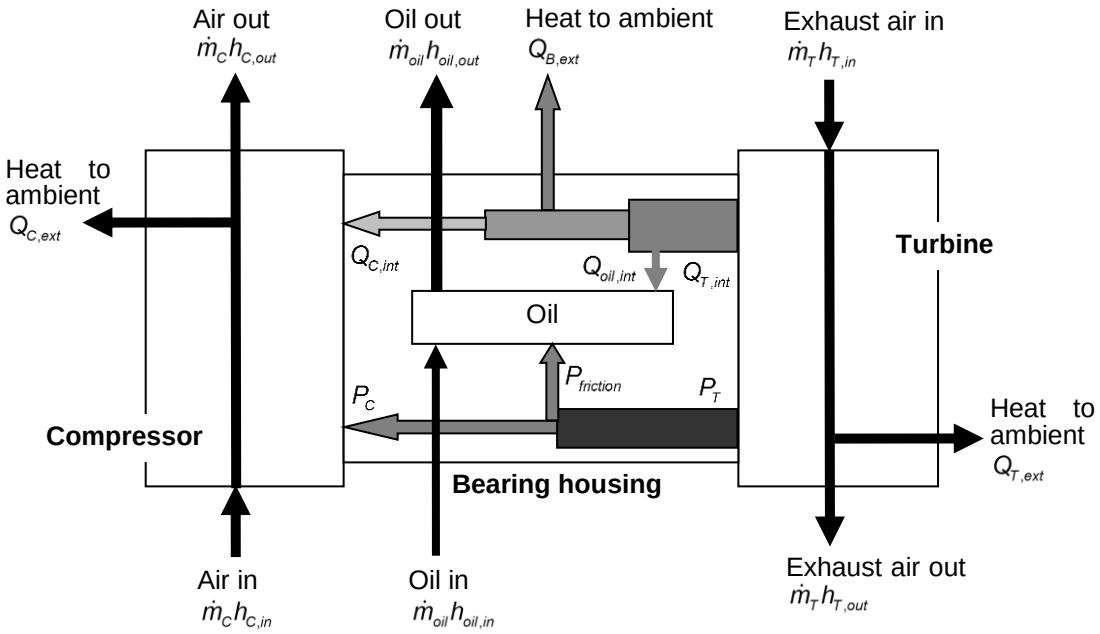


Note: $\dot{m}$ = mass flow rate; $h$ = enthalpy; $Q$ = heat flow; $P$ = power

**Figure 3. Schematic view of energy flows in a turbocharger [3].**

An increase in delivery of lubricant flow rate into the bearing system to carry away heat and to cool components may be counterproductive because a cold lubricant has a large viscosity that determines a larger mechanical drag power loss that is not favorable to the TC mechanical efficiency [1]. However, if the lubricating oil flow rate is not sufficient, it can easily bring severe performance and operation penalties. The oil overheats and could even flash with formation of oil-coke [1]. Furthermore, the large thermal growth of the bearing components could induce severe film clearance changes that may cause sudden shaft seizure [1]. Additionally, if the lubricated bearing system fails to act as a heat sink, more heat can be transferred from the hot turbine to the compressor through the shaft. Warmer air at the compressor intake and hotter air at its

discharge has a negative effect on the overall engine efficiency [4].

Thus, there is a pressing need to model adequately the transport of thermal energy flows in the bearing subsystem of a TC to design an effective thermal management. Accordingly, it is necessary to perform accurate predictions of the temperature field in the fluid films of a floating ring bearing (FRB) to correctly estimate the mechanical drag power loss and heat flows. The analysis must determine safe operating conditions ensuring the TC component mechanical integrity and the robustness of the bearing system.

# 2. OBJECTIVE AND TASKS

The current investigation proposes to study the effect of thermal energy transport on the performance of oil lubricated (semi) floating ring bearings for automotive TCs. The fluid film flows and temperature fields, inner and outer, are governed by lubrication equations and the thermal energy transport equations, respectively. The heat flow conduction equation for the (semi) FRB is solved using the finite element method. Implementation of the finite element method and the control volume method gives solutions to the Reynolds equations and the thermal energy transport equations, respectively. An efficient algorithm couples the solution of the Reynolds equations and the thermal energy transport equations and updates the temperature-dependent viscosity and film clearances during the iterative process.

The tasks performed are:

(1) To calculate the temperature distribution in a (semi) floating ring and to predict the thermal energy flows in the bearing system of a TC.

(2) To compare numerical predictions against published experiment data to validate the model [5].

(3) To analyze performance characteristics of a (semi) floating ring bearing with an actual configuration in a TC application for typical TC operating conditions.

(4) To study the possible impact of some physical and operating parameters on the performance of the actual (semi) floating ring bearing. These parameters include

the lubricant supply pressure and temperature, the bearing clearances, the number and the dimensions of axial grooves.

# 3. LITERATURE REVIEW

## Heat Transfer Flows in Automotive Turbochargers

An engine turbocharger aims at increasing the amount of air supplied to an engine of a given size. However, one of the important factors affecting TC performance is the heat transfer between the components of the TC and also between the TC and ambient [4]. To understand the thermal energy transport behavior, various heat transfer models have been developed. There are simple models based on empirical formulas [4, 6], experiment-based models with heat transfer coefficients obtained from test results [2, 3], and advanced conjugate heat transfer models which couple the interaction between the solid and the various fluid flows [7, 8]. With the aid of these models, engineers estimate the TC thermal energy transport flows and balance and to improve the engine simulation tools coupled with the TC model, particularly at low shaft speeds when the total amount of heat transfer from the turbine is in the same order of magnitude as the turbine extracted mechanical power [4].

In 1983, Rautenberg et al. [6] present one of the first theoretical and experimental studies of heat transfer effects on the performance of TCs. The authors indicate that the heat transfer between TC components and between the TC and ambient cause an underestimation of the measured compressor efficiency and an overestimation of the turbine efficiency, both leading to an inaccurate estimation of the power for both the compressor and the turbine. According to measured results, the authors state that the geometrical arrangements of turbine and compressor, as well as the turbine inlet

temperature, have a considerable impact on the heat flux from the turbine towards the compressor. Malobabic and Rautenberg [9] state further that the turbine inlet temperature and the mass flow rate are the main factors that determine the turbine mechanical output power out of the total energy obtained from the hot gas, and that at conditions of high inlet temperature and low mass flow, the majority of the energy from the hot gas is dissipated by the turbine to the compressor and environment rather than converted into mechanical power.

Shaaban [4] confirms numerically and experimentally that heat transfer has negative effects on both the turbine and compressor. The author defines the total turbine heat loss as the sum of the amount of heat transfer from the turbine to ambient, plus the heat to the oil, and plus the heat to the compressor through the bearing center housing. For the studied speed range with a fully open guide vane position, the results show that heat transfer from the turbine to ambient by convection and radiation accounts for the majority of total turbine heat loss, about 60-70% at the lowest shaft speed (60 krpm). This percentage increases as the shaft speed grows, becoming as high as 90% at the highest shaft speed (120 krpm) and the largest exhaust gas temperature at the turbine entry (973 K). Besides, the lubricating oil also plays an important role in removing heat from the turbine, taking up 10-49% of the total amount of turbine heat loss. This percentage depends on the shaft speed and the exhaust temperature at the turbine inlet. The author provides the percentage range for the exhaust temperature range at each specific shaft speed. The remaining heat loss from the turbine, less than 10% of total heat loss, is transported to the compressor through the bearing center housing. Note that

this small amount of heat transfer causes significant deterioration of the compressor performance at very low shaft speeds because of the very small compressor aerodynamic work at low speeds. Additionally, the overall heat losses from turbine can be as high as 8 times the turbine mechanical power at the lowest journal speed when the gas temperature at the turbine inlet is the highest, and the sum of the total heat losses from turbine and the turbine mechanical power only accounts for a small fraction of energy from the exhaust, the majority of exhaust energy (~ 90%) is lost at the turbine outlet. The author uses the mean oil temperature and an empirical formula to calculate the bearing friction power loss with good accuracy. The mean oil temperature, used to estimate the lubricant viscosity, equals to the average of the oil temperatures at the inlet and outlet. The empirical formula is based on the test data at some speeds (60 -100 krpm) showing a good match with the test data at even higher speeds.

In addition, both Cormerais et al. [2] and Bohn et al. [10] verify experimentally the effect of the turbine inlet temperature on a TC compressor performance. Ref. [2] reports larger differences in temperature between the compressor outlet and inlet when the turbine inlet temperature changes. Ref. [10] documents the potential factors influencing the maximum casing temperatures of the turbine and compressor and concludes that the turbine inlet temperature and mass flow rate are the main factors determining the total heat flow from the turbine to compressor. Ref. [10] also points out that heat radiation from both the turbine and compressor has a minor influence on the heat flow from turbine to compressor.

Other researchers have explored further the paths of thermal energy flows by

performing extensive experiments on ad-hoc test rigs. Experiment-based methods are used to obtain correlation for heat transfer coefficients, to determine the TC non-adiabatic efficiency and the mechanical power loss. Baines et al. [3] focus on obtaining accurate convective heat transfer models by fitting the measured temperatures to the proposed heat transfer model. As for the other modes of heat transfer, surface emissivity of the casings to calculate thermal radiation is based on thermograph measurements [10], and the thermal conductivities of components are known from published data. Based on the test data, the authors calculate the internal heat flux from the turbine gas to the TC structure and from there to the oil and the compressor, and the external heat flux to the ambient. Comparing magnitudes, at the compressor side, the internal heat transfer is more than 10 times greater than the external heat transfer for most of conditions with different exhaust inlet temperatures and ventilation rates. However, for a compressor with a low flow rate, the intake air is in actuality heated by the compressor housing. Additionally, the effect of turbine inlet temperature on the external heat transfer of the compressor is weaker than that of the turbine, because the lubricating oil acts as a heat barrier. Though the compressor external heat transfer is consistently low for the studied model (< 50 W against 400 W for the internal heat transfer), it is not a negligible fraction of the overall heat transfer. On the other hand, at the turbine side, the internal heat transfer is nearly twice the external heat transfer, and the external heat transfer of turbine is almost four times that of compressor. The analysis of the heat transfer in a TC proves the cooling effect of the lubricating oil is very important in maintaining efficient operation of the whole system.

Cormerais et al. [11] use the equivalent heat transfer resistance (EHTR) method to quantify the conductive heat transfer from the turbine to the compressor, as well as the heat transfer among other components and the oil and the heat loss to the surroundings. With regards to the heat transfer between the oil and the bearing housing, non-adiabatic and also insulated test results are used to correlate the constants of the Nusselt number formula. The authors point out the location of the heat loss to surroundings is near the scrolls of the turbine and compressor. The results show the predictions by the EHTR method are in good agreement with measured results; yet the authors fail to clearly state the portion of each energy flow. Additionally, this method requires performing many experiments to correlate the heat transfer coefficients for each TC, which is both time-consuming and expensive.

Nguru [12] confirms experimentally that the turbine flow and compressor temperature ratio[2] have a direct effect on the heat transfer to the oil and cooling water system through the entire operating range of a large test TC (8 ~14 krpm). A CFD analysis is carried out on the flow of the gas through the TC to determine the portion of heat loss as a result of heat transfer through the casing by radiation and convection to the surrounding surfaces and ambient air, respectively. The total heat transfer values are a sum of the heat transfer through the casing, to the lubricating oil, and to the cooling water. The rate ratios of heat transfer to the oil-water cooling system over the total heat transfer for both the compressor and turbine are around 85% and 40%, respectively, regardless of shaft speed. For the TC tested case, because of the high resistance offered

[2] Compressor temperature ratio: the ratio of absolute temperature at compressor outlet to that at inlet.

by the materials and the heat sink forced by the oil-water cooling system, there is no heat flow along the rotor assembly from the turbine end to the compressor wheel.

For the purpose of calculating the power loss due to the oil shearing effect, researchers use different methods to get accurate results. Lamquin and Gjika [13] brief an experimental facility with a bladeless compressor (no compression work), thus the power dissipation in a semi-floating ring bearing only depends on the inlet and outlet turbine gas temperature since the kinetic energy of the compressor can be ignored. The authors observe that the thrust bearing is the largest contributor to the bearing system power loss when the rotor spins at 180 krpm with a higher oil feed temperature (100 ℃), and that an increase of the oil feed pressure can slightly increase the power loss for the studied journal bearings.

Incidentally, Deligant et al. [14] present a 3D CFD model for TC bearing friction losses. This 3D model is developed for the half of a symmetric bearing with four supply holes. The predictions show a substantial decrease in the bearing friction power against the ones from an isothermal model because of a significant decrease of the lubricant viscosity as the lubricant heats. Additionally, the authors indicate that the changes of journal eccentricity and supply pressure have slight effects on the bearing power loss.

San Andrés and Kerth [15] give full consideration of the modification of the oil viscosity due to temperature changes by introducing a flow model for the floating ring bearing (FRB). The model includes a lumped-parameter thermal energy balance to estimate an effective lubricant viscosity and changes in clearances due to the thermal growth of the journal, ring and bearing. That thermal model serves efficiently to predict

the exit lubricant temperature, power loss, and floating ring speed. The model is fully integrated into a rotordynamics nonlinear model to evaluate the amplitude and the frequency of shaft motions. Note that the authors assume the lubricant temperatures are constant in the inner and outer flow domains.

San Andrés et al. [1] extend the earlier lumped-parameter thermal energy transport model to take into account the thermal energy transport in the films, inner and outer, and through the floating ring. Predictions for a commercial semi FRB configuration show that the lubricant temperature in the inner film rises quickly along the axial direction because, for most shaft speeds, the axial fluid velocity is not large (fast) enough to remove the local drag power loss induced by the shear (circumferential) fluid speed. The oil flow in the inner film carries away much more energy than the outer film. The total thermal energy carried away by lubricant in both films is no less than 70% of the total energy generated by mechanical drag power and heat from the hot shaft. The heat from shaft to the inner film is overwhelming, especially at the lubricant inlet plane where the temperature difference with the cold oil is the largest. The authors demonstrate that an adequate thermal management with well designed flow paths in the bearing system is paramount to remove quickly the heat generated and to keep the lubricating oil temperature well below its flashing point.

In Ref. [16], Chun introduces a similar model to the one in Ref.[15], and also considers the effects of oil aeration[3] and oil mixing. The study indicates that the type of oil inlet port and the shaft speed have a strong influence on the film temperature and

[3] Oil aeration refers to the entrapment of air in the lubricating oil.

pressure distributions. An oil inlet configuration with four supply holes has a better cooling effect than one with an axial groove because the predictive temperatures on bearing midplane for the former are much lower than the latter. As the oil aeration level or the shaft speed increases, the temperature usually increases under a constant load operating condition. The assumption that the convective heat transfer coefficients at the lubricant-bearing and air-bearing interfaces are constant deserves the engineers' attention.

The aforementioned methods calculating the thermal energy flows are conventional ones that decouple the fluid mechanics problem from the heat transfer problem between the fluid and the structure. Since the temperature of the structures relies on that of the adjacent fluid, and the fluid flow mechanics in turn depends on the thermal boundary conditions in the adjacent structures, the fluid and the bounding solid influence each other through thermal boundary interfaces. The decoupled method is strongly dependent on the heat convection transfer coefficients that must be prescribed at the fluid-solid interface. For a complex geometry or flow phenomenon, well known empirical heat transfer coefficients from too simple flow conditions may be inadequate [11].

Thanks to the development of fast computers and numerical methods, the conjugate heat transfer (CHT) method is applied successfully to fluid-solid coupled problems. The CHT method takes into account the interdependency of the heat transfer between the fluid flow and solids simultaneously. The physical domain is divided into different blocks for fluid flow and solid body regions, so that no boundary conditions at

the interior walls but at the exterior boundaries are required. Bohn et al. [7] provide an example of applying the CHT method to estimate the TC performance aiming to ensure no thermal stress overloading. The authors conduct a CHT analysis that describes the heat fluxes in a TC divided into three regions: a turbine, an oil-cooled center housing, and a compressor region. The authors develop 3D TC energy transfer models with boundary conditions obtained from experiments [10]. The authors include the thermal boundary condition on the temperature distribution on the surface of the casing and also the boundary conditions for gas at the inlet and outlet of both compressor and turbine. One part of the energy from the exhaust (hot) gas in the turbine becomes the mechanical power that drives the compressor. One other part of the remaining energy, a kinetic energy, leaves as the gas exits the turbine. Another portion leaves the system as heat that equals to the heat loss to ambient and the casing due to natural convection and thermal radiation, as well as the heat taken away by the lubricating oil. Note also that drag power losses in the films also generate heat. The CHT helps the authors to quantify the thermal flows between adjacent regions. The results show that the total heat flux from the turbine to the compressor is mainly influenced by the turbine inlet temperature. Some of the heat entering the compressor does not pass away to the surrounding area, but heats up the compressor gas at some operating points.

The analysis of heat fluxes for turbine wheels with the CHT method conducted by Heuer et al. [8] shows one part of the wheel surface absorbs heat from the hot gas, while the other part could deliver heat into the gas flowing through the turbine due to the great different temperature levels and the high thermal conductivity of the solid. The

authors also undertake the analysis of thermal stress analysis of a twin-entry turbine housing with integrated manifold using the same method in Ref. [17]. The heat transfer coefficients obtained at full load serve as a boundary condition for a subsequent transient solid body thermal stress calculation. The authors find the intensification of flow turbulence improves the heat transfer near the waste gate area. The analysis can determine the location of the potential mechanical fatigue and unmask design deficiencies. Unfortunately the authors provide no details on the thermal energy carried away by the lubricant and ignore the fact that the fluid films can also act as a source of mechanical drag power.

# 4. THERMOHYDRODYNAMIC ANALYSIS OF A (S)FRB SYSTEM[*]

Figure 4 depicts a schematic view of a turbine or compressor FRB[4] with the journal and ring rotating with constant angular speeds $\Omega$ and $\Omega_R$, respectively. A lubricant is fed into the center housing at supply pressure $P_{SUP}$ and temperature $T_{SUP}$, then flows through the supply holes or a ½ moon groove ($z = 0$)[5] into the outer film with thickness $h_o$. A portion of the lubricant flows axially towards the bearing discharge planes $z = \pm ½ L_o$ with an outer film pressure $P_o$ and temperature $T_o$ generated in this area. The remaining lubricant continues to flow thought holes in the ring and into the inner film with thickness $h_i$ where it generates the hydrodynamic pressure field $P_i$ with temperature $T_i$, the lubricant eventually leaves the inner flow region with the energy due to the heat transfer and mechanical dissipated power.

[*] Part of the content presented in this Chapter is reprinted with permission from San Andrés, L., 2011, "On the Effect of Thermal Energy Transport to the Performance of(Semi)Floating Ring Bearing Systems for Turbocharger Applications," Annual Progress Report to Honeywell Turbo Technologies, Texas A&M University.

[4] No other obvious configuration differences exist between a SFRB and a FRB, except there is a pin or button in the SFRB configuration preventing its rotation.

[5] The study focuses on a bearing system supplied at its middle plane. Actual configurations have a variety of feed ports.

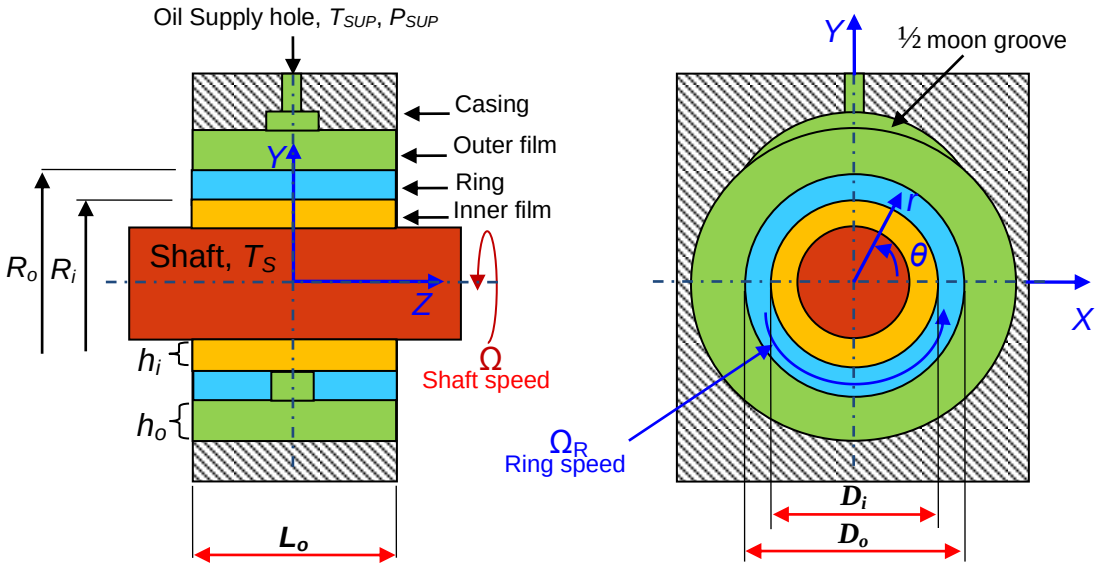


**Figure 4. Schematic view of a floating ring bearing system[6] [1].**

Figure 5 presents a schematic view for the journal and ring kinematics [1]. The figure notes the position of the ring center with respect to the bearing ($e_{Rx}$, $e_{Ry}$), and ($e_{Jx}$, $e_{Jy}$) refers to the journal eccentricity relative to the ring center. In operation, the inner film $h_i$ and the outer film $h_o$ are

$$h_i = c_i(\theta, z_i, T_i) - e_{Jx}\cos\theta - e_{Jy}\sin\theta \tag{1a}$$

$$h_o = c_o(\theta, z_o, T_o) - e_{Rx}\cos\theta - e_{Ry}\sin\theta \tag{1b}$$

where $c_i$ and $c_o$ are the inner and outer film operating clearances, which depend on the

[6] The actual inner film axial length may differ from the outer film length.

film temperature distribution and the thermal expansion material properties of the ring, shaft and casing. See later for the details on the clearance thermal growth model.

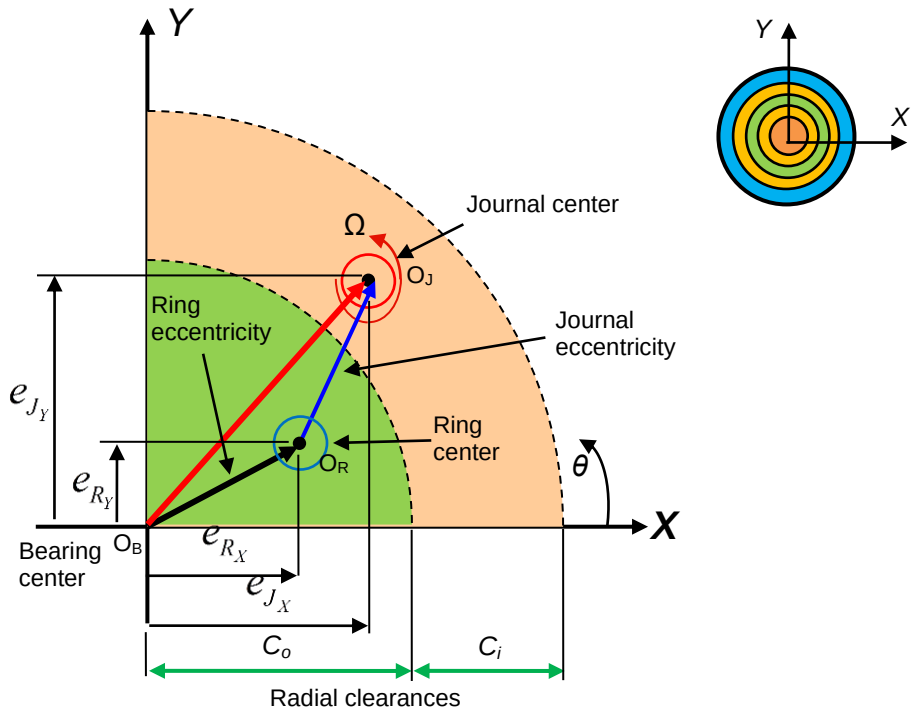


**Figure 5. Kinematics of journal and ring center and nomenclature for eccentricities [1].**

## Equations for Generation of the Hydrodynamic Pressure and Transport of Thermal Energy in the Fluid Films

Reynolds equation describes the generation of hydrodynamic pressure *P* in a thin

fluid film laminar flow[7] region under steady-state conditions [18]. For the inner and outer films the steady-state equations are:

$$\frac{1}{R_J^2}\frac{\partial}{\partial\theta}\left(\frac{h_i^3}{12\mu_i}\frac{\partial P_i}{\partial\theta}\right)+\frac{\partial}{\partial z_i}\left(\frac{h_i^3}{12\mu_i}\frac{\partial P_i}{\partial z_i}\right)=\frac{\Omega_J+\Omega_R}{2}\frac{\partial h}{\partial\theta} \tag{2a}$$

$$\frac{1}{R_{R_o}^2}\frac{\partial}{\partial\theta}\left(\frac{h_o^3}{12\mu_o}\frac{\partial P_o}{\partial\theta}\right)+\frac{\partial}{\partial z_o}\left(\frac{h_o^3}{12\mu_o}\frac{\partial P_o}{\partial z_o}\right)=\frac{\Omega_R}{2}\frac{\partial h}{\partial\theta} \tag{2b}$$

where $(P_i, T_i, h_i)$ and $(P_o, T_o, h_o)$[8] denote the pressure, the temperature and the film thickness of the inner and outer films, respectively; and $\Omega_J$ and $\Omega_R$ represent the rotating speed of the journal and floating ring. Above $\mu$ denotes the viscosity, which is determined by the local temperature and the shear rate, $\gamma$. Ref. [19] introduces a formula for lubricant viscosity as

$$\mu=\mu_\infty+\frac{\mu_*-\mu_\infty}{1+|\gamma/\gamma_c|} \tag{3}$$

where $\mu_*=\kappa e^{(a/(b+T))}$, with $\kappa$, a, b are constants for a given lubricant. Here, $\mu_*$ and $\mu_\infty$ correspond to the viscosity at null and infinite shear rates, and $\gamma_c$ is the critical shear rate that determines a 50% reduction in viscosity between the low and high shear rate conditions.

The bulk-flow thermal energy transport equation for the inner film is [20]

$$C_v\left[\frac{1}{R_J}\frac{\partial}{\partial\theta}\left(\dot{m}_\theta T\right)_i+\frac{\partial}{\partial z_i}\left(\dot{m}_z T\right)_i\right]+H_{R_i}(T_i-T_{R_i})+H_J(T_i-T_S)=\Phi_i \tag{4}$$

---

[7] Analysis and practice demonstrates that $\mathrm{Re}=\rho\Omega R/\mu<2{,}000$, thus both fluid inertia and turbulent flow effect are negligible.

[8] Subindices *i and o* denote the inner and outer films, respectively.

where $(T_S, T_{R_i})$ denote the temperature of shaft and ring ID surface; $(H_J, H_{R_i})$ are the heat convection coefficients to the shaft OD surface and the ring ID surface, respectively. Thus, $Q_i = H_{R_i}(T_i - T_{R_i}) + H_J(T_i - T_S)$ represents the heat flowing into the ring through its inner surface and into the journal; $\left(\dot{m}_{\theta_i}, \dot{m}_{z_i}\right)$ denote the lubricant mass flow rates in the circumferential and axial directions,

$$\dot{m}_{\theta_i} = \left(\rho U h\right)_i = -\frac{\rho h^3}{12\mu_i}\frac{\partial P_i}{R_J \partial \theta} + \left(\rho h\right)_i U_m \tag{5a}$$

$$\dot{m}_{z_i} = \left(\rho W h\right)_i = -\frac{\rho h_i^3}{12\mu_i}\frac{\partial P_i}{\partial z_i} \tag{5b}$$

and the shear energy dissipation function ($\Phi_i$) equals

$$\Phi_i = 12\frac{\mu_i}{h_i}\left[W_i^2 + \frac{1}{12}\left(U_S - U_R\right)^2 + \left(U_i - U_m\right)^2\right] \tag{5c}$$

with $U_S = R_J\Omega$, $U_R = R_{R_i}\Omega_R$, $U_m = \frac{1}{2}\left(U_S + U_R\right)$. The mean flow velocities in the circumferential and axial direction are, from Eqs. (5a) and (5b),

$$U_i = -\frac{h_i^2}{12\mu_i}\frac{\partial P_i}{R_J \partial \theta} + U_m \tag{6a}$$

$$W_i = -\frac{h_i^2}{12\mu_i}\frac{\partial P_i}{\partial z_i} \tag{6b}$$

Similarly, the thermal energy transport equation for the outer film is [20]

$$C_v\left[\frac{1}{R_{R_o}}\frac{\partial}{\partial\theta}\left(\dot{m}_\theta T\right)_o + \frac{\partial}{\partial z_o}\left(\dot{m}_z T\right)_o\right] + H_{R_o}(T_o - T_{R_o}) + H_C(T_o - T_C) = \Phi_o \tag{7}$$

with

$$\dot{m}_{\theta_o} = \left(\rho U h\right)_o = -\frac{\rho h_o^{\,3}}{12\mu_o}\frac{\partial P_o}{R_{R_o}\partial\theta} + \frac{1}{2}\left(\rho h\right)_o \Omega_R R_{R_o} \tag{8a}$$

$$\dot{m}_{z_o} = \left(\rho W h\right)_o = -\frac{\rho h_o^{\,3}}{12\mu_o}\frac{\partial P_o}{\partial z_o} \tag{8b}$$

and

$$\Phi_o = 12\frac{\mu_o}{h_o}\left[W_o^{\,2} + \frac{\left(\Omega_R R_{R_o}\right)^2}{12} + \left(U_o - \frac{\left(\Omega_R R_{R_o}\right)}{2}\right)^2\right] \tag{8c}$$

Above ($T_C, T_{R_o}$) denote the temperatures of the TC casing ID surface and ring OD surface; ($H_C, H_{R_o}$) are the heat convection coefficients to the casing ID surface and the ring OD surface, respectively. Thus, $Q_o = H_{R_o}(T_o - T_{R_o}) + H_C(T_o - T_C)$ represents the heat flow into the ring through its outer surface plus that into the bearing casing. Above, $\left(\dot{m}_{\theta_o}, \dot{m}_{z_o}\right)$ denote the outer film lubricant mass flow rates in the circumferential and axial directions. The mean flow velocities are from Eqs. (8a) and (8b)

$$U_o = -\frac{h_o^{\,2}}{12\mu_o}\frac{\partial P_o}{R_{R_o}\partial\theta} + \frac{1}{2}\Omega_R R_{R_o} \tag{9a}$$

$$W_o = -\frac{h_o^{\,2}}{12\mu_o}\frac{\partial P_o}{\partial z_o} \tag{9b}$$

Incidentally, for the semi-floating ring bearing, the ring cannot rotate so that $\Omega_R$=0, and there is no shearing of the outer film.

Notes that the heat convection coefficients ($H_C, H_{R_o}, H_{R_i}, H_J$) depend on the

Prandtl number $\mathrm{Pe} = \frac{C_v \mu}{\kappa}$ and the flow condition defined by the local Reynolds number $\mathrm{Re} = \frac{\rho U h}{\mu}$ relative to the ring and journal surfaces. Refs. [21, 22] provide a number of heat convection models including those for fully developed or developing wall temperatures.

**Equations for Film Pressure and Temperature in the Lubricant Cavitation Region**

The Reynolds and energy transport equations are valid within a full film zone where the fluid flow completely fills the gap between the bounding solids. The oil lubricated film will cavitate (liquid vaporization or release of dissolved gases) in regions when the fluid film pressure drops to ambient or the cavitation pressure $P_{cav}$. Figure 6 shows a schematic view of the oil cavitation region with the gas/vapor region attached to the inner surface of the ring. Note that the following analysis is valid only when the ring does not rotate.

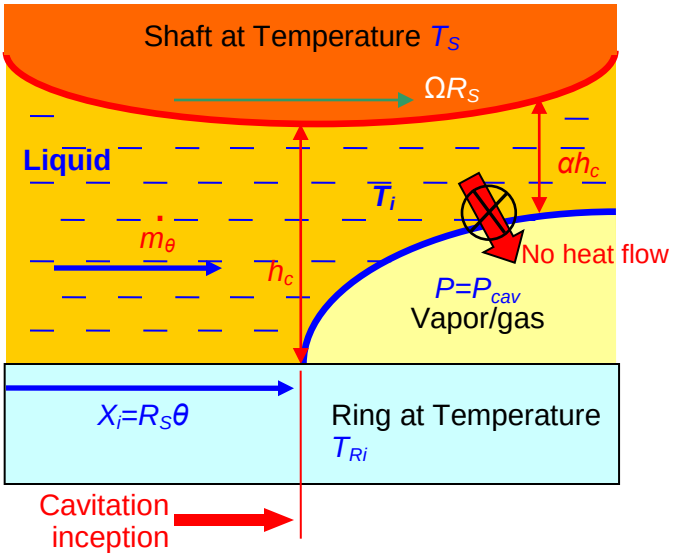


**Figure 6. Schematic view of flow path in lubricant cavitation zone (inner film) [23].**

Within the cavitation zone, there is no generation of hydrodynamic pressure, hence $\left(\partial P/\partial\theta, \partial P/\partial z\right)=0$ .Therefore, the axial flow within the cavitation zone is null. For the inner film,

$$\dot{m}_{z_i}=0 \tag{10}$$

and the circumferential flow is

$$\dot{m}_{\theta_c}=\frac{1}{2}\rho h_c \Omega R_J \tag{11}$$

where $h_c$ denotes the film thickness at the inception of the oil cavitation region.

As for the thermal energy transport in the cavitation region, Ref. [23] introduces a model that accounts for heat conduction across the film in contact with the rotating

shaft and assumes no shear power generation. The heat diffusivity into the gas or vapor *bubble* is negligible. Hence, the thermal energy transport equation simplifies to

$$C_v\left[\frac{\dot{m}_{\theta_c}}{R_J}\frac{dT_{i_c}}{d\theta}\right]+H_J\left(T_{i_c}-T_S\right)-\kappa\left[\frac{d^{\,2}T_{i_c}}{R_J^2 d^2\theta}\right]h_*=0 \tag{12}$$

where $h_* = \alpha h_c$ is the liquid film thickness, and $\alpha$ is an ratio between the lubricating oil and the actual gap (liquid plus vapor) separating the rotating shaft from the ring surface. $H_J$ is the heat convection coefficients to the shaft OD surface, and $H_J\left(T_{i_c}-T_S\right)$ represents the heat flow into the shaft surface in oil cavitation zone. $\kappa$ is the thermal conductivity of the film flow.

**Temperature Field in a (Semi) Floating Ring**

At a thermal steady state condition, Ref. [24] shows the derivation of the heat conduction equation in a rotating floating ring in a fixed reference frame ($r, \theta, z$):

$$\frac{\partial}{r\partial r}\left(r\kappa_R\frac{\partial T_R}{\partial r}\right)+\frac{\partial}{r\partial\theta}\left(\kappa_R\frac{\partial T_R}{r\partial\theta}\right)+\frac{\partial}{\partial z}\left(\kappa_R\frac{\partial T_R}{\partial z}\right)=\rho_R C_{P_R}\left(\Omega_R r\right)\frac{\partial T_R}{r\partial\theta} \tag{13}$$

where $\kappa_R$ , $\rho_R$ and $C_P$ are the thermal conductivity, density and specific heat of the ring material. Above, the term on the right denotes the effect of rotation on the ring temperature and denoting the transport of thermal (internal) energy acting by advection

The heat conduction in the axial direction of the ring is neglected for simplicity and ignorance [1]. Hence, Eqn. (13) reduces to

$$\frac{\partial}{r\partial r}\left( r\kappa_R \frac{\partial T_R}{\partial r}\right)+\frac{\partial}{r\partial\theta}\left( \kappa_R \frac{\partial T_R}{r\partial\theta}\right)=\nabla^2 T_R(r,\theta)=\rho_R C_{P_R}\left(\Omega_R r\right)\frac{\partial T_R}{r\partial\theta} \tag{14}$$

The heat flow (boundary) conditions at the inner and outer surfaces of the ring are:

$$H_{R_i}(T_{R_i}-T_i)=-q_r\big|_{r=R_i,\theta,z}=+\kappa_R\left.\frac{dT}{dr}\right|_{r=R_i,\theta,z} \quad \text{for} \quad \theta\in\{0,2\pi\}, z\in\left\{-\tfrac{1}{2}L_i,\tfrac{1}{2}L_i\right\} \tag{15a)}$$

$$H_{R_o}(T_{R_o}-T_o)=+q_r\big|_{r=R_o,\theta,z}=-\kappa_R\left.\frac{dT}{dr}\right|_{r=R_o,\theta,z} \quad \text{for} \quad \theta\in\{0,2\pi\}, z\in\left\{-\tfrac{1}{2}L_o,\tfrac{1}{2}L_o\right\} \tag{15b)}$$

where $T_{R_i}$ and $T_{R_o}$ are the (to be determined) temperatures of the ID and OD surfaces of the ring, respectively. $H_{R_i}$ and $H_{R_o}$ are the heat convection coefficients for the inner and outer films bounding to the ring. These coefficients are identical to those defined in the thermal transport equations for the inner and outer flows, see Eqs (4) and (6).

In a semi-floating ring the thermal advection term disappears since $\Omega_R = 0$. Hence, the heat conduction equation reduces to

$$\frac{\partial}{r\partial r}\left( r\kappa_R \frac{\partial T_R}{\partial r}\right)+\frac{\partial}{r\partial\theta}\left( \kappa_R \frac{\partial T_R}{r\partial\theta}\right)=\nabla^2 T_R(r,\theta)=0 \tag{16}$$

with the same boundary conditions as stated by Eqns. (15a) and (15b).

Note that Ref.[1] presents the thermal energy transport analysis and predictions for (semi) floating ring bearing system based on the assumption that the ring temperature only varies along the radial direction. However, there is no experimental data to support this simplification. Presently, the proposed heat transfer model in a semi-floating ring will account for heat conduction in both the circumferential and radial directions. It is

assumed that there is a large temperature change of the ring inner surface in the oil cavitation region where heat convection from the oil vapor/gas transfers is negligible. In the regions wetted fully by lubricant, the heat transfer process from the inner film into the ring inner surface is more effective because the oil liquid conductivity is much higher than when oil entraps some air[9].

The heat flowing from the inner film into the ring inner surface equals [1]

$$Q^{i\to R} = \int_{-L_i/2}^{L_i/2}\int_0^{2\pi}\left[H_{R_i}(T_i - T_{R_i})\right]R_{R_i}\,d\theta dz_i \tag{17}$$

and the heat flow from the ring outer surface into the outer film is

$$Q^{R\to o} = \int_{-L_o/2}^{L_o/2}\int_0^{2\pi}\left[H_{R_o}(T_{R_o} - T_o)\right]R_{R_o}\,d\theta dz_o \tag{18}$$

Similarly, the heat flow from the shaft and the heat flow into the casing are calculated, respectively, by

$$Q^{J\to i} = \int_{-L_i/2}^{L_i/2}\int_0^{2\pi}\left[H_{R_i}(T_S - T_i)\right]R_{R_i}\,d\theta dz_i = -Q^{i\to J} \tag{19}$$

$$Q^{o\to C} = \int_{-L_o/2}^{L_o/2}\int_0^{2\pi}\left[H_{R_o}(T_o - T_C)\right]R_{R_o}\,d\theta dz_o = -Q^{C\to o} \tag{20}$$

Note that the above heat flows are obtained from the solution of the energy transport equations in the inner and outer films. Since there is no accumulation of heat in the floating ring, the heat flow from the inner film into the ring must equal the heat from the ring into the outer film, $Q^{i\to R} = Q^{R\to o}$.

[9] This paragraph paraphrases Dr. San Andres' personal note in July, 2012

**Global Form of the Energy Transport Equation in the Flow Domains**

Integration of the energy transport Eqns.(4) and (6) in the circumferential and axial directions leads to a global balance of energy transport in the inner and outer flow domain, respectively.

For the inner film,

$$\int_{-L_i/2}^{L_i/2}\int_0^{2\pi} C_v\left[\frac{1}{R_J}\frac{\partial}{\partial\theta}\left(\dot{m}_\theta T\right)_i+\frac{\partial}{\partial z_i}\left(\dot{m}_z T\right)_i\right]R_J d\theta dz_i + Q^{i\to R} + Q^{i\to J} = \wp_i \tag{21}$$

where

$$\wp_i = \int_{-L_i/2}^{L_i/2}\int_0^{2\pi} \Phi_i R_J d\theta dz_i \tag{22}$$

is the total mechanical drag power converted into heat; $Q^{i\to R}$ and $Q^{i\to J}$ are the heat flows from the inner film into the bounding surface defined by Eqns.(17) and (19) .

The integral term in Eqn.(21) represents the total heat convected to the inner film,

$$\begin{aligned} E_i &= C_v\int_{-L_i/2}^{L_i/2}\int_0^{2\pi}\left[\frac{1}{R_J}\frac{\partial}{\partial\theta}\left(\dot{m}_\theta T\right)_i+\frac{\partial}{\partial z_i}\left(\dot{m}_z T\right)_i\right]R_J d\theta dz_i \\ &= 2C_v\left\{\int_0^{2\pi}\left(\left[\left(\dot{m}_{z_i} T_i\right)_{z_i=L_i/2}\right]-\left[\left(\dot{m}_{z_i} T_i\right)_{z_i=0}\right]\right)R_J d\theta\right\} \end{aligned} \tag{23}$$

with the first integral term $\int_0^{2\pi}\left[\frac{1}{R_J}\frac{\partial}{\partial\theta}\left(\dot{m}_\theta T\right)_i\right]d\theta = 0$ because of periodicity, i.e., $\left(\dot{m}_{\theta,z}, T\right)_\theta = \left(\dot{m}_{\theta,z}, T\right)_{\theta+2\pi}$.

Similarly, for the outer film, the global balance of energy transport over the whole flow domain is

$$E_o + Q^{o\to R} + Q^{o\to C} = \wp_o \tag{24}$$

where

$$\wp_o = \int_{-L_o/2}^{L_o/2}\int_0^{2\pi} \Phi_o R_{R_o}\, d\theta dz_o \tag{25}$$

$$E_o = 2C_v \left\{ \int_0^{2\pi} \left( \left[ \left( \dot{m}_{z_o}\, T_o \right)_{z_o = L_o/2} \right] - \left[ \left( \dot{m}_{z_o}\, T_o \right)_{z_o = 0} \right] \right) R_{R_o}\, d\theta \right\} \tag{26}$$

Figure 7 depicts a schematic view of the heat flows and drag powers in the films of a FRB system. The flow path through both films must be designed carefully to ensure the lubricant flow rates cool effectively the bearing components without actually increasing the drag power loss that impacts adversely a TC mechanical efficiency, as also stressed earlier.

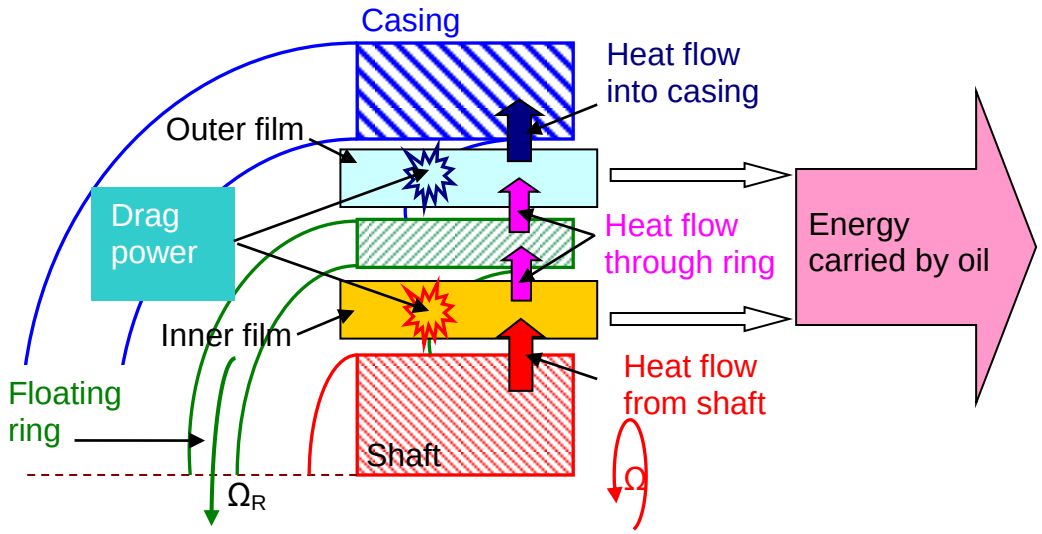


**Figure 7. Schematic view of heat flows in floating ring bearing system [1]**

**Estimation of the Exit Temperature of the Lubricant Leaving the Bearing System**

The energy convected to the lubricant inner and outer flows equals to the sum of the energy transported by the inner and outer films, $E = E_i + E_o$, see Eqns.(23) and (26).

The mass flow rate of lubricant leaving the bearing system equals to the total lubricant supply mass flow at $z_{i,o}$=0 by flow continuity, $\dot{M} = \dot{M}_i + \dot{M}_o$, where

$$M_i = 2\int_0^{2\pi} \left( \dot{m}_{z_i} \Big|_{z_i=0} \right) R_J d\theta \tag{27a}$$

$$M_o = 2\int_0^{2\pi} \left( \dot{m}_{z_o} \Big|_{z_o=0} \right) R_{R_o} d\theta \tag{27b}$$

Hence, the lubricant temperature rise ($\Delta T_E$) is estimated by a simple balance of thermal energy,

$$C_v \dot{M} \Delta T_E = E = E_i + E_o \tag{28}$$

Note that the mixed flow rate at the discharging plane ignores the potential flow streams leaving the thrust bearings, thus $\Delta T_E$ is representative only when the lubricant flows out from the inner and outer films.

**Boundary Conditions for the Pressure and Temperature Fields [25]**

The boundary conditions for the solution of the pressure generation and energy transport equations depend on the type of bearing analyzed. Presently, the bearings for analysis are symmetric about the axial mid plane (z=0), and it is also assumed there is no

axial misalignment between the rotor and its ring or between the ring and the bearing casing. The pressure must satisfy

$$P_i(\theta, z_i) = P_i(\theta, -z_i); \quad P_o(\theta, z_o) = P_o(\theta, -z_o) \tag{29a}$$

$$T_i(\theta, z_i) = T_i(\theta, -z_i); \quad T_o(\theta, z_o) = T_o(\theta, -z_o) \tag{29b}$$

Additionally, in both inner and outer films, the pressure and temperature must be periodic in the circumferential direction,

$$P_i(\theta, z_i) = P_i(\theta + 2\pi, z_i); \quad P_o(\theta, z_o) = P_o(\theta + 2\pi, z_o) \tag{30a}$$

$$T_i(\theta, z_i) = T_i(\theta + 2\pi, z_i); \quad T_o(\theta, z_o) = T_o(\theta + 2\pi, z_o) \tag{30b}$$

As for the locations where the pressure and temperature are specified, such as in the supply holes and in a ½ moon groove,

$$P_i(\theta_{k_i}, z = 0) = P_{SUP}; \quad T_i(\theta_{k_i}, z = 0) = T_{SUP} \tag{31a}$$

$$P_o(\theta_{k_o}, z = 0) = P_{SUP}; \quad T_o(\theta_{k_o}, z = 0) = T_{SUP} \tag{31b}$$

where $(\theta_k)_{k=1,..N_{holes}}$ indicates the angle location of the orifice port where the boundary condition is prescribed.

In addition, the pressure at the bearing discharge plane is specified as the ambient pressure ($P_A$),

$$P_i(\theta, z = \tfrac{1}{2} L_i) = P_o(\theta, z = \tfrac{1}{2} L_o) = P_A \quad , \quad 0 \le \theta \le 2\pi \tag{32}$$

Other boundary conditions denoting the heat flows into the ring, casing and shaft

were stated earlier.

**Estimation of Operating Film Clearances**

The operating film clearances represent the difference in diameter between the bounding solids. Specified nominal clearances $(c_*)_{i,o}$ are at cold or room temperature condition ($T_* \approx 20°C$) and derived from drawing or direct measurement of components.

When TCs operating the temperatures of the shaft, ring, and casing are well above ambient, the thermal growth of each component is significant with regard to the nominal clearance, and then affect directly the operating clearance. In addition, the typical thermal expansion coefficients ($\alpha$) of these components are dissimilar, so that the thermal expansion rates of them are different, which may lead to sudden shaft seizure. Thus, it is necessary to estimate the clearance between the bounding solids and to ensure its value within the acceptable range for TCs' reliable operation.

Presently, an approximate model takes the film clearances as invariant both along the axial and circumferential directions. The operating clearances are determined from the formulas

$$c_i(T_i) = c_i(T_*) - \alpha_S R_S \left(\bar{T}_{S\&i} - T_*\right) + \alpha_R R_{R_i} \left(T_{R_i\&i} - T_*\right) \tag{33a}$$

$$c_o(T_o) = c_o(T_*) - \alpha_R R_{R_o} \left(T_{R_o\&o} - T_*\right) + \alpha_C R_C \left(\bar{T}_{C\&o} - T_*\right) \tag{33b}$$

where $\bar{T}_{S\&i} = \frac{1}{2}\left(T_S + \bar{T}_i\right)$; $T_{R_i\&i} = \frac{1}{2}\left(T_{R_i} + \bar{T}_i\right)$; $\bar{T}_{C\&o} = \frac{1}{2}\left(T_C + \bar{T}_o\right)$; $T_{R_o\&o} = \frac{1}{2}\left(T_{R_o} + \bar{T}_o\right)$.

Here, $\overline{T}_i$ and $\overline{T}_o$ are the average lubricant film temperatures over the whole inner and outer flow regions, respectively. $\alpha_S$, $\alpha_R$, and $\alpha_C$ are the thermal expansion coefficients of the shaft, ring and bearing casing, respectively, all of which are constant.

**Numerical Solution Procedure**

Figure 8 depicts a flow chart for the entire solution procedure to obtain both pressure and temperature fields in the inner and outer films. The model that calculates the temperature field within the ring couples the inner and outer fluid flows with the balance of heat flows through the ring. The entire procedure also couples the temperature distribution of the film flows and the film reaction forces satisfying the static load balance while updating the operating clearances.

**Closure**

An engineered management of the thermal energy flows within an engine-oil lubricated floating ring bearing system is vital to warrant the reliable operation of a turbocharger (TC). Not only the temperature fields of both fluid films, but also the temperature field in the floating ring are indispensable to predict the thermal energy paths in a TC bearing. Adequate thermal management aims at ensuring the maximum film temperature is well below the lubricant flash temperature, and that most heat from the (hot) shaft and fluid shear drag power loss is carried away by the lubricant flowing

through the inner and outer films. In order to better estimate the mechanical drag power loss, the temperature-depend lubricant viscosity and operating clearances are updated with the predicted temperature fields for the oil and the floating ring. The improvements in the thermal energy model for a (semi) floating ring bearing system are essential to improve predictions of the overall thermal energy transfer and mechanical efficiency of TCs.

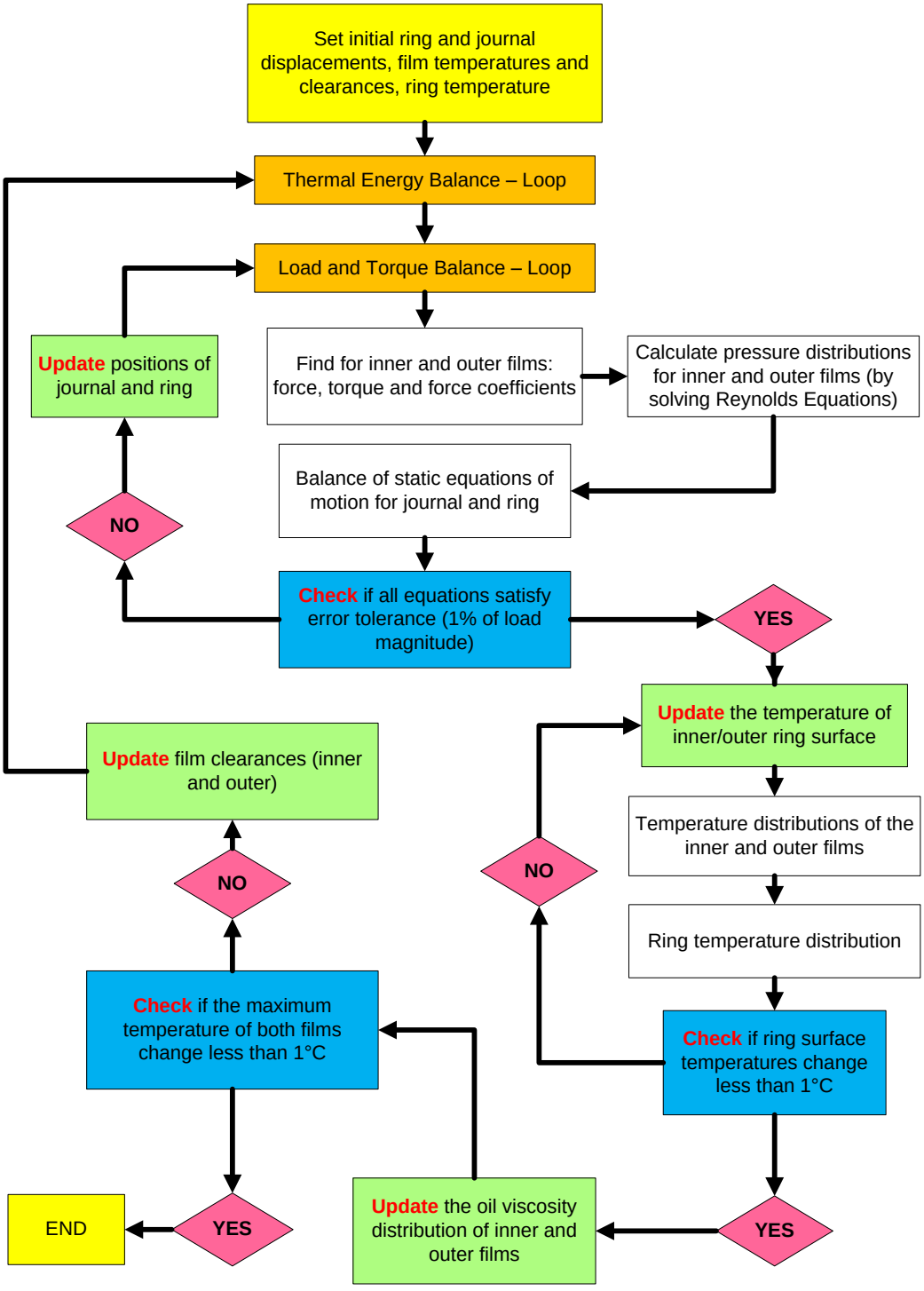


**Figure 8. Flowchart showing the solution procedure (pressure and temperature) for the inner and outer films in a floating ring bearing**

# 5. VALIDATION OF THE THERMOHYDRODYNAMIC MODEL FOR BEARING PERFORMANCE

Presently, there are few if any experimental data available to benchmark performance predictions of the thermohydrodynamic (THD) tool for a typical (semi) floating bearing in a turbocharger. However, there are a number of published papers that present measurements of journal bearing surface temperatures for typical industrial journal bearings [5, 26, and 27]. Some references also include numerical predictions of whole 3D temperatures fields [28].

Among these publications, Ref. [5] provides experimental data of pressure and temperature profiles recorded at the midplane of a bearing with two oil supply holes and two oil supply grooves (180 ° apart). This bearing has a similar inlet geometry as that of the inner film in a turbocharger. Besides, Ref. [5] gives details on the shaft temperatures for various operating conditions. That data helps to simulate better the actual physical condition (rather than assuming an adiabatic shaft model, e.g., no heat transfer between the shaft and lubricant film in a steady thermal condition).

Figure 9 shows a schematic view of a bearing test rig in Ref. [5]. Referring to Figure 9, one or more steel disks are mounted onto the bearing housing. The (stationary) steel disk provides the static load, in combination with the external load from the loading system, which can deliver a maximum load of 10 kN vertically. The test bearing bush is fitted with a light press into a cylindrical bearing housing, so that the clearance between the bearing bush and bearing housing is nil. The bearing bush is machined from bronze

C93700 and its thermal conductivity is 46.9 W/m ·℃. The bearing housing and disks are made of steel, whose average thermal conductivity is around 35~50 W/m ·℃. Lubricant is supplied to the test bearing from a gear pump and its available supply pressure is 0~10 bar. The oil inlets are always at 90 ºto the vertical load line.

Two pairs of capacitance displacement sensors are installed to measure the journal position along the vertical and horizontal directions. The oil film pressure distribution is measured in the bearing midplane. Sixteen equally-spaced pressure sensors are inserted in holes in the bearing housing to provide the static pressure data. The temperature distribution is measured at the midplane of the bearing bush inner surface via sixteen thermocouples. One additional thermocouple, within 0.5mm of the journal OD surface, provides the journal surface temperature data. The thermocouple signal is transmitted by a mercury slip-ring to a recorder. Note that the shaft temperature varies little compared to that of the bearing housing.

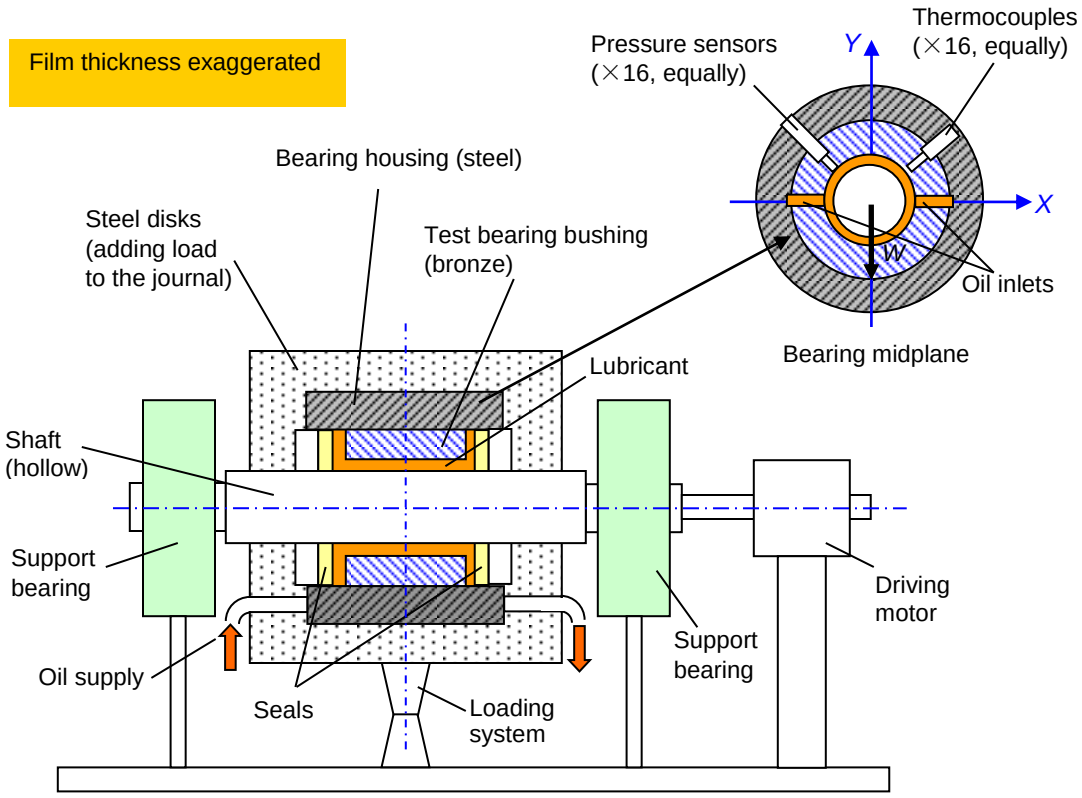


**Figure 9. Schematic view of a journal bearing test rig [5]**

Figure 10 shows schematic views comparing the bearing in Ref. [5] and one equivalent model as a (S)FRB. Apart from the heat carried away by the lubricant, the remaining heat is conducted through the bearing bushing, then through the bearing housing and the steel disks, and eventually convected into the ambient[10]. To simulate the

[10] In practice, heat transfer due to radiation is much less than the heat convection, so the heat transfer mechanism only accounts for heat conduction, convection, and drag power dissipation.

test bearing and describe the heat flow through it, some adaptations on the generic model for a (S)FRB are needed. Firstly, both the thermal conductivity coefficient of the outer film and the heat convection coefficient between the outer film and the casing are increased by 1,000 times. This value is arbitrarily chosen to "force" the coefficients to be high enough as to produce a constant uniform outer film temperature field and close to the casing temperature. The outer film of the (S)FRB is used to simulate the air surrounding the test rig, and the air temperature can be set by assigning the casing temperature in the (S)FRB model. Second, the heat convection coefficient between the outer film and the ring outer surface is reduced to 50 $W/m^2 \cdot ℃$. This is an approximate value for the natural convection coefficient to ambient [29]. Thus, the adapted model can simulate the natural convection that occurs on the steel disk wall.

Note that the magnitude of the outer film clearance is of no relevance to the accuracy of the adapted numerical model, but the stiffness of the anti-rotation button should be modified and be high enough to fix the floating ring. In addition, the thermal conductivity coefficients of the bearing housing and steel disk are equal to that of the test bearing. The ring inner radius in the (S)FRB is equal the test bearing inner radius, and the ring outer radius is taken to equal the outer radius of the steel disks. In other words, the test bearing, the bearing housing and the steel disks are taken together to act as the ring in the (S)FRB.

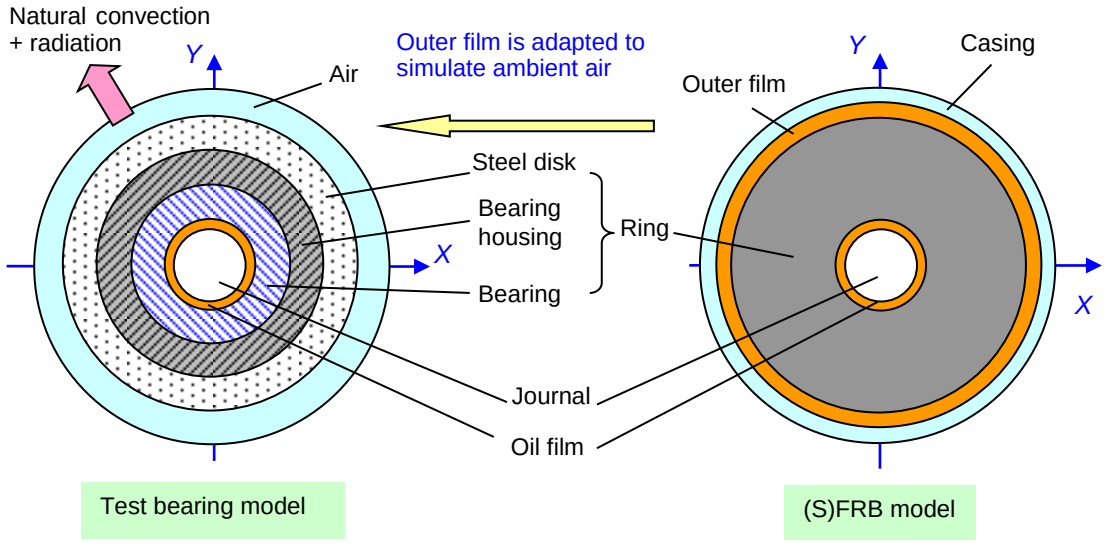


**Figure 10. Schematic views of the test bearing in Ref. [5] and its (S)FRB idealization.**

Table 1 lists the test bearing dimensions and operating conditions as in Ref. [5]. It is reported that the lubricant supply temperature ($T_{SUP}$) is adjusted to the thermal condition of the test rig, e.g., at low journal speeds the monitored mid range of $T_{SUP}$ is typically about 30 ℃; for high journal speeds $T_{SUP}$ is thermostatically controlled to be under 48 ℃. The shaft temperature depends on the journal speed and the lubricant viscosity, and is also influenced by the load and the method of oil supply (holes or grooves). For example, with a load of 9,000 N and operating with lubricant (ISO VG 32), the shaft temperature increases from 35 ℃ to 81 ℃ as the journal speed grows from 400 rpm to 6,400 rpm.

**Table 1. Journal bearing dimensions and operating conditions for bearing in Ref.[5]**

| | |
|---|---|
| Bearing diameter, $D$ | 100 mm |
| Bearing length, $L$ | 55 mm |
| Bearing wall thickness, $d$ | 10 mm |
| Cold radial clearance at 20 ℃, $C_0^*$ | 75 μm |
| Lubricant supply pressure, $P_{SUP}$ | 2 bar |
| Lubricant supply temperature, $T_{SUP}$ | 30~48 ℃ |
| Shaft temperature, $T_S$ | 31 ~ 91 ℃ (measured) |
| Applied load range, $W$ | 0 ~ 10,000 N |
| Shaft rotational speed, $N$ | 40 ~ 8,000 RPM |
| Conductivity of bearing bushing, $\kappa$ | 46.9 W/m ·℃ (Bronze, C93700) |
| Conductivity of bearing housing and steel disk | 46.9 W/m ·℃ (assumed) |
| Natural heat convection coefficient | 50 W/m$^2$ ·℃ (assumed) |
| Ambient temperature | 30 ℃ (assumed) |
| Oil type : **ISO VG32** | |
| Density, $\rho$ | 860 kg/m$^3$ |
| Specific Heat, $C_V$ | 2000 J/kg ·℃ |
| Viscosity (at 40 ℃), $\mu_0$ | 0.0278 Pa s |
| Viscosity (at 100 ℃), $\mu_0$ | 0.0046 Pa s |

Figure 11 depicts the predicted film pressure and temperature field for the test

bearing with a load of 5,000 N and shaft speed at 3,200 rpm. Two supply grooves deliver lubricant to the bearing. The temperature of the shaft outer surface is at 62 ℃ from measurement. The pressure field shows that the entire fluid flow separates into a loaded zone and an unloaded zone. In the unloaded zone where oil cavitation takes place, the gas or vapor zone (*bubble*) attached to the bearing has negligible heat conduction and there is no drag power generation. The film temperature near the oil inlet plane heats more quickly in the loaded zone due to drag power loss. Note that both the peak film temperature and the peak pressure occur in the loaded zone.

Figure 12 compares the predicted and measured pressure profiles at the bearing midplane for operation at 3,200 rpm and with 5,000 N. The results show that the predictions and the test data are in good agreement. Note that in oil cavitation zone, the fluid pressure drops below ambient to its vapor pressure ($P_{CAV}$), which is assumed to be at -0.01 bar.

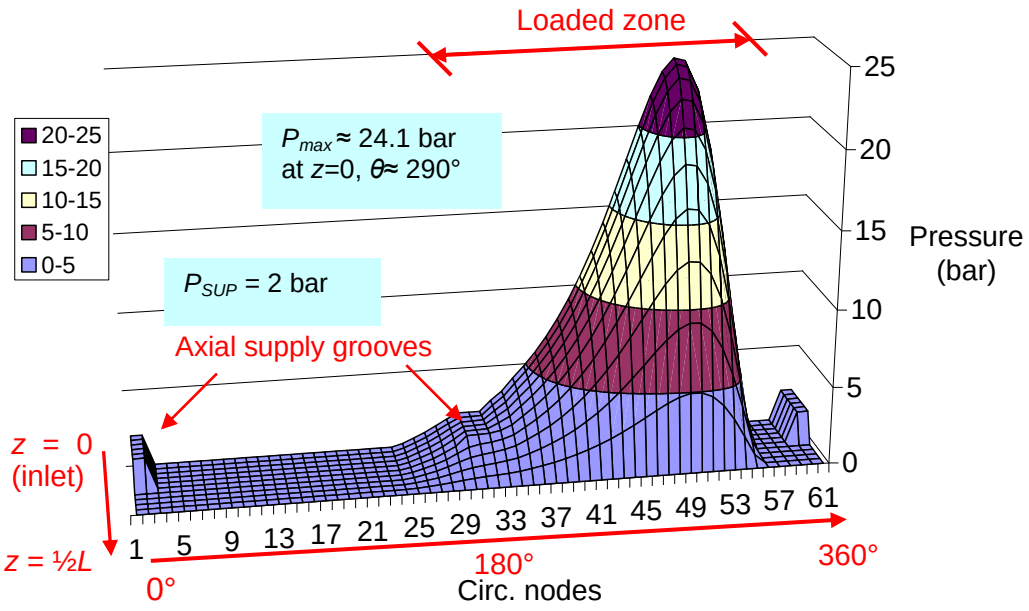


**(a) Film pressure field**

**Figure 11. Predicted pressure field (a) and temperature field (b) for journal bearing film. Shaft speed = 3,200 rpm, $W$ = 5,000 N, ($e$,$\Phi$) ≈ (45μm, 50°). $T_{SUP}$ = 40°C, $P_{SUP}$ = 2 bar, $T_{shaft}$ = 62 °C (measured).**

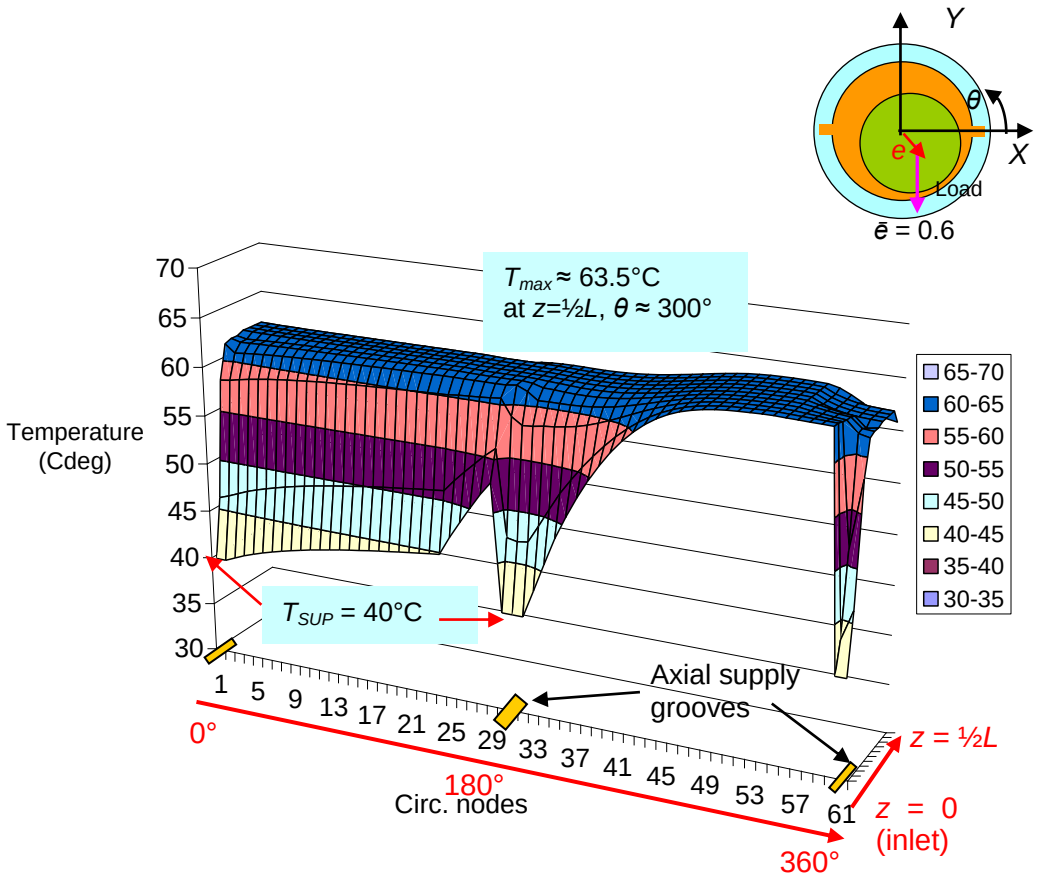


**(b) Film temperature field**

**Figure 11** Continued.

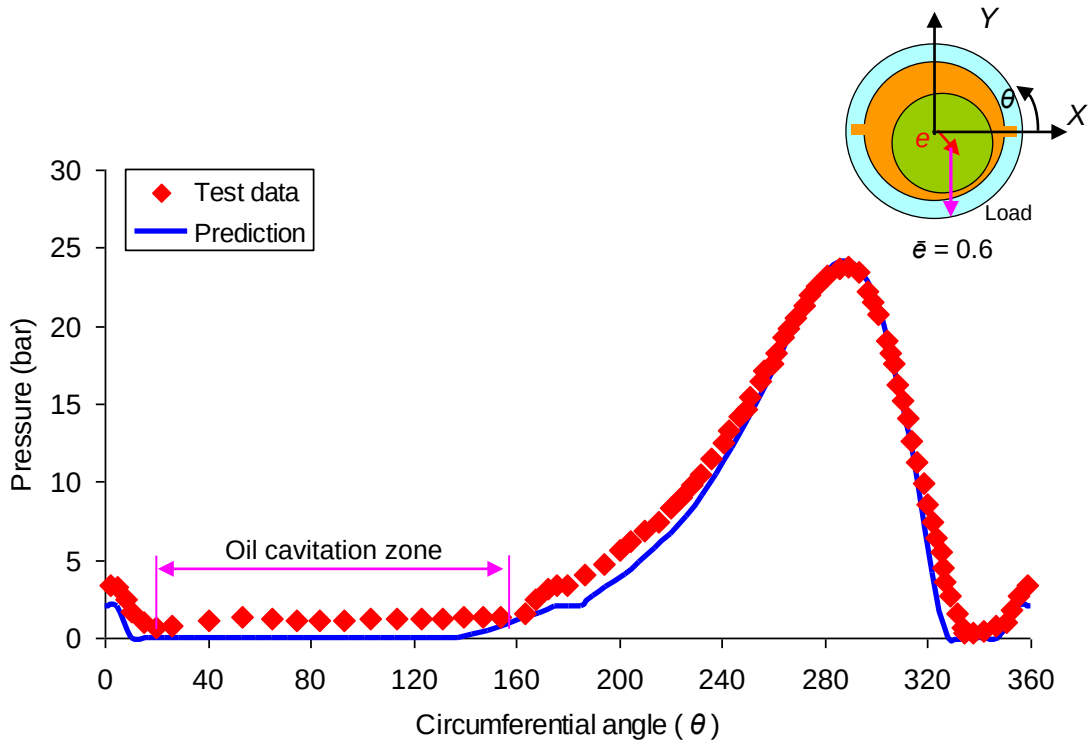


**Figure 12. Pressure fields at the bearing midplane: test data from Ref. [5] and prediction. Shaft speed = 3,200 rpm, $W$ = 5,000 N, ($e$,$\Phi$) ≈ (45μm, 50°). $T_{SUP}$ = 40°C, $P_{SUP}$ = 2 bar. $T_{shaft}$ = 62 °C (measured).**

Figure 13 shows a comparison of the predicted and measured temperature profiles at the midplane of the bearing bushing inner surface for operation at 4,800 rpm and with a null load. Since there is no load on the journal, the journal rotates nearly concentrically to the casing. The measured temperature of the shaft outer surface is at 83 ℃. The measured temperatures at the *film-bushing* interface in Ref. [5] refer to temperatures just below the inner surface of the bearing bushing, at a depth of 0.5 mm.

The results show that the predicted temperatures are a little higher than the measured ones, but the prediction is satisfactory considering the deviation is less than 5% of the average temperature (~77 ℃) of the measured temperatures.

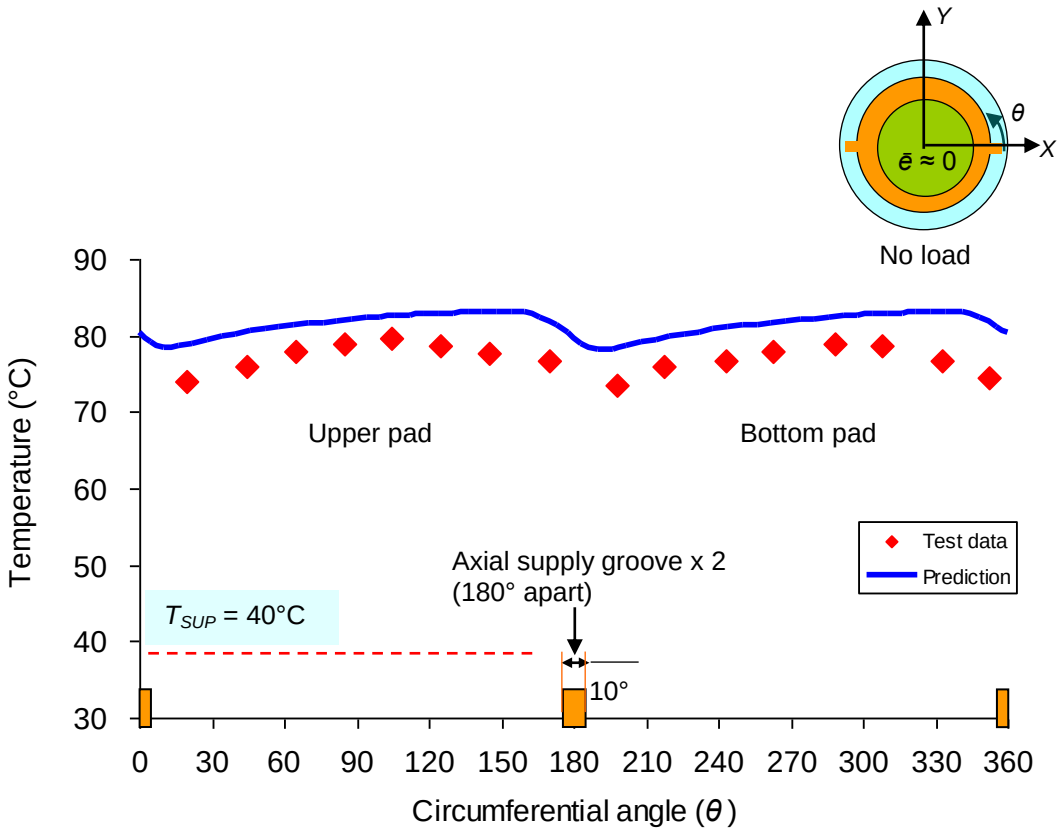


**Figure 13. Temperature fields at the bearing midplane: test data from Ref. [5] and prediction. Shaft speed = 4,800 rpm, no load. ($e$,$\Phi$) ≈ (0, 0). $T_{SUP}$ = 40°C, $P_{SUP}$ = 2 bar. $T_{shaft}$ = 83 °C (measured).**

Figure 14 shows a comparison of the predicted and measured temperature

profiles at the midpane of the bearing bushing for operation at 6,400 rpm and an acting vertical load of 5,000 N. The prediction shows a similar temperature trend as the test data. The bushing temperature remains nearly invariant in the upper pad, but increases in the film loaded area (the bottom pad) where shear drag power generation occurs. The deviations of the predicted results from the test data near the oil supply groove ($\theta$=180 °) is due to the assumption that the axial temperature gradient within the bushing is negligible.

The predicted temperatures of the bearing bushing vary only along the circumferential direction, depending on the film temperature profile along the axial direction for the corresponding circumferential angle. The film temperature increases quickly as the lubricant flows through the film clearance. The bearing bushing is cooler near the oil supply holes rather than near the bearing outlet plane. Measurements in Refs. [30, 31] prove that the bushing temperatures near the supply holes are lower than other areas, while measured bushing temperatures on regions far from the oil supply holes are nearly invariant along the axial direction.

Figure 15 shows a comparison of the predicted and measured journal center locus for operation at 3,200 rpm with loads ranging from 100 N to 9,000 N. Only a recorded temperature (~62 ℃) with a load of 9,000 N is reported in Ref. [5]. However, Ref. [32] states that the shaft temperature ($T_{shaft}$) is not affected by the load, but it is significantly influenced by the journal speed[11]. Thus, it is reasonable to assume the shaft temperature

[11] According to the measurements in Ref.[32], the shaft temperature increases by 3 ℃ as the load increases from 2 kN to 10 kN for operation at 4,000 rpm, but it increases by as high as 20 ℃ as the journal speed increases from 1,000 rpm to 4,000 rpm with a load of 2 kN.

is constant at 62 ℃ for operation at 3,200 rpm as the load grows from 100 N to 9,000 N. The comparison reveals that the maximum deviation in journal locus occurs at the maximum load, while diminishing for small loads[12]. The deviation is probably caused by the changes in clearance due to mechanical over stress as the shaft is heavily loaded[13].

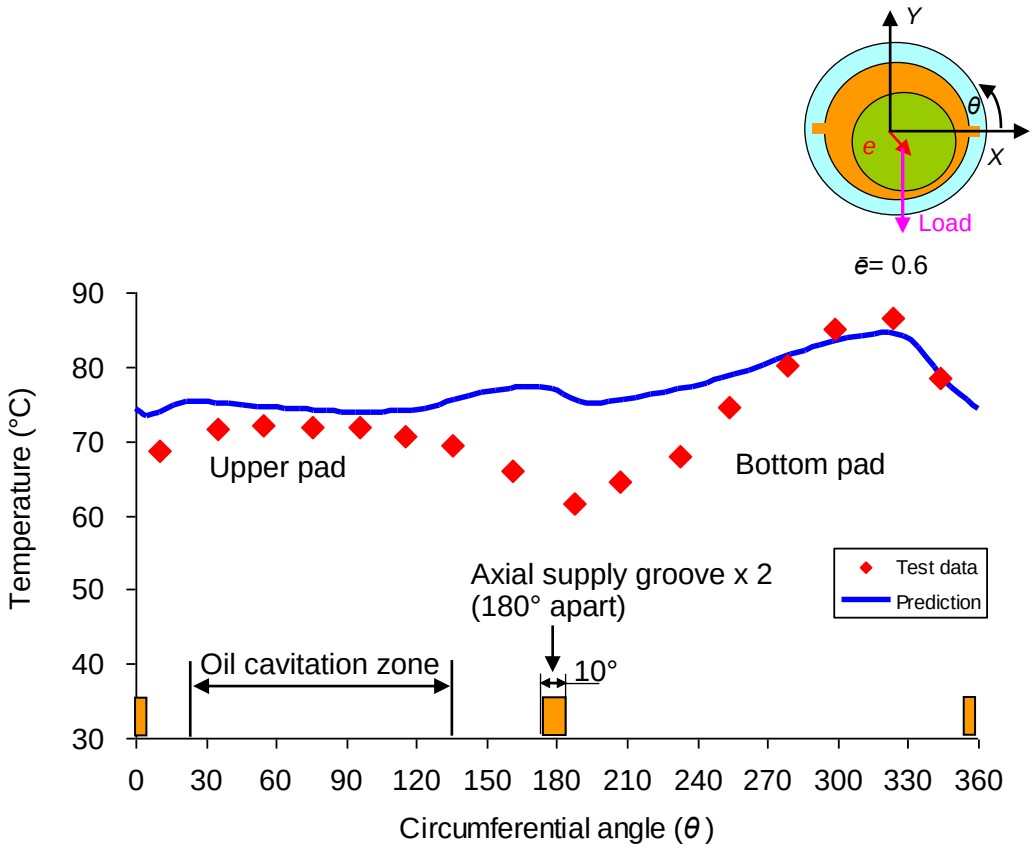


**Figure 14. Temperature fields at the bearing midplane: test data from Ref. [5] and prediction. Shaft speed = 6,400 rpm, $W$ = 5,000 N, ($e$,$\Phi$) ≈ (45μm, 50°). $T_{SUP}$ = 40°C ,$P_{SUP}$ = 2 bar. $T_{shaft}$ = 82 °C (measured).**

[12] The authors in Ref. [5] present a similar predictive journal locus curve, which also shows that the maximum deviation occurs at the largest load.

[13] For the maximum recorded load (9,000N), the specific load ($W/LD$) on the shaft is about 16 bar.

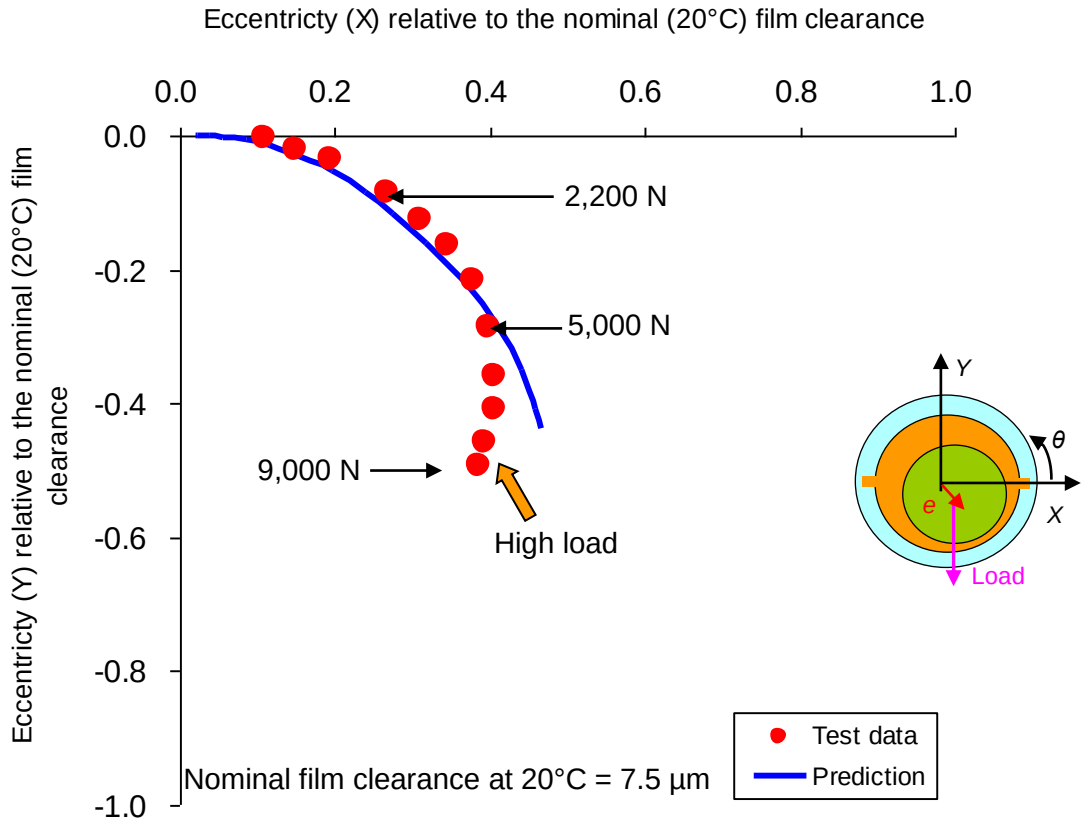


**Figure 15. Journal center locus: test data from Ref. [5] and prediction. Shaft speed = 3,200 rpm, $W$ = 100 ~ 9,000 N, $T_{SUP}$ = 40°C, $P_{SUP}$ = 2 bar. $T_{shaft}$ = 62°C (for all loads).**

In summary, this chapter presents a few predictions aiming to validate the thermohydrodynamic model by comparing the pressure and temperature distributions of the inner film in the current (S)FRB model, as well as the journal locus curve, against available test data for a journal bearing lubricated with two supply axial grooves. Some

necessary adaptations to the current (S)FRB model were required. The comparison reveals that the majority of predictions are in good agreement with the test data, in particular for operation at low loads.

Considering that the static load on the (S)FRB of a turbocharger is usually small[14], the results of the thermohydrodynamic tool for predicting the bearing performance of a (S)FRB are most likely reliable.

[14] For reference, the specific load ($W/LD$) for the test in Ref.[5] ranges from 0 to 16 bar, but for a typical (S)FRB it is around 0.25 bar (see an example of the (S)FRB detailed in the next chapter).

# 6. PREDICTIONS OF PERFORMANCE FOR A SEMI-FLOATING RING BEARING

Figure 16 shows a schematic view of a semi-floating ring bearing reproducing an actual configuration in a turbocharger application. The ring has four equally spaced axial grooves on its inner surface, and four radial holes at its middle plane. Table 2 describes the geometry of the (S)FRB and its typical operating conditions in a turbocharger. The diameter of the holes, 1 mm, equals the width of an axial groove. On the ring outer surface there is a circumferential groove of depth 0.35 mm with the same depth and axial length as the ½ moon groove (140 ° extent) machined on the bearing casing inner surface.

Figure 17 shows that at 150 ℃ the commercial lubricant (SAE 5W-30) used in the application is shear thinning [33], i.e., its viscosity decreases 10% as the journal speed increases from 30 to 240 krpm. When the journal spins at a high rotational speed, both the operating temperature and the shear thinning effect contribute to decrease the lubricant viscosity.

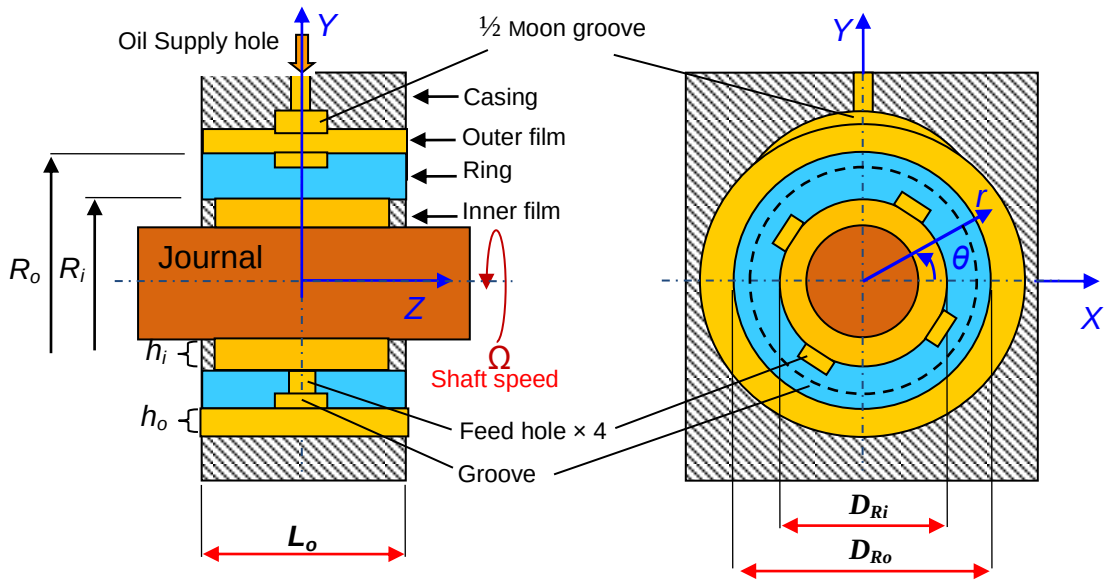


**Figure 16. Schematic view of a semi-floating ring bearing system [1]**

**Table 2. Geometry and operating condition of a (S)FRB for a typical TC application[15]**

| | | | | |
|---|---|---|---|---|
| **RBS geometry** | Diameters | | | |
| | Shaft OD | $D_s$ | 7.90 | mm |
| | Ring ID | $D_{Ri}$ | 7.92 | mm |
| | Ring OD | $D_{Ro}$ | 14.10 | mm |
| | Casing ID | $D_c$ | 14.17 | mm |
| | Ring thickness | $t_R$ | 3.10 | mm |
| | Ring mass | $m_R$ | 98 | g |

[15] The data is the proprietary property to Honeywell Turbo Technologies.

**Table 2** Continued

| | | | | |
|---|---|---|---|---|
| **RBS geometry (continued)** | Inner film | | | |
| | Length | $L_i$ | 4.6 | mm |
| | Outer film | | | |
| | Length | $L_o$ | 6.2 | mm |
| | Clearance (at 20 ℃) | | | |
| | Inner film | $C_{i*}$ | 7.5 | μm |
| | Outer film | $C_{o*}$ | 35.0 | μm |
| | Grooves | | | |
| | Inner groove (axial) | Width | 1 | mm |
| | | Depth | 0.0375 | mm |
| | Outer groove (circumferential) | Axial length | 2 | mm |
| | | Depth | 0.35 | mm |
| | ½ moon groove （140 °extent） | Axial length | 2 | mm |
| | | Depth | 0.35 | mm |

| | | | | |
|---|---|---|---|---|
| **RBS material properties (at 20 ℃)** | | Ring | Casing | Rotor |
| | Material | brass | cast iron | steel |
| | Thermal Exp. [1/ ℃], α | $1.80\times10^{-5}$ | $1.25\times10^{-5}$ | $1.24\times10^{-5}$ |
| | Specific heat [J/kg ℃], $C_p$ | 377 | 550 | 519 |
| | Conductivity [W/m ℃], $\kappa$ | 58.1 | 53.6 | 43.2 |
| | Density [kg/m$^3$], $\rho$ | 8,500 | 7,170 | 7,833 |

| | | | | |
|---|---|---|---|---|
| **Operating conditions** | Oil Supply pressure | Oil supply temp. | Casing Temp. | Shaft temp. |
| | bar | ℃ | ℃ | ℃ |
| | $P_{sup}$ | $T_{sup}$ | $T_c$ | $T_s$ |
| | 4.0[16] | 120 | 120 | 213 |

| | | |
|---|---|---|
| **Lubricant SAE 5W30 Flash point temperature Tflash ≈ 230 ℃** | Density [kg/m$^3$], $\rho$ | 850 |
| | Specific Heat [J/kg], $C_p$ | 1,880 |
| | Conductivity [W/m ℃], $\kappa$ | 0.127 |
| | Viscosity at $T_{sup}$ [c-Poise], $\mu$ | 5.85 |

| | | | |
|---|---|---|---|
| **Static load** | Rotor weight [N] | Compressor bearing load [N] | Turbine bearing load [N] |
| | 1.27 | 0.36 | 0.91 |

[16] The pressure at the upstream of the TC casing is 4 bar. The actual pressure into the film is lower, ~ 3.6 bar. The inlet pressure loss factor is estimated at 90%.

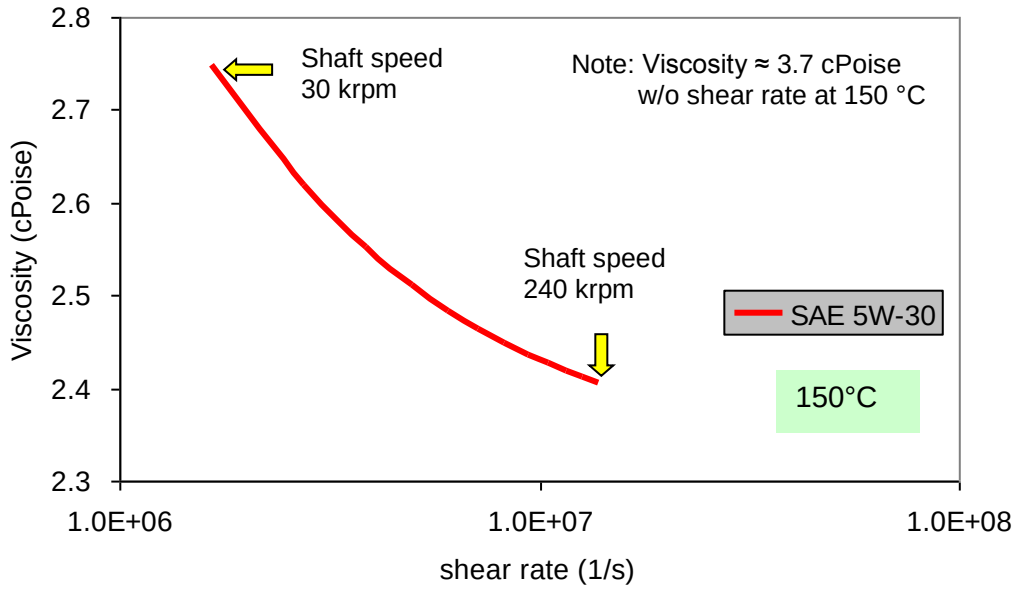


**Figure 17. Variation of viscosity with shear rate for lubricant SAE 5W-30 at 150°C**

Figure 18 depicts the mesh generated for numerical analysis of the inner and outer film flows as well as the semi-floating ring that separates both films. The outer film is modeled as a complicated geometry with $N_{EX}$=45 and $N_{EY}$=12 elements in the circumferential and axial directions, respectively. For the inner film, $N_{EX}$=52 and $N_{EY}$=12, since the axial grooves require of more elements to model. The floating the ring is modeled with $N_{\theta}$=40 and $N_R$=8 elements in the circumferential and radial directions, respectively. An element axial thickness equals the ring axial length[17]. The mesh density

[17] The film axial length of the ring inner diameter is shorter than that of its outer diameter for the bearing geometry shown in Table 2.

for each film and the ring is based on the particular geometry and should be suitable to obtain accurate predictions without an excessive time in computational cost.

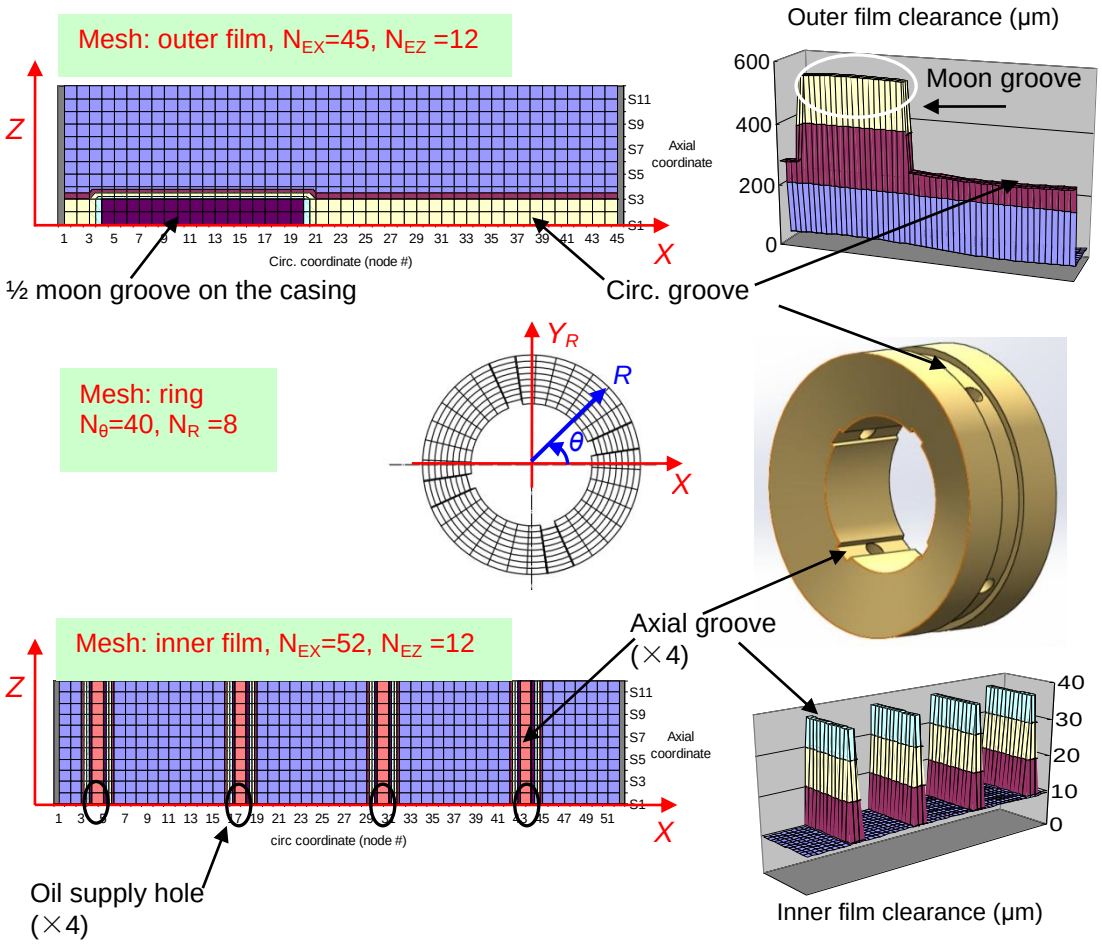


**Figure 18. Computational meshes for analysis of flow in the inner and outer films and in the floating ring**

Figure 19 depicts the predicted pressure and temperature fields on the inner film for operation with shaft speed at 240 krpm. The static load equals 0.9 N along the gravity direction and causes small eccentricities[18] of the journal relative to the ring, $\bar{e}_X$ =0.01 and $\bar{e}_Y$ =0. At the midplane of the inner film ($z$=0), the temperature leaves a supply hole at 120 ℃ to increase downstream because of shear drag due to journal rotation, until the lubricant mixes with the downstream supply oil from the next hole. The maximum temperature of the inner film occurs near the outlet plane ($z=L_i/2$) and just before the next axial groove. More details about the peak temperature are discussed later.

Under the same operating conditions, Figure 20 depicts the pressure and temperature fields for the outer film. The increase of temperature from $T_{SUP}$ to the peak magnitude (~7 ℃ higher) is much lower than the temperature rise in the inner film (~80 ℃). Since the semi-floating ring cannot spin, there is no power dissipation due to shear drag in the outer film. The heat conducted through the ring is the energy source heating the outer film. For the region near the ½ moon groove, the temperature is close to $T_{SUP}$. The peak temperature of the outer film flow occurs at the outlet plane ($z=L_o/2$) and near the region of the minimum outer film thickness.

[18] Presently, the predicted eccentricity is shown in dimensionless form ($\bar{e} = e/c$). The eccentricity of the journal and ring are divided by the nominal radial clearances of the inner and outer films, respectively. The nominal clearances at hot temperatures are based on shaft, ring and casing temperatures.

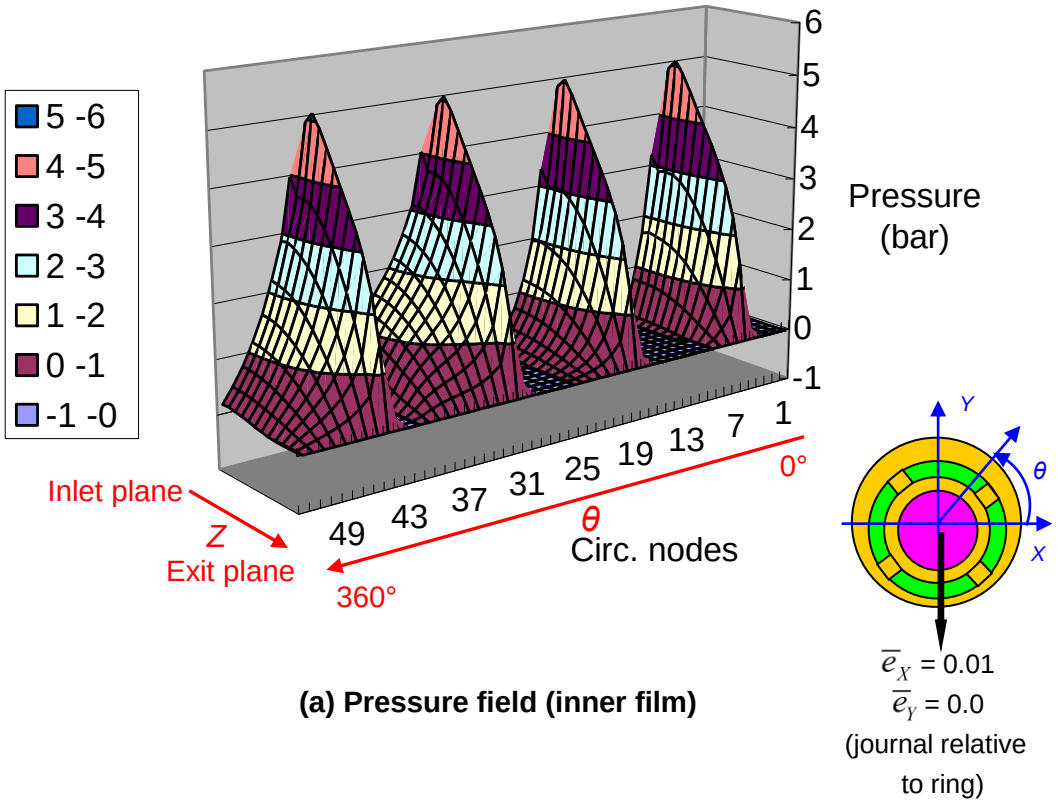


**(a) Pressure field (inner film)**

**Figure 19. Prediction of pressure field (a) and temperature field (b) for the inner film of (S)FRB on the turbine side. Shaft speed = 240 krpm. $P_{SUP}$ = 4 bar, $T_{SUP}$ = 120°C, static load = 0.9 N.**

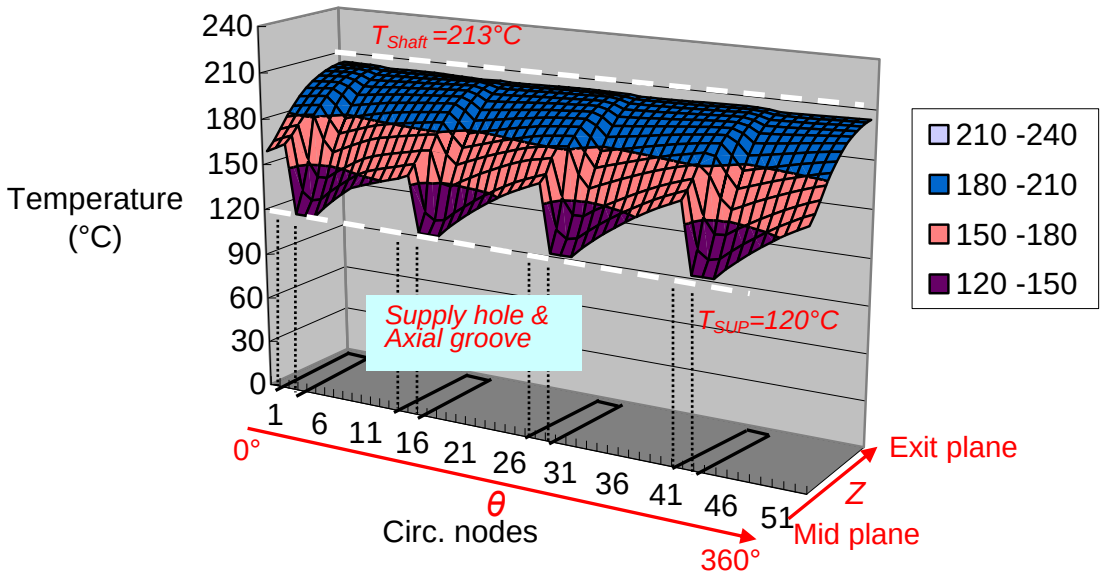


**(b) Temperature field (inner film)**

**Figure 19** Continued.

Figure 21 shows the predicted flow rates for the inner and outer films as the journal speed increases. The flow rates through the outer film are higher than the inner film flow rates because the outer film clearance is larger than that of inner film, i.e. $c_o^*/c_i^*$ =4.7 at 20 ℃. The increase of the inner film flow rate is because the inner film lubricant viscosity becomes smaller as its temperature rises.

Figure 22 shows the operating eccentricities of the journal ($e_J/c_i$) and ring ($e_R/c_o$) over the entire journal speed range (30~240 kprm) and for a static load equal to 0.9 N. The eccentricity of the ring, decreasing with shaft speed, leads to a smaller outer film thickness; and thus to the drop of the flow rate through the outer film, as shown in

Figure 21. Note that the eccentricity of the ring is determined by the stiffness of the anti-rotation button or pin. The minimum outer film thickness (~ 0.07 $c_o$) occurs at the lowest journal speed.

Due to the light static load on the bearing, as the journal speed grows the variation of journal eccentricity relative to the ring is very small relative to the hot inner film clearance ($e_J < 0.05\ c_i$).

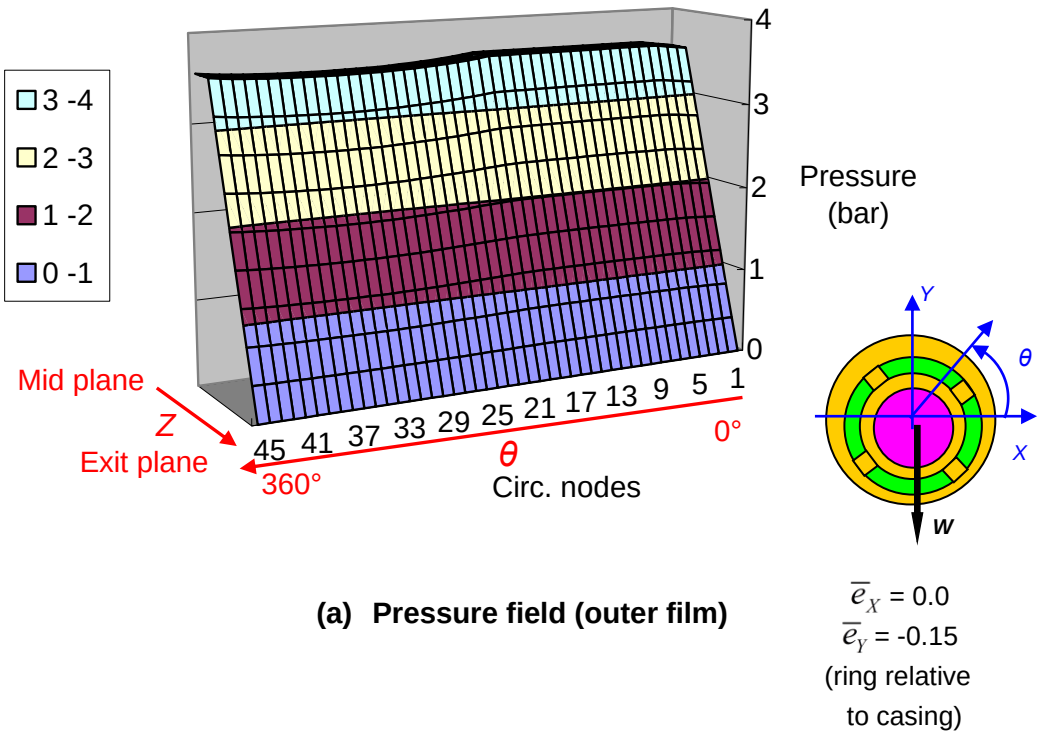


**(a) Pressure field (outer film)**

**Figure 20. Prediction of pressure field (a) and temperature field (b) for the outer film of a (S)FRB on turbine side. Shaft speed = 240 krpm. $P_{SUP}$ = 4 bar, $T_{SUP}$ = 120°C, static load = 0.9 N.**

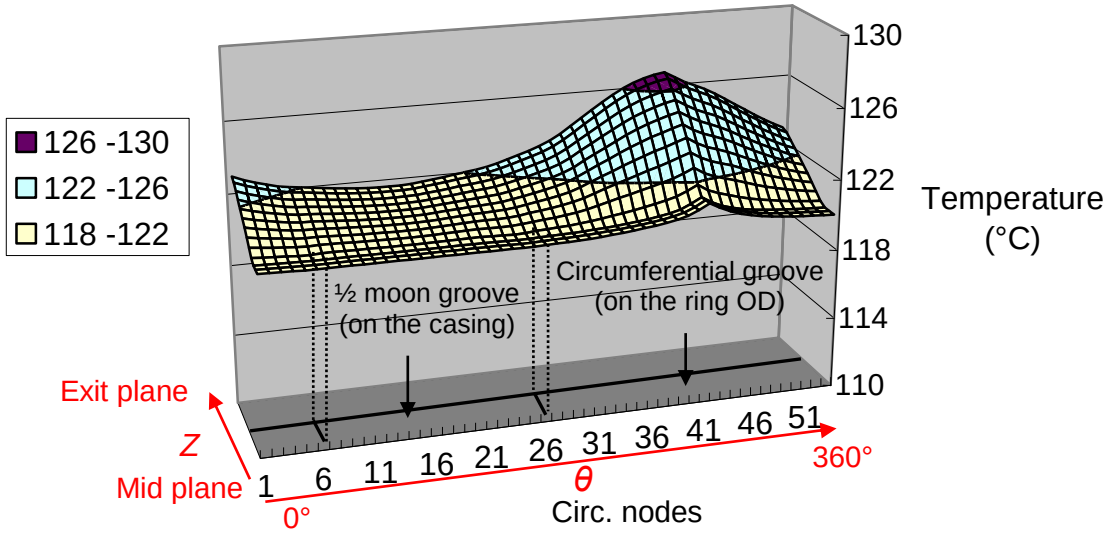


**(b) Temperature field (outer film)**

**Figure 20** Continued.

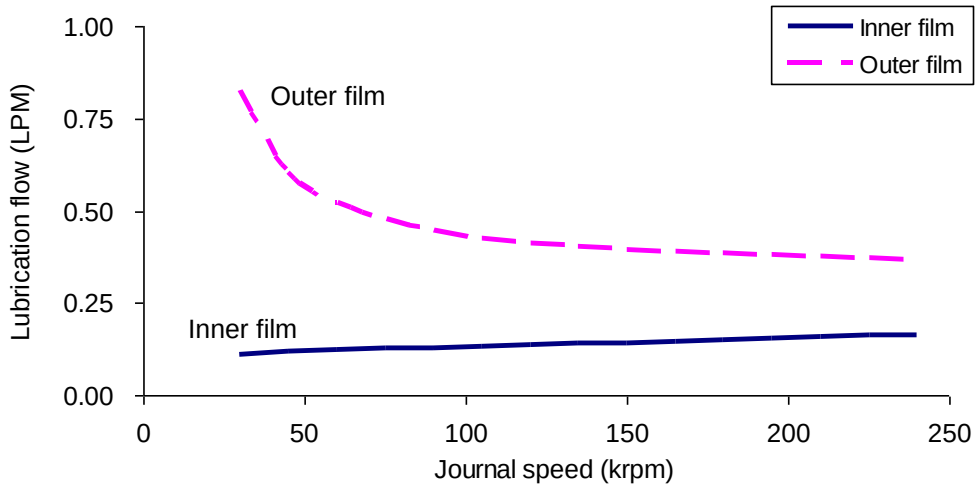


**Figure 21. Flow rates through the inner and outer films vs. shaft speed. $P_{SUP}$ = 4 bar, $T_{SUP}$ = 120°C, static load = 0.9 N.**

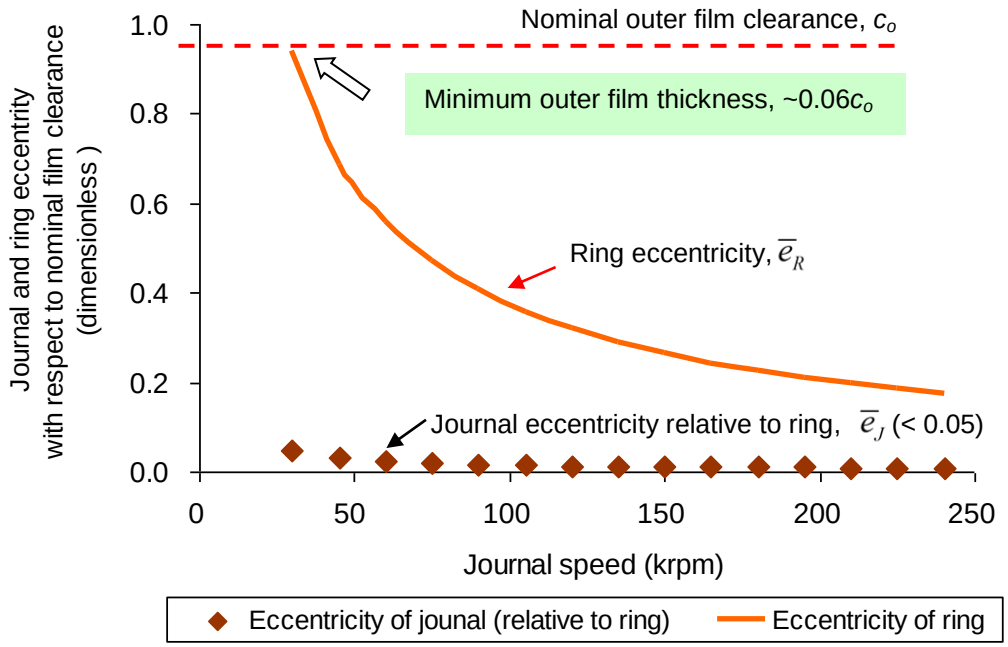


**Figure 22. Dimensionless eccentricities of ring and journal vs. shaft speed. $P_{SUP}$ = 4 bar, $T_{SUP}$ = 120°C, static load = 0.9 N.**

Figure 23 shows the viscosity fields for the inner and outer films for operation with $T_{SUP}$ = 120 ℃ and $P_{SUP}$ = 4.0 bar, as the journal spins at 240 krpm. Note that the lubricant viscosity has a sharp decline along the axial direction of the bearing since the film temperature increases sharply along this direction.

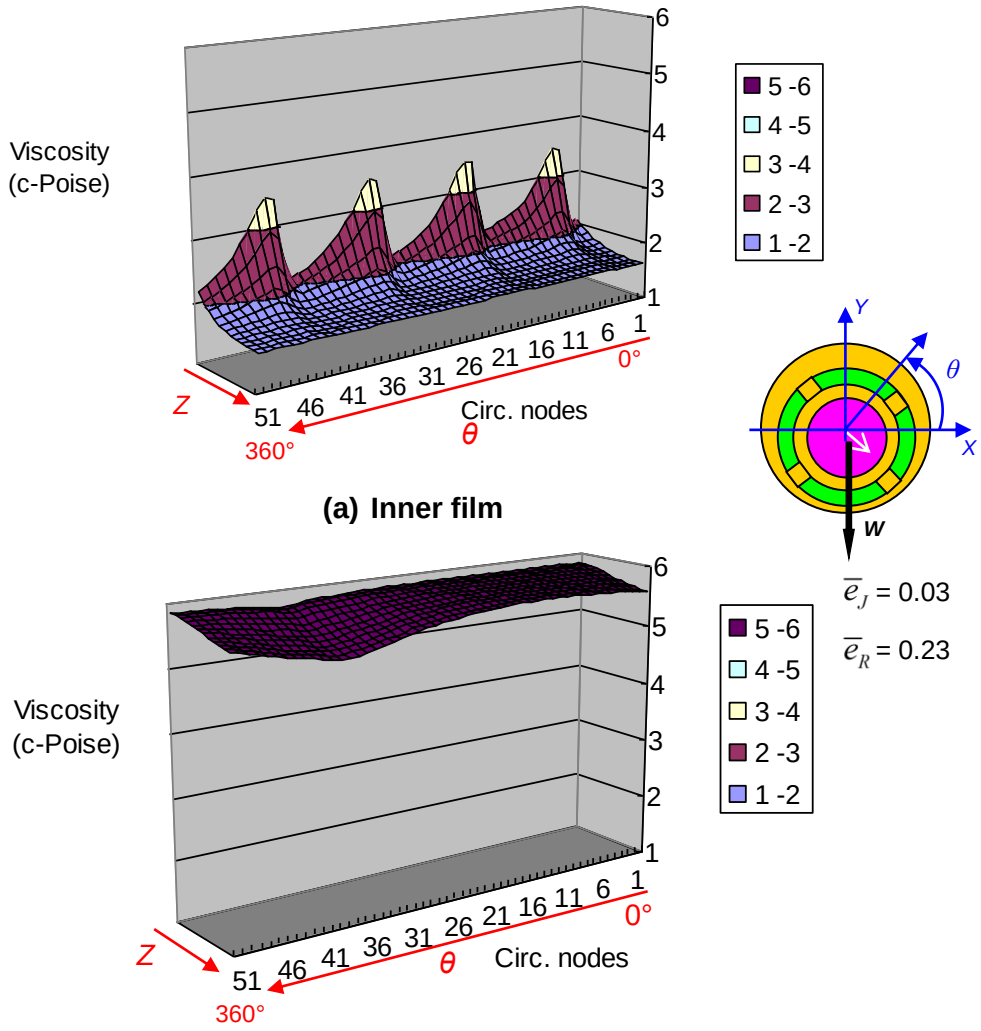


**Figure 23. Viscosity fields for the inner and outer films of a (S)FRB. Shaft speed = 240 krpm. $T_{SUP}$ = 120°C, $P_{SUP}$ = 4 bar, static load = 0.9 N, $\mu_{supply}$ = 5.85 cPoise.**

Figure 24 shows the exit temperatures for the inner and outer films and the outlet temperature of the oil mixed streams versus journal speed. The film exit temperature is

the average temperature around the bearing circular perimeter at the exit plane ($z=L/2$). The exit temperature of the inner film grows steadily with shaft speed, reaching a temperature as high as 203 ℃. It is not only lower than the temperature of the hot journal surface (~213 ℃), but also well below the oil flash temperature (~230 ℃). This means that over the whole inner film flow region there is always heat flow from the journal towards the film. On the other hand, the exit temperature of the outer film is almost invariant and remains cold, near $T_{SUP}$, over the entire journal speed range. This occurs because the flow rate through the outer film is large enough to carry away the small amount of heat conducted through the ring and convected into the outer film. In addition, the outlet mixing temperature, which results from the mixing of the inner and outer flow streams leaving the bearing, has a moderate growth with an increase in journal speed. Note that the flow rate through the outer film is much larger than that through the inner film, hence the outer film flow influences most the outlet mixing temperature[19].

[19] This result shows that recording the temperature of the outlet lubricant is not representative of the temperature in the inner film.

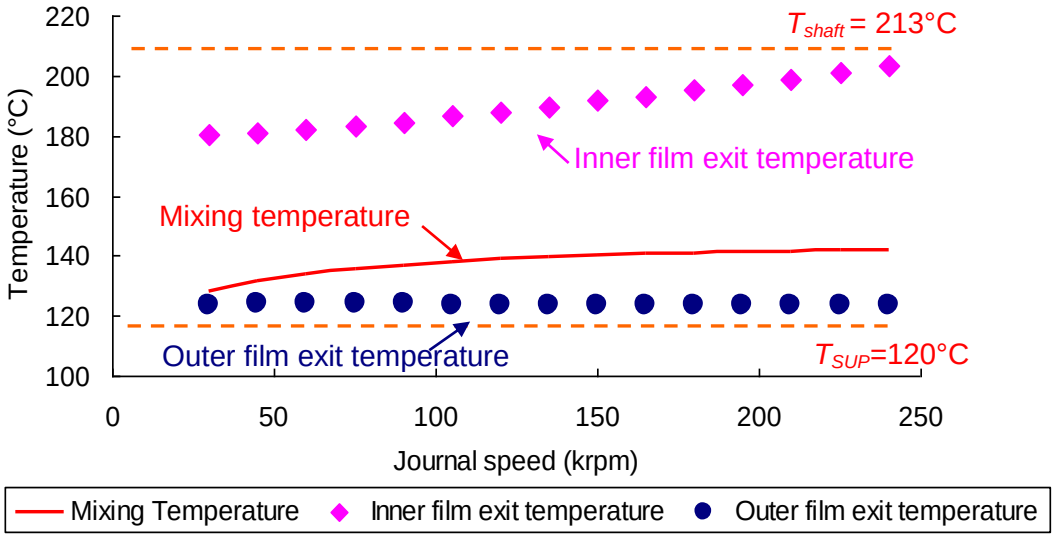


**Figure 24. Film exit temperatures of the inner and outer films and lubricant films mixing exit temperature vs. journal speed. $P_{SUP}$ = 4 bar, $T_{SUP}$ = 120°C, static load = 0.9 N.**

Figure 25 shows the thermal energy flows and the drag power loss in the inner film versus shaft speed. The change of heat flow from the shaft indicates that the cooling effect of the inner film on the journal becomes stronger as the journal speed increases towards 90 krpm, and then decreases since the inner film temperature grows steadily for the journal speeds exceeding 90 krpm. Due to the increase of the drag power loss, which is proportional to the journal speed (squared), the total energy (drag power loss plus heat flow) advected by the inner film eventually levels off after a steady increase at low speeds. The majority of the total energy is carried away by the inner film, while the

remaining energy is conducted as heat flow into the ring. Note that the heat flow conducted into the ring is nearly invariant over the entire speed range (30~240 krpm).

In contrast, in the outer film the only source of heating is the heat transfer conducted from the ring, since the shear drag power loss is negligible. The nearly invariant thermal energy conducted through the ring and into the casing indicates that the heat carried by the outer film is also constant and hence its temperature does not vary significantly as the shaft speed increases to 240 krpm. Note that the heat conduced into the casing is much lower than the heat flow carried by the inner film.

Figure 26 presents that the portion of the total energy carried away by the inner film starts at 65% and then approaches around 80% with an increase in journal speed. It indicates that the inner film flow is more effective in removing the heat entering into the inner film than the heat conducted into the ring, in particular at high speeds.

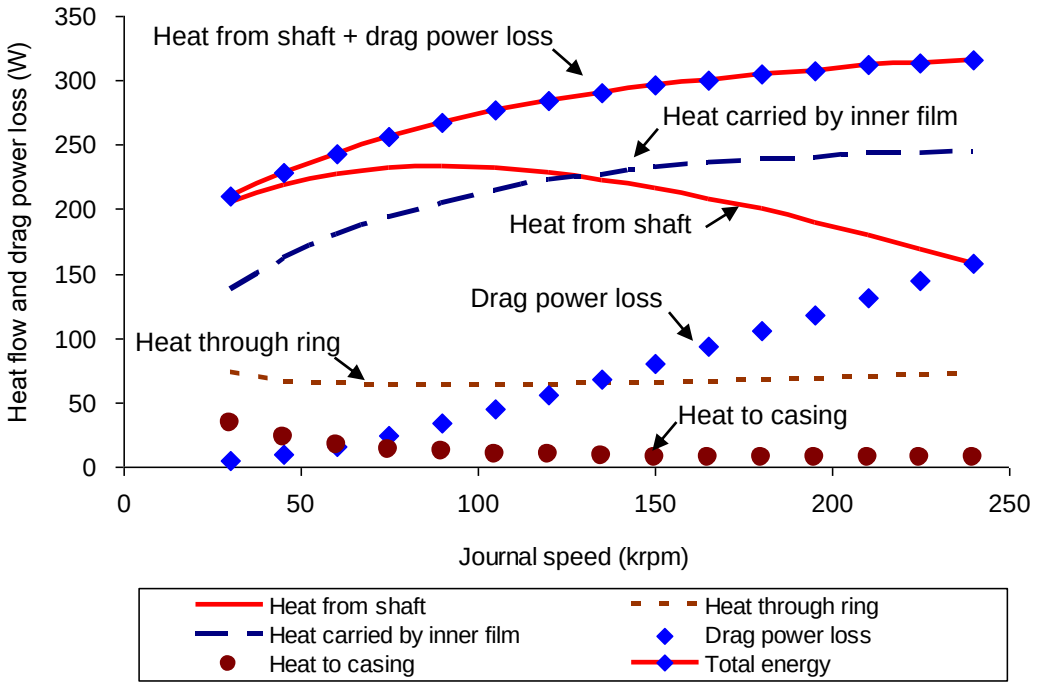


**Figure 25. Heat flows and drag power loss in a (S)FRB bearing vs. journal speed. $P_{SUP}$ = 4 bar, $T_{SUP}$ = 120°C, static load = 0.9 N.**

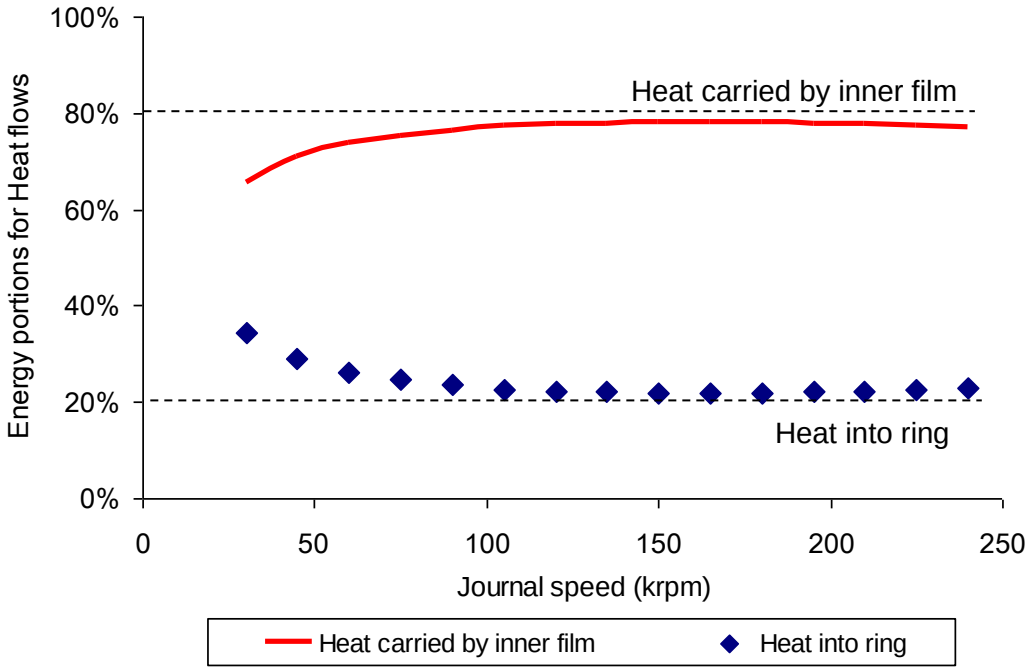


**Figure 26. Portion of energy carried away by the inner film and conducted into the ring in a (S)FRB vs. journal speed. $P_{SUP}$ = 4 bar, $T_{SUP}$ = 120°C, static load = 0.9 N.**

Figure 27 depicts the pressure contours in the inner film for operation at three journal speeds with a static load equal to 0.9 N. The darkest colored areas (highlighted by the dashed ellipses) denote oil cavitation zones where the film pressure is below ambient. The oil cavitation zone grows with an increase in journal speed. The extent of the cavitation area will directly influence the magnitude of heat conducted into the floating ring and its temperature; and hence, affect the temperature distribution in the film flow region.

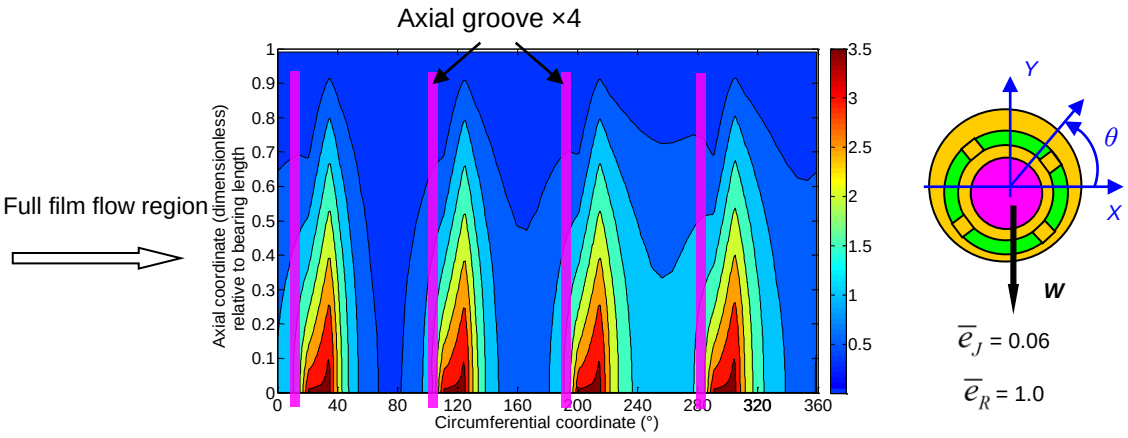


(a) Journal speed = 30 krpm, static load = 0.9 N

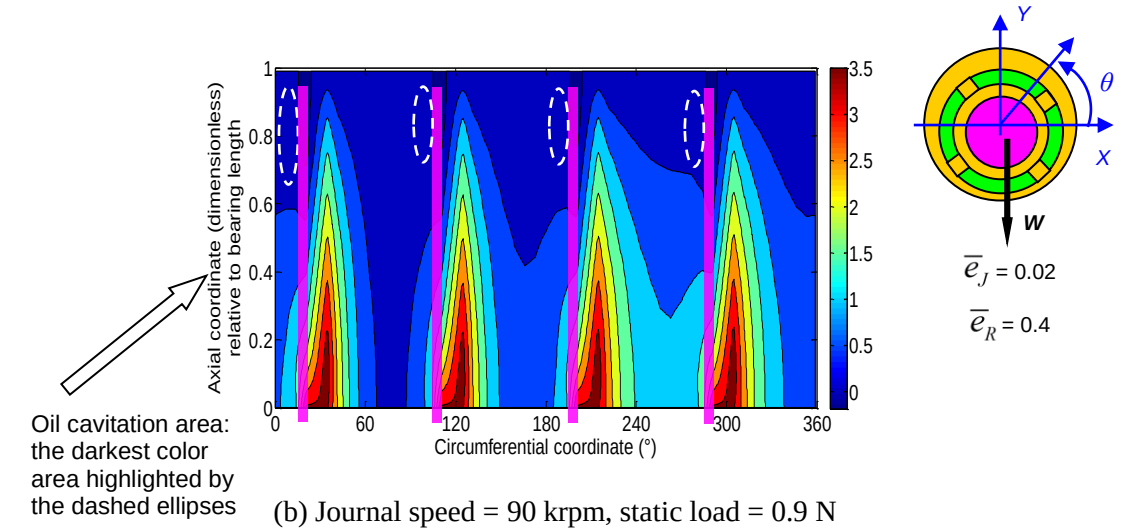


(b) Journal speed = 90 krpm, static load = 0.9 N

**Figure 27. Pressure contours in the inner film flow region. Shaft speed = 30, 90 and 240 krpm. $P_{SUP}$ = 4 bar, $T_{SUP}$ = 120°C, static load = 0.9 N.**

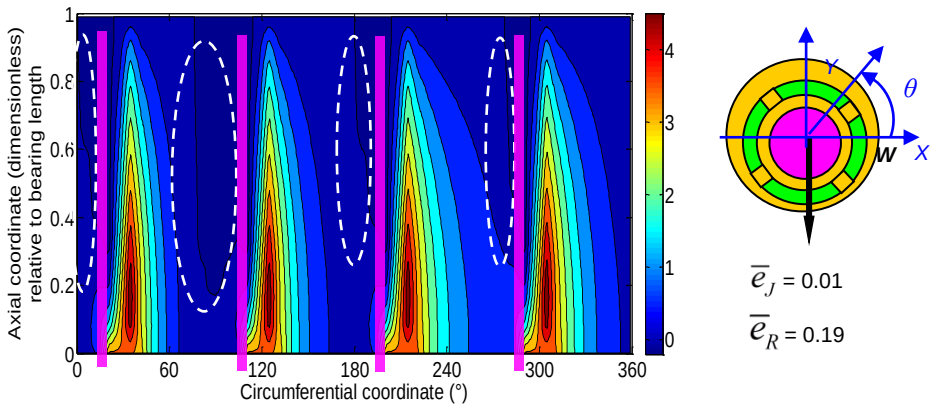


(c) Journal speed = 240 krpm, static load = 0.9 N

**Figure 27** Continued.

For operation at a mid-range journal speed (105 krpm), Figure 28 shows that the peak film temperature occurs immediately after the oil cavitation region ends. The inner film temperature evolves from a low temperature (= $T_{SUP}$) downstream from the supply holes, and increases along the journal rotational direction until mixing with the cool fluid emerging from the next axial groove. Some hot lubricant leaves the bearing through the outlet, and it gets hotter as it flows along the shaft.

Under the same operating conditions, Figure 29 depicts the variation of the inner film temperature in the circumferential direction at the axial location where the peak film temperature occurs. Between two axial grooves, the increase of the inner film temperature, from one valley to the next crest, can be as high as 15 ℃.

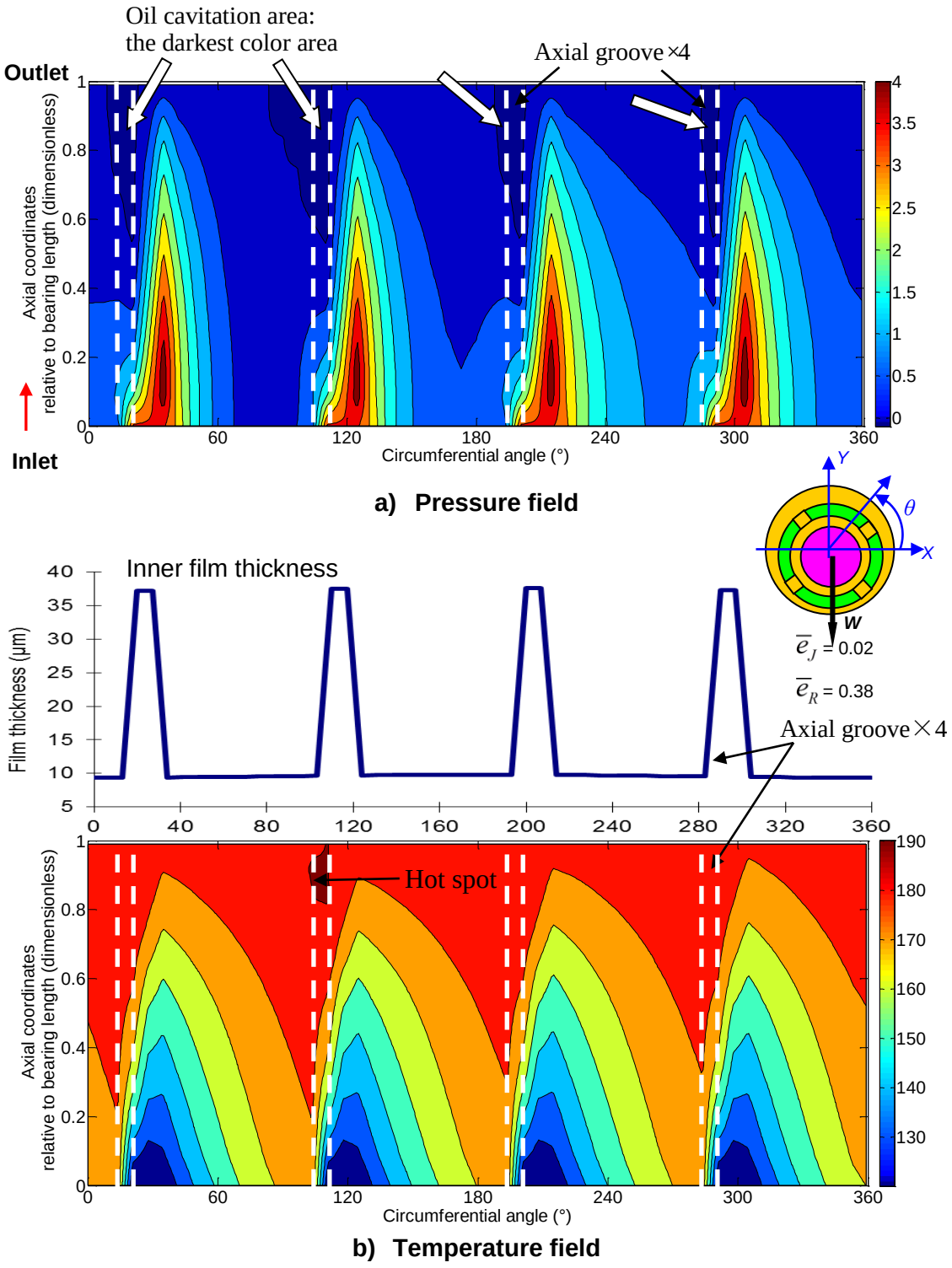


**Figure 28. Pressure and temperature fields in the inner film. Journal speed = 105 krpm. $P_{SUP}$ = 4 bar, $T_{SUP}$ = 120°C, static load = 0.9 N.**

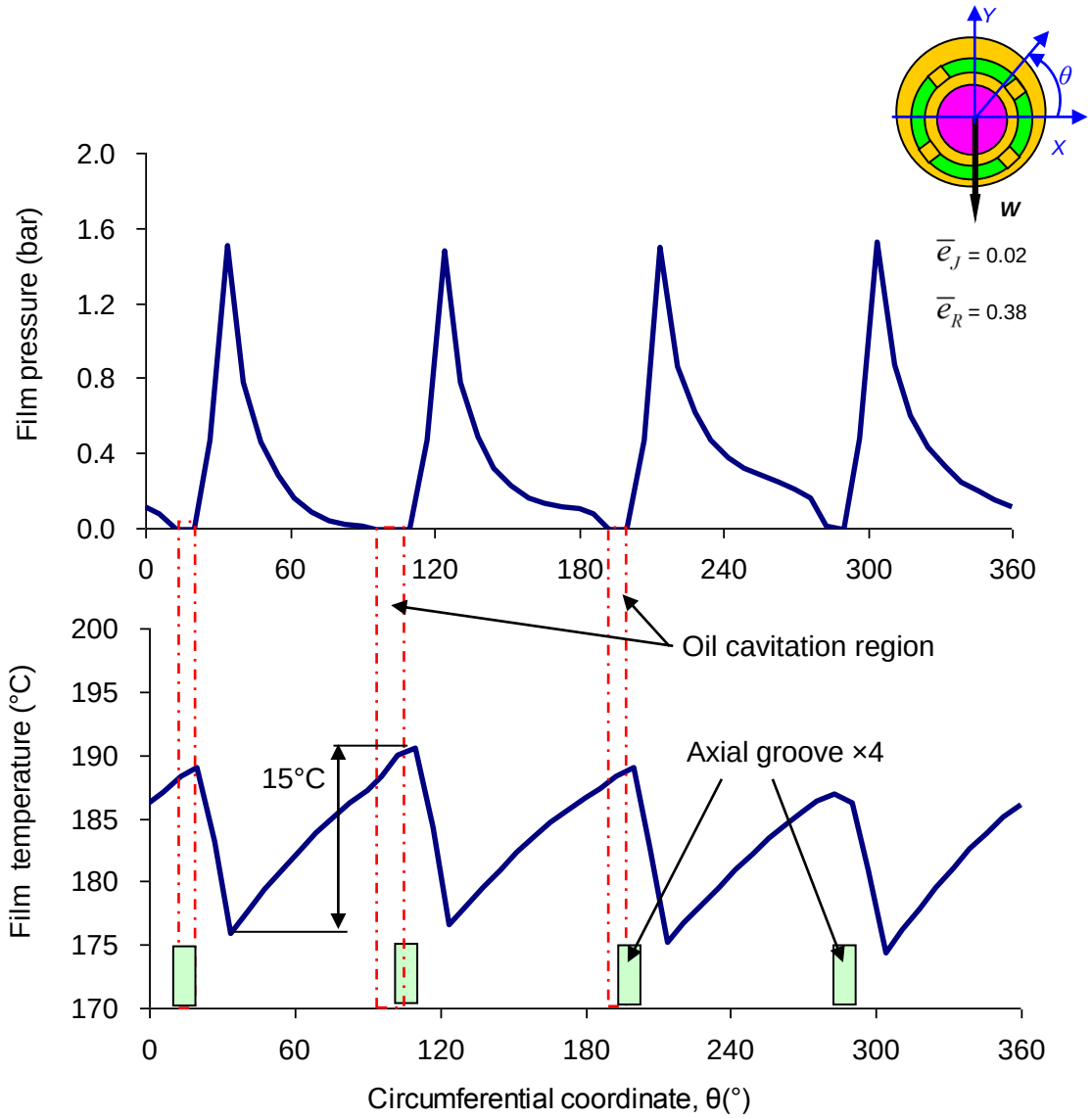


**Figure 29. Circumferential variation of the inner film temperature at the axial location where the peak film temperature occurs. Shaft speed = 105 krpm, $P_{SUP}$ = 4 bar, $T_{SUP}$ = 120°C, static load = 0.9 N.**

Figure 30 shows the peak (maximum) lubricant temperature in the inner film versus increasing journal speeds. As the journal speed goes up from 30 krpm to 240 krpm, the peak film temperature begins with a slight decrease and then quickly grows. It eventually reaches up to as high as 204 ℃, which is 15 ℃ higher than the peak film temperature at low speeds (<100 krpm). The increase in the peak film temperature is because the drag power loss intensifies with faster journal rotation, which makes the (hot) fluid from the full film lubricant zone advects more energy. The hotter fluid, which is attached to the rotating shaft, enters into the oil cavitation zone where the peak film temperature usually occurs. This fluid continues receiving heat from the hot shaft, but cannot drop heat into the ring.

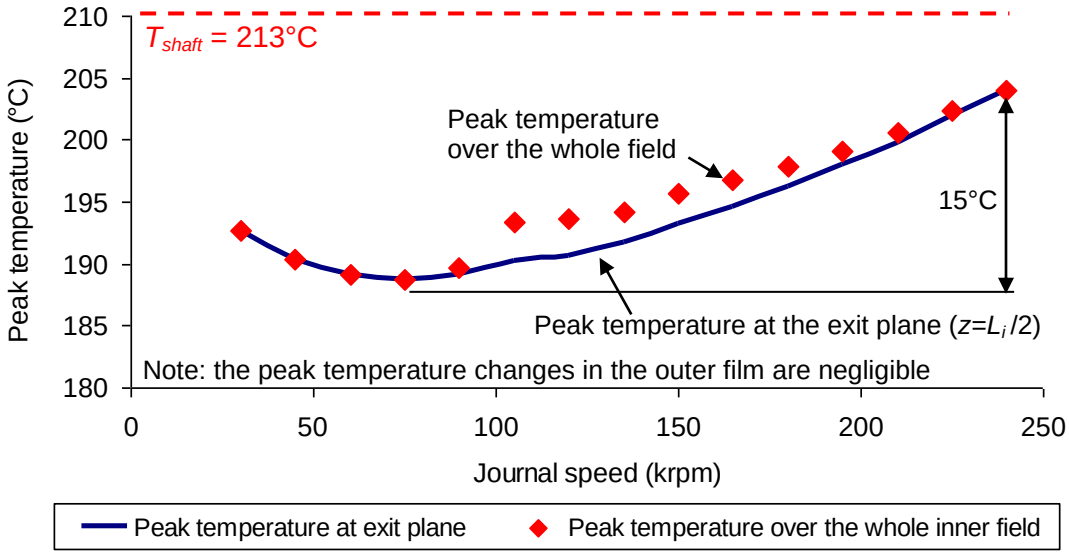


**Figure 30. Inner film peak temperature at the exit plane and over the whole flow field vs. journal speed. $P_{SUP}$ = 4 bar, $T_{SUP}$ = 120°C, load = 0.9 N.**

For operation at 240 krpm, Figure 31 depicts the temperature distribution in the ring, showing considerable variations in the circumferential and radial directions. The lowest temperature on the inner surface of the ring does not coincide with the location on an axial groove, where the cool lubricant is supplied, but it is instead located at the corresponding oil cavitation area.

In the (S)FRB, the shaft, the ring and the casing are made of different materials, and thus have dissimilar thermal expansion coefficients, as shown in Table 2. As these components experience thermal growth, the relative expansion of the surfaces bounding the clearance space may lead to bearing seizure [34]. Recall the eccentricities of the journal and ring shown in Figure 22, the predictions indicate the bearing can operate safely over the entire journal speed range (30~240 krpm). Note that since the ring has the largest thermal expansion coefficient among the three components, the actual operating clearance of the inner film is larger than its nominal value ($c_i/c_i^* \approx 1.3$), but the operating clearance of the outer film is smaller than its nominal value ($c_o/c_o^* \approx 0.85$).

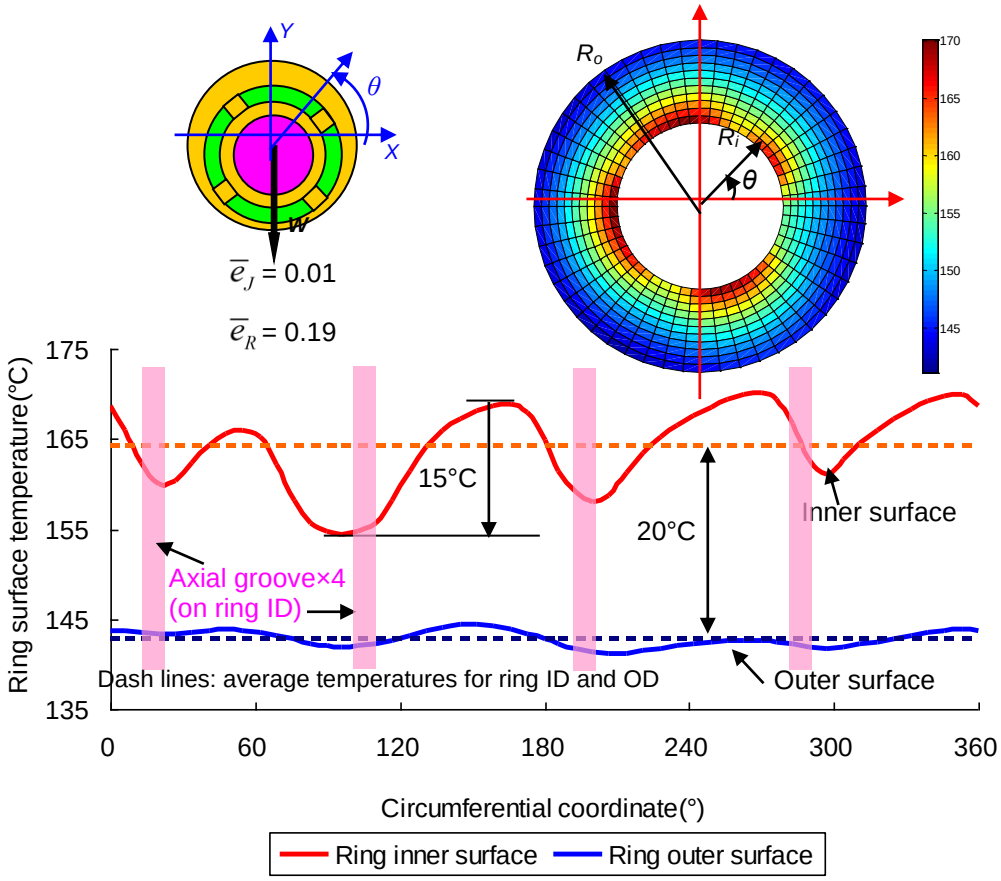


**Figure 31. Ring temperature distribution in the circumferential and radial directions. Journal speed = 240 krpm, $P_{SUP}$ = 4 bar, $T_{SUP}$ = 120°C, static load = 0.9 N.**

Figure 32 shows a schematic representation of the drag power and thermal energy flows in the bearing system for operation at two journal speeds, 45 krpm and 240 krpm. At the low journal speed, the heat from the shaft overwhelms the drag power loss, but as the journal speed increases, the contribution from the drag power loss to the total

energy flow increases significantly from 6% to 50%. The lubricant carries away the vast majority of the heat flow and drag power over the entire journal speed range, from 90% up to 98% at the highest journal speed. This indicates the importance of designing a bearing configuration that promotes the flow rates to remove effectively the thermal energy. Note that the ring conducts a considerable portion of energy from the inner film into the outer film, 23-29% of the total energy (heat from shaft plus drag power loss). The energy conducted through the ring remains nearly invariant with journal speed, and so does the small amount of heat conducted into the casing. The heat portion of the total energy flowing into the casing decreases from about 15% at the lowest shaft speed (~ 30 krpm), then approaches less than 5% quickly as the journal speed increases towards 90 krpm, and eventually remains nearly constant, around 3%.

For comparison, Ref. [1] also shows the energy flow patterns for a similar (S)FRB and displays similar traits as in the current model, i.e., the inner film takes away the majority of the shaft heat and drag power, and the contribution by the drag power loss to the total energy flow increases considerably as the journal speed increases, etc. However, Ref. [1] presents a larger portion of energy conducted into the casing than the one from the current model for operation over the entire journal speed range. For example, the portion of energy conducted into the casing levels off at about 19% for high rotor speeds (>150 krpm), but this portion from the current model for the same speeds remains at around 3%.

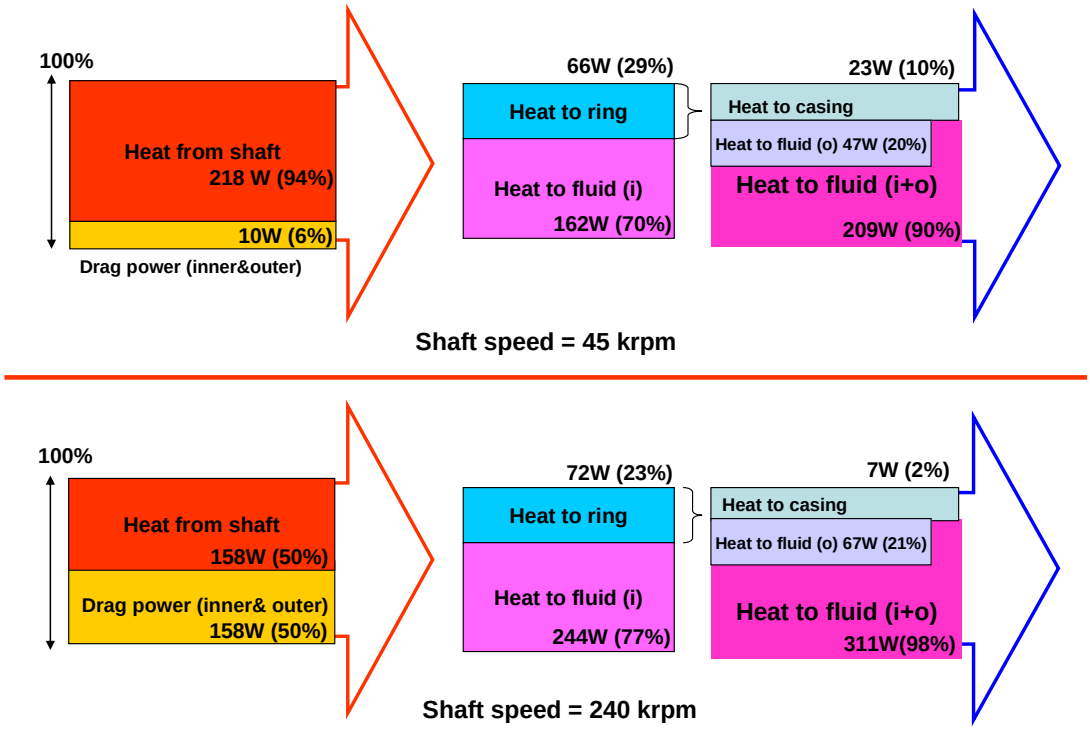


**Figure 32. Schematic representation of energy flows in (S)FRB at a low speed (45 krpm) and a high speed (240 krpm). $P_{SUP}$ = 4 bar, $T_{SUP}$ = 120°C.**

The major reason for this difference is that the authors in Ref.[1] selected the Reynolds/Colburn analogy[20] to estimate the heat convection coefficients between the fluid and its bounding solid surface. The current model, however, adopts an empirical heat convection coefficient[21] that assumes a condition of constant heat flux through the wall, i.e., the heat flow into the ring is uniform. The model in Ref. [1] predicts a larger

[20] The Reynolds/Colburn analogy estimates the Nusselt number according to the fluid property, $Nu=3\,Pr^{0.33}$, here $Pr=C_P\mu/\kappa$. This model is strictly applicable to laminar flow.
[21] This is the Kays and Crawford model [21], that assumes a constant Nusselt number, $Nu=8.22$.

heat flow through the ring than the current one, and hence the heat conducted into the casing grows correspondingly. On the other hand, Ref. [1] assumes that the ring is at a uniform temperature in the circumferential direction. The simplified heat flow model through the ring in Ref. [1] also has an effect on the energy flows in the (S)FRB.

Figure 33 shows the comparison of predicted energy flows for the current model and the simplified model versus journal speed and with both using with the same heat convection coefficient ($Nu$=8.22), i.e., the one for constant heat flow. The current model, taking into account that the ring temperature varies along both the radial and circumferential directions, generates similar predictions as the simplified model in the heat flows related to the inner film, such as the heat from the shaft, the heat through the ring and the heat carried by the inner film, as well as the drag power loss. However, the current model predicts that the outer film carries more energy than that from the simplified model by about 10% of the total thermal energy, and shows less heat flow conducted into the casing. This occurs because the current model predicts a larger outer film clearance that causes a slightly greater flow rate and thus carries away more energy.

The earlier model [1] that considers a radial temperature variation infers using a very large thermal conduction coefficient in the circumferential direction. As the predicted heat flow through the ring is similar for both models, as shown in Figure 33 (a), the simplified model predicts a larger ring outer surface temperature, so that the ring outer surface experience more thermal growth, which makes the outer film clearance shrink to a smaller magnitude than the current model.

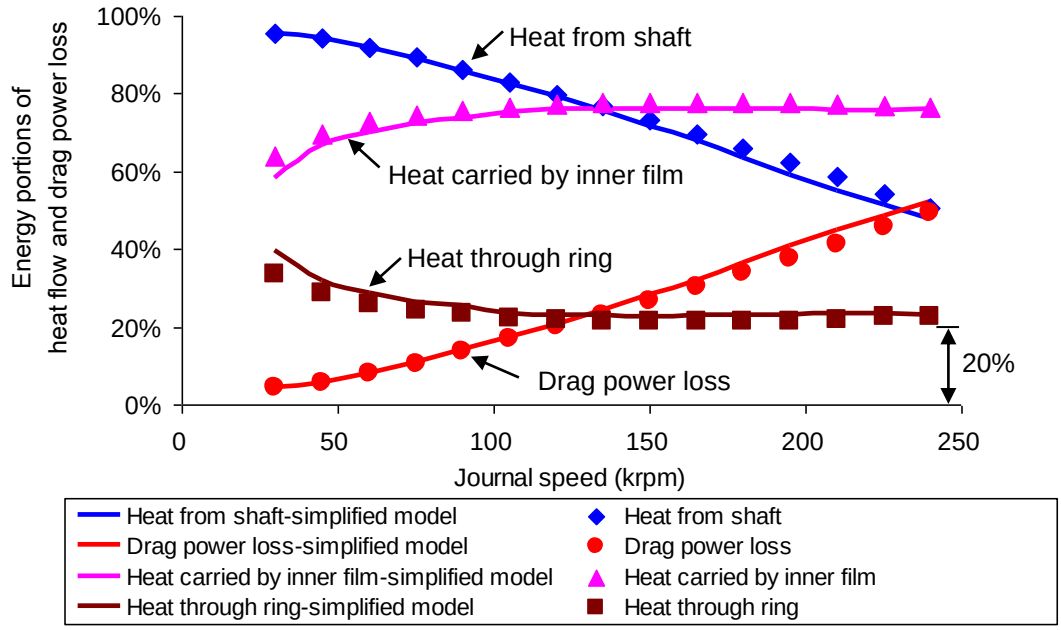


(a) Heat flows from the shaft, heat carried by the inner film, heat flow through the ring and drag power loss.

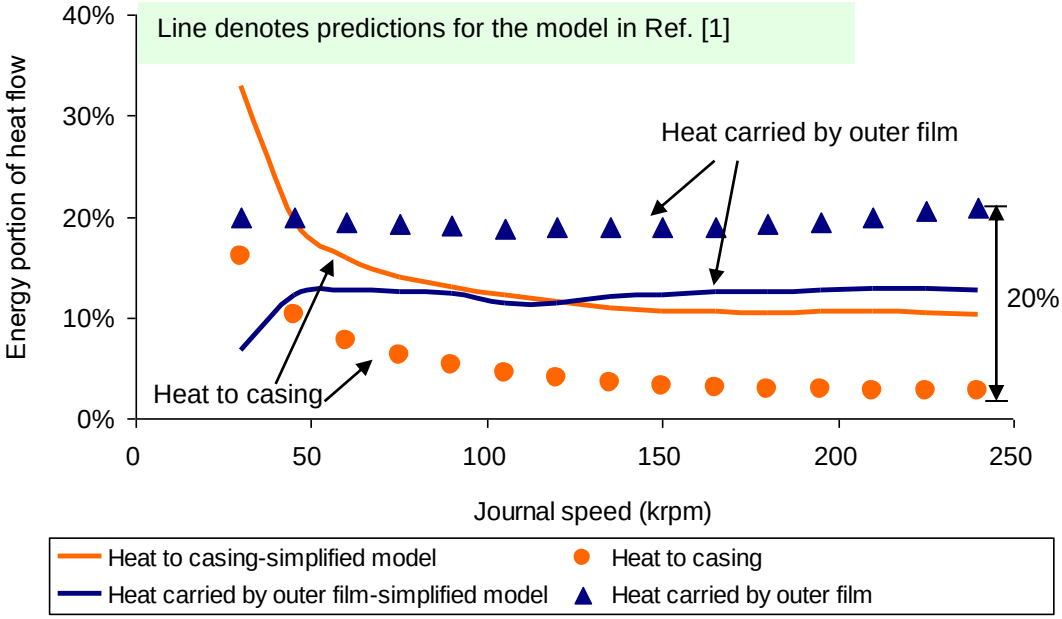


(b) Heat flows to the casing and heat carried by the outer film

**Figure 33. Comparison of energy portions of heat flows and drag power loss in (S)FRB for the current model and the simplified model in Ref. [1] vs. journal speed. $N_u$ = 8.22. $P_{SUP}$ = 4 bar, $T_{SUP}$ = 120°C.**

In summary, the current predictive tool calculates the pressure and temperature fields for the inner and outer films. It also predicts the ring temperature field, radial and circumferential, in a typical (S)FRB used in TCs for passenger vehicles. The bearing performance parameters and energy flow patterns are derived from the pressure and temperature fields. The predictions of bearing performance with typical TC operating conditions reveal distinct knowledge summarized as:

a) The inner film temperature increases dramatically along the axial direction, since the axial flow rate is not large enough to remove the local power dissipation due to the shear drag and the heat flow from the hot shaft. The sharp temperature increase also causes a rapid decrease of the oil viscosity along the axial direction[22].

b) Heat flow from the hot journal into the inner film is overwhelming at low shaft speeds. With an increase in the shaft speed, the heat flow from the hot journal decreases since the average temperature of the inner film approaches the shaft temperature. However, the drag power loss in the inner film grows considerably. As a result, the total energy entering into the film levels off at high journal speeds.

c) The flow rate through the outer film is higher than the inner film flow rate. The inner film flow, however, carries away the majority of the total energy available (heat from the hot shaft plus drag power converted into heat). The heat conducted into the casing is small, which steadily decreases and

[22] Ref.[1] reveals the same conclusion.

approaches less than 5% of the total energy as the journal speed exceeds 100 krpm. Nevertheless, the heat conducted through the ring remains almost invariant over the entire journal speed (30 krpm ~ 240 krpm).

d) The peak temperature in the inner film flow increases with shaft speed, and its location is immediately after the oil cavitation region ends. The outer film flow carries a small amount of thermal energy, so the outer film temperature remains a little higher than the lubricant supply temperature, regardless of the shaft speed.

e) The floating ring shows a temperature field varying along the radial and circumferential directions. For operation at the highest journal speed (240 krpm), the temperature difference between the ring inner and outer surfaces can be as high as 25 ℃. On the ring inner surface, the temperature difference along the circumferential direction from peak to peak can reach 15 ℃. This difference is much larger than the temperature variation on the ring outer surface. Note that the temperature field in the ring depends on the ring material conductivity and the (S)FRB operating conditions.

# 7. ON THE INFLUENCE OF VARIOUS LUBRICANT SUPPLY CONDITIONS, FILMS CLEARANCES AND FEED HOLES SIZES ON (S)FRB PERFORMANCE

The prior chapter discussed the performance of a (S)FRB operating under typical conditions in a passenger vehicle turbocharger (TC). The bearing performance depends on various parameters, not only the lubricant viscosity and its supply conditions, but also on the bearing geometrical configuration for oil supply and its distribution. Occasionally, the selection of one particular parameter to improve a certain performance characteristic could be detrimental to other characteristics. To trade off between the various performance characteristics of a (S)FRB, it is necessary to assess the possible impact of some physical and operating parameters on bearing performance.

As the hot exhaust gas (> 500~600 ℃) from the engine flows through the turbine impeller, the shaft in a TC withstands a severe axial temperature gradient. Thus, the performance parameters related to heat flow become significantly important. For instance, if heat cannot be effectively removed from the bearing system, the bearing components could experience large thermal growths that may result in localized surfaces contacting one another [34]. Additionally, excessive film peak temperatures drop dramatically the lubricant viscosity, which negatively affects the bearing load-carrying capacity and could also be responsible for lubricant degradation.

Figure 34 shows a schematic view of a (S)FRB and notes the geometrical parameters related to the supply of lubricant into the inner film. These parameters include the magnitudes of the inner and outer film clearances, the depth and width of the

axial grooves in the ring inner surface, the number of axial grooves[23], and the depth and axial length of the entire circumferential groove in the ring outer surface.

The present study also discusses the influence of lubricant supply pressure and temperature ($P_{SUP}$, $T_{SUP}$) on the (S)FRB performance with a particular type of lubricant and operating conditions (shaft speed and load). The lubricant type and operating conditions are determined by engine operational requirements and its running conditions, so they cannot be studied independently. Note that presently, when considering one specific parameter, other parameters remain unchanged.

**Influence of Lubricant Temperature**

The lubricant operating temperature has a strong effect on its material viscosity. The oil viscosity is the physical parameter affecting most the hydrodynamic pressure generation within the fluid film and determines the magnitude of the lubricant shear drag torque. Since the lubricant supply temperature ($T_{SUP}$) could affect the entire film temperature field, it is likely that a variation in $T_{SUP}$ will influence the flow pattern and drag power loss in the films, and thus also affect the heat flows and the peak film temperature, for example.

[23] Each axial groove has one supply hole in the middle of the ring. The diameter of the hole is equal to the width of an axial groove.

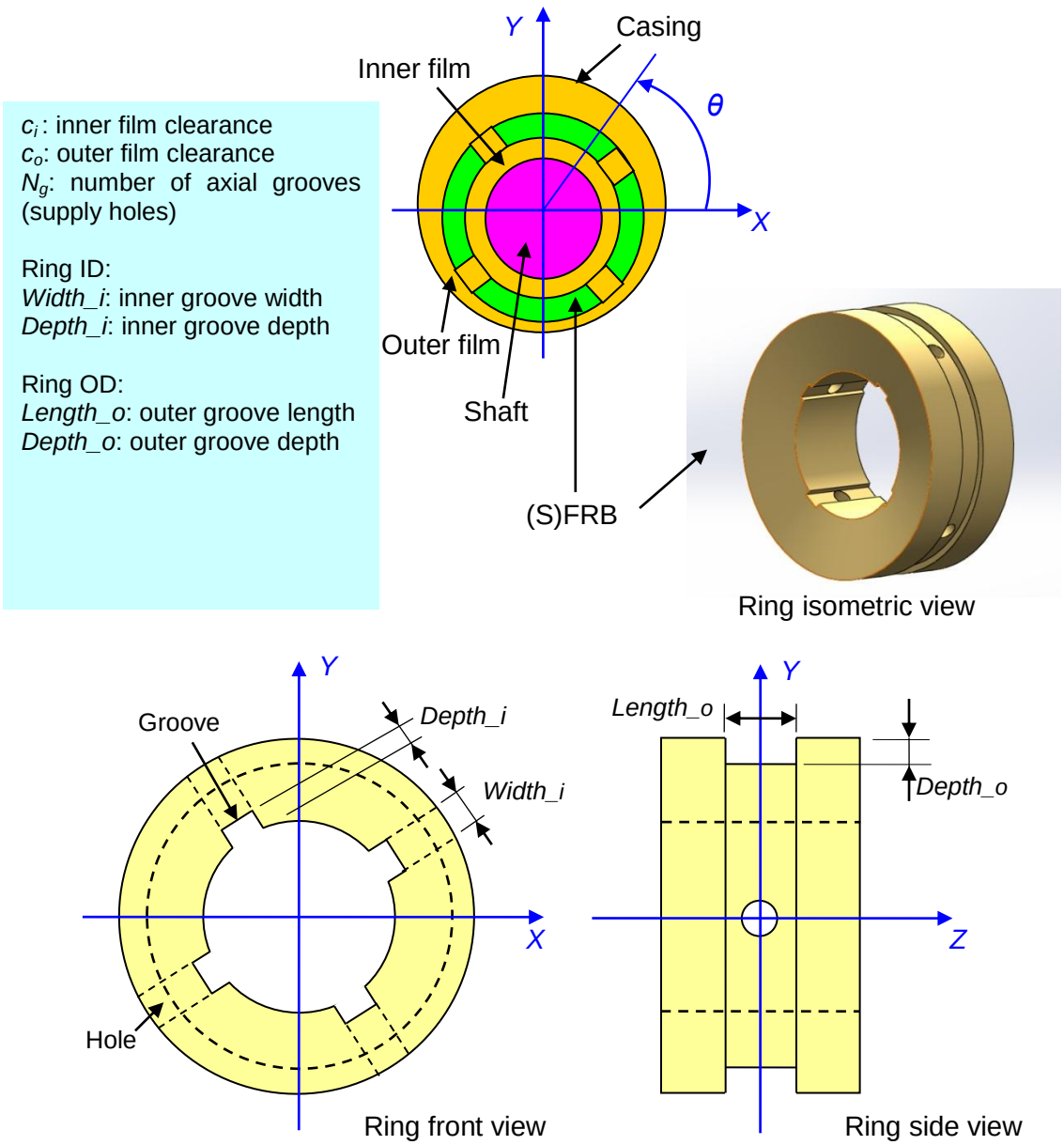


**Figure 34. Schematic views of a semi-floating ring bearing and notation for geometry of oil supply arrangement.**

Three $T_{SUP}$[24] values (100 ℃, 120 ℃, 140 ℃)[25] are considered with a constant $P_{SUP}$ (4 bar) over a typical speed range (30~240 krpm). The bearing casing temperature is taken to equal $T_{SUP}$[26] since the passage channels for feeding lubricant into the bearing are casted in the bearing casing. Hence, the variation of $T_{SUP}$ will directly and strongly influence the bearing casing temperature. Note that the shaft temperature ($T_{shaft}$) is 213 ℃, a constant, in all cases.

Figure 35 displays the temperature profiles in the inner film for operation at three lubricant supply temperatures (100 ℃, 120 ℃, and 140 ℃) and at two axial locations ($z$ = 0 and $z = \frac{1}{4} L$) as the journal spins at 240 krpm. The graph shows that a lower $T_{SUP}$ can lead to a lower temperature profile at the oil inlet plane ($z$ = 0), but as the lubricant heats, flowing through the small inner film clearance, the three temperature profiles at $z = \frac{1}{4} L$ reach a similar magnitude that approaches the shaft temperature (213 ℃).

For the same operating condition, Figure 36 depicts how the inner film temperature grows along the axial direction at $\theta = 240°$ for the three oil inlet temperatures ($T_{SUP}$). The graph shows that the film temperature steadily increases as the lubricant flows axially through the film land. Regardless of $T_{SUP}$, the film exit temperatures at $z = \frac{1}{2} L$ are virtually identical. This occurs mostly due to the large heat

[24] The International Lubricant Standardization and Approval Committee (ILSAC) introduced the GF-4 test standard in 2004 for passenger car engine oils [35]. Some Tests for GF-4 are designed for more severe conditions like in turbocharged engines (small capacity, high power output). Different oil test temperatures (100 ℃~150 ℃) are required for these specific tests, so that the normal temperature of lubricant circulating into the TC should be in the same range.

[25] Lubricant (5W-30) viscosity is a function of temperature, which is 8.56 cPoise at 100 ℃, 5.85 cPoise at 120 °, and 4.22 cPoise at 140 °, respectively. Ref. [36] shows a typical product specifications of 5W-30 for reference.

[26] This oversimplification stems from the model simplicity rather than actual practice.

flow from the hot shaft kept at a fixed temperature[27] ($T_{shaft}$ = 213 ℃). APPENDIX A shows the influence of shaft temperature on the bearing performance characteristics.

Note that the inner film temperature with a lower $T_{SUP}$ climbs up faster in a short axial distance from the oil inlet plane ($z$ = 0) than the one with a higher $T_{SUP}$. This is so since the lubricant flow rate for the lower $T_{SUP}$ is smaller (shown in Figure 42) and is less effective in carrying away the heat from the hot journal.

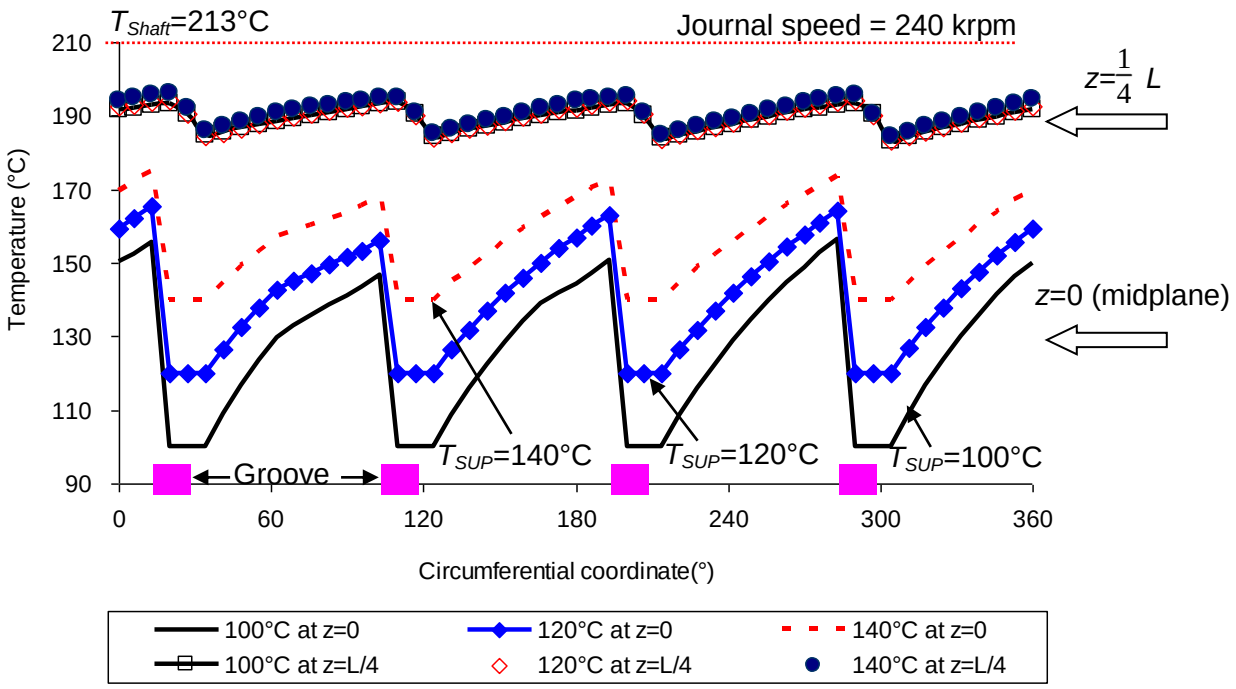


**Figure 35. Influence of oil supply temperature ($T_{SUP}$) on the inner film circumferential temperature distribution at two axial locations, $z$ = 0 and $z$ = $L$/4. $T_{SUP}$ = 100~140°C, $P_{SUP}$ = 4 bar, static load = 0.9 N. Journal speed = 240 krpm. $T_{shaft}$ = 213°C.**

[27] In practice, the heat flow model must be systemic and incorporate the shaft. The interaction between the shaft temperature and the oil supply temperature exists over the entire journal speed range. However, in the current simplified shaft model, the shaft is assumed as a source of thermal energy with a constant temperature at 213 ℃, regardless of $T_{SUP}$.

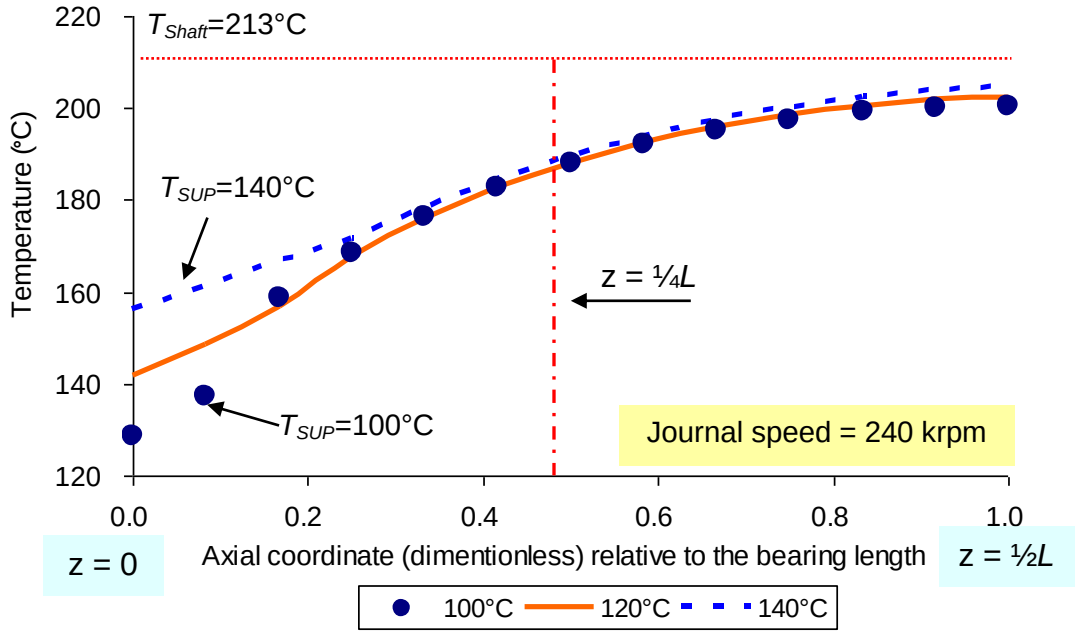


**Figure 36. Axial temperature growth in the inner film at $\theta$ = 240° for $T_{SUP}$ = 100°C, 120°C, and 140°C. Shaft speed = 240 krpm, $P_{SUP}$ = 4 bar, static load = 0.9 N. $T_{shaft}$ = 213°C.**

Figure 37 shows the influence of the oil inlet temperature ($T_{SUP}$) on the average temperatures[28] and peak temperatures of the inner and outer films for operation at the maximum journal speed (240 krpm) with $P_{SUP}$ = 4 bar. The results indicate that $T_{SUP}$ does not influence much the average and peak temperatures of the inner film, and that the peak temperature in the inner film is close to the temperature of the hot shaft ($T_{shaft}$ =213 ℃). This occurs because the thermal energy from the hot shaft into the film is

[28] The film average temperature is the arithmetic mean of the temperatures predicted over the whole film region.

overwhelming, lubricant heats quickly in the inner film. That is the shaft temperature rather than the oil inlet temperature largely determines most of the film temperature field. In other words, based on a fixed shaft temperature[29], lowering $T_{SUP}$ is not an effective method to decrease the peak film temperature when attempting to avoid oil flash or burning, since the decrease of the peak temperature in the inner film (<5 ℃) is much smaller than the corresponding decrease of $T_{SUP}$ from 140 ℃ to 90 ℃. However, $T_{SUP}$ strongly influence the outer film temperature, since the thermal energy advected by the outer film is small and thus its temperature closely follows $T_{SUP}$.

Figure 38 shows the influence of oil inlet temperature ($T_{SUP}$) on the oil average viscosity[30] of the inner and outer films for operation at 240 krpm. Since the oil viscosity tends to decrease as its temperature increases, the steady increase of the average temperature of the outer film shown in Figure 37 leads to a decrease of average oil viscosity. Similarly, the oil average viscosity of the inner film remains almost invariant as the oil inlet temperature increases.

[29] In reality, a lower oil inlet temperature will definitely cool the shaft to some extent. However, there is no available measured results to satisfactorily describe the cooling effect of $T_{SUP}$ on the shaft for an actual operating condition, in which there is continuously a large amount of heat flow from the hot turbine side. Presently, it is not feasible to model the heat transfer for the shaft when the amount of heat received from the exhaust gas flowing through the turbine impellers is not known. This requires of integration of the current model with the other heat flows in the TC system. Therefore, the shaft temperature is taken to be constant at 213 ℃ for simplicity.

[30] The oil average viscosity is calculated at the average temperature of the temperature field in the inner or outer film.

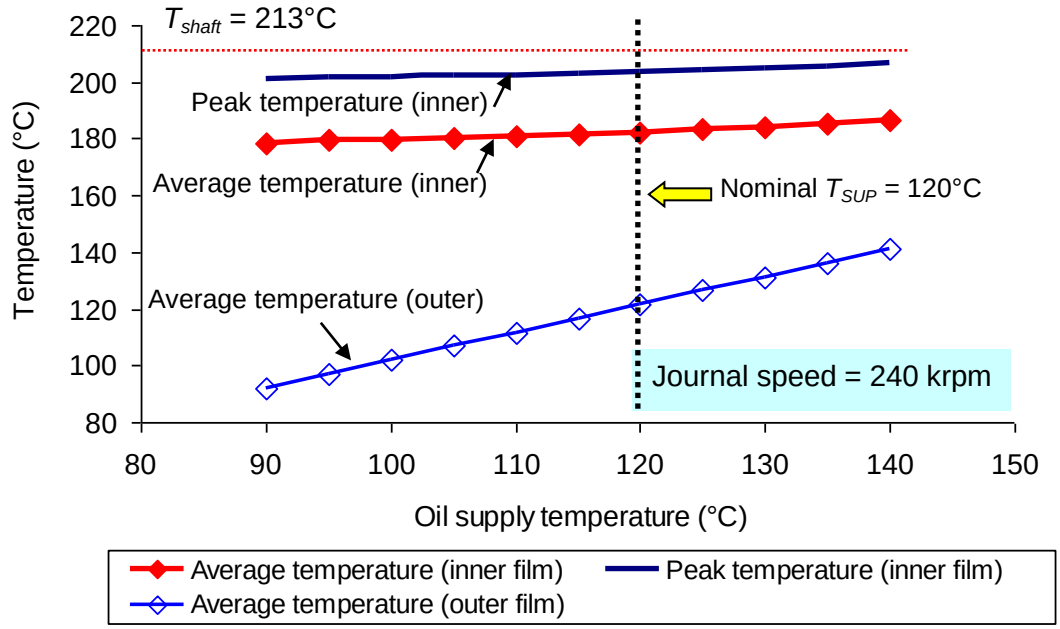


**Figure 37. Influence of oil inlet temperature ($T_{SUP}$) on the maximum temperature of the inner and outer films. Journal speed = 240 krpm, $P_{SUP}$ = 4.0 bar, $T_{SUP}$ = 100~140 °C, static load = 0.9 N. $T_{shaft}$ = 213°C.**

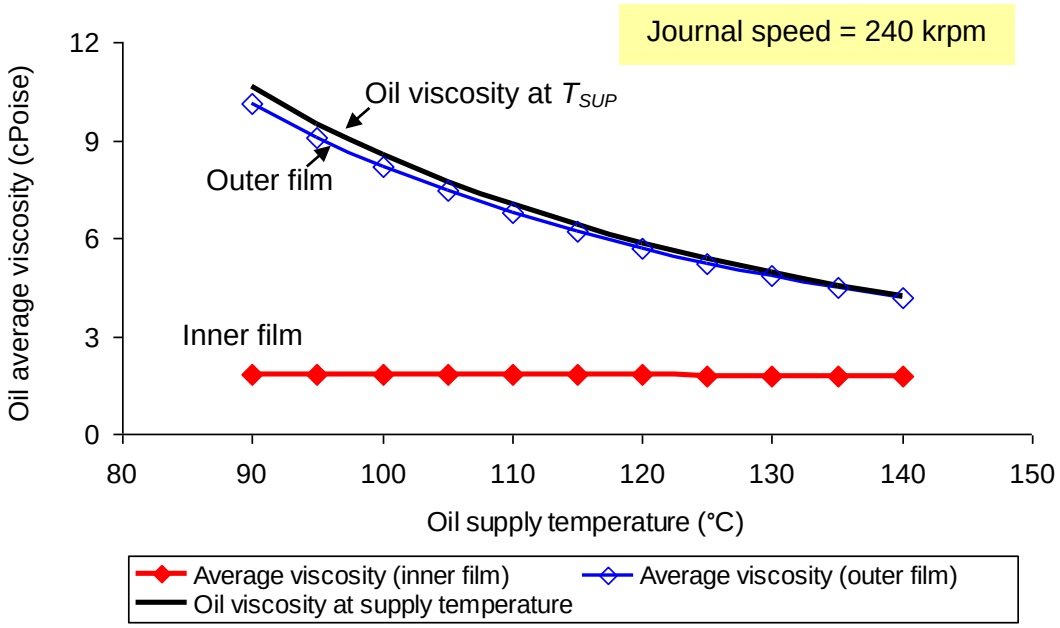


**Figure 38. Influence of oil supply temperature ($T_{SUP}$) on the oil average viscosity of the inner and outer films. $T_{SUP}$ = 90°C ~ 140°C. Shaft speed = 240 krpm, $P_{SUP}$ = 4 bar, static load = 0.9 N. $T_{shaft}$ = 213°C. $\mu_{supply}$ = 5.85 cPoise at 120°C.**

Figure 39 shows the drag power loss (inner film) versus journal speed for operation with an increasing oil inlet temperature ($T_{SUP}$). The predictions demonstrates that $T_{SUP}$ has a negligible effect on the drag power loss in the inner film. This occurs because the influence of $T_{SUP}$ on the film temperature field is felt only near the oil inlet region, and the oil average viscosity of the inner film is nearly the same for all $T_{SUP}$ (see Figure 38). The drag power loss in the outer film (not shown in Figure 39) is negligible.

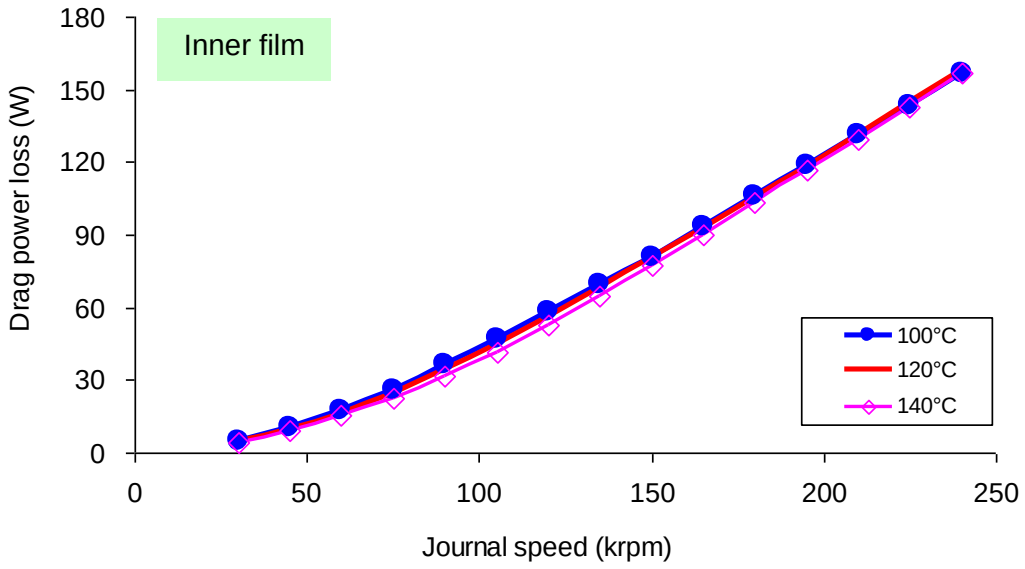


**Figure 39. Influence of oil inlet temperature ($T_{SUP}$) on the drag power loss in the inner film vs. journal speed. $P_{SUP}$ = 4.0 bar, $T_{SUP}$ = 100~140 °C, static load = 0.9 N. $\mu_{supply}$ = 5.85 cPoise at 120°C.**

Figure 40 depicts the influence of the oil inlet temperature ($T_{SUP}$) on the heat flow taken from the hot journal versus journal speed. The results show that (a) a lower $T_{SUP}$ leads to a larger heat flow from the journal, and (b) that the trends of this heat flow versus journal speed for three $T_{SUP}$ are similar. For (a), the film temperatures at the region near the oil inlet plane with a lower $T_{SUP}$ are lower than the ones with a higher $T_{SUP}$ (see Figure 36). Hence, the heat flow from the hot journal whose temperature is fixed at 213 ℃ increases correspondingly.

For a certain $T_{SUP}$, the heat flow from the journal increases until the journal speed reaches about 90 krpm and then decreases with further raises in journal speed. An explanation for this can be traced to the influence of the oil inlet temperature on the average temperature of the inner film, as shown in Figure 41. Note that the heat convection coefficient between the shaft and the film remains invariant in a laminar flow of the inner film, and the "wet" area of the shaft outer surface also keeps unchanged. Therefore, the heat flow from the shaft is a strong function of the temperature difference between the shaft (213 ℃) and the inner film temperature field. The results in Figure 40 show that the greatest temperature difference between the shaft and the average film temperature occurs at 90 krpm, so that the maximum heat flow from the shaft takes place at the same speed.

Figure 41 depicts the influence of the oil inlet temperature ($T_{SUP}$) on the average temperature of the inner film versus journal speed. For operation at low journal speeds (< 90 krpm), the drag power loss is so small (less than 30 W) that cannot strongly effect the inner film temperature. Hence, the (average) inner film temperature decreases due to the larger flow rate induced by a faster journal rotation. However, as the journal speed exceeds 90 krpm, drag power loss, which is eventually converted into thermal energy, is largely generated in the inner film (see Figure 39), causing the inner film temperature to increase with journal speed and then to decrease the heat flow from the hot journal. Note that for high journal speeds, the film temperature increases sharply along the axial direction (see Figure 36), so it is reasonable to assume that there is more drag power loss generated near the oil inlet plane where the oil viscosity is the largest.

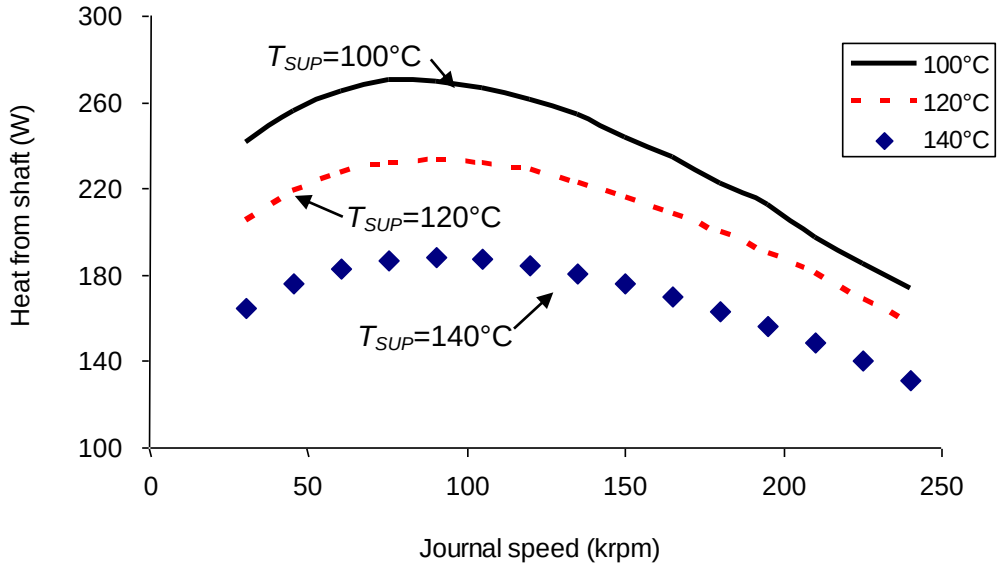


**Figure 40. Influence of oil inlet temperature ($T_{SUP}$) on heat flow from the journal vs. journal speed. $T_{SUP}$ = 90~140°C, $P_{SUP}$ = 4 bar, static load = 0.9 N. $T_{shaft}$ = 213°C.**

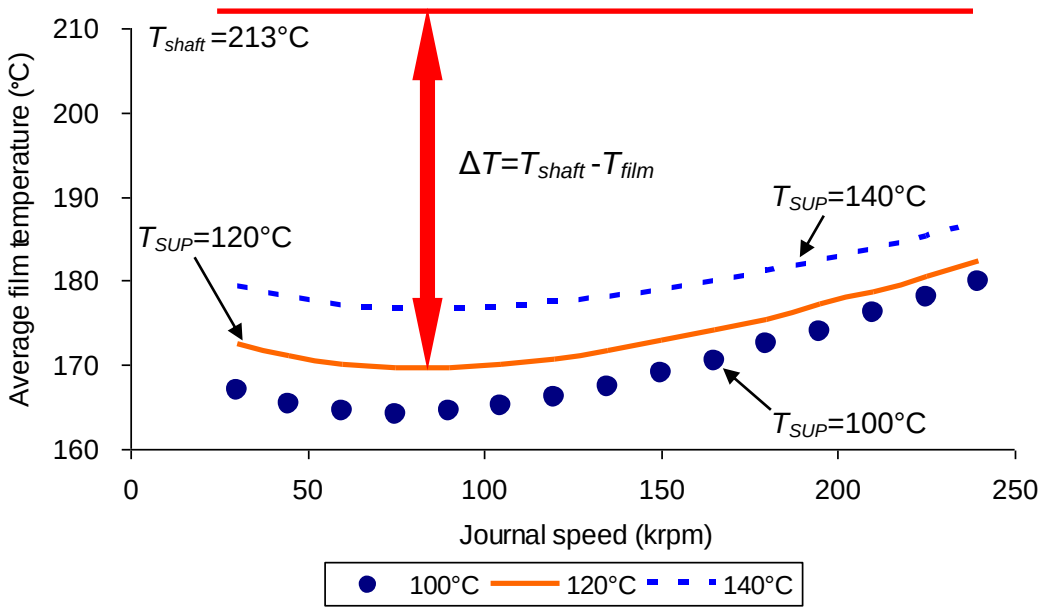


**Figure 41. Influence of oil inlet temperature ($T_{SUP}$) on the average temperature of the inner film vs. journal speed. $T_{SUP}$ = 90~140°C, $P_{SUP}$ = 4 bar, static load = 0.9 N. $T_{shaft}$ = 213°C.**

Figure 42 presents the influence of the oil inlet temperature ($T_{SUP}$) on the flow rates through the inner and outer film regions versus journal speed. The graphs (a) and (b) show that a higher $T_{SUP}$ leads to a larger flow rate through the inner and outer films, respectively. The increase of the flow rate through the inner film results from the larger thermal growth of the inner film clearance. For one thing, the temperature of the ring inner surface increases with a higher $T_{SUP}$ (see Figure 43), which leads to a larger

thermal growth[31]. Note that as $T_{SUP}$ increases, the oil viscosity is not a factor responsible for the increase of flow rate in the inner film, since inner film viscosity is determined mainly by the shaft temperature, a constant at 213 ℃.

On the other hand, the flow rate in the outer film also increases with the oil inlet temperature ($T_{SUP}$). Note that the average temperature of the outer film is close to the oil inlet temperature. As the oil inlet temperature increases from 100 ℃ to 140 ℃, the corresponding increase in the outer film temperature field results in a drop of oil viscosity, i.e., for lubricant SAE 5W-30, $\mu_{100°C} / \mu_{140°C} \approx 2$. This is the reason for the flow rate in the outer film to increase with $T_{SUP}$.

Figure 43 presents the influence of oil inlet temperature ($T_{SUP}$) on the average temperatures of both the inner and outer ring surfaces. The results show that a lower $T_{SUP}$ cools the floating ring, effectively decreasing the average temperatures of both the ring inner and outer surfaces.

[31] In the current model, the temperature, which is used to estimate the thermal growth of one component (ring or shaft) surface, is the average of the component surface temperature and the temperature of the (inner or outer ) film contacting the component.

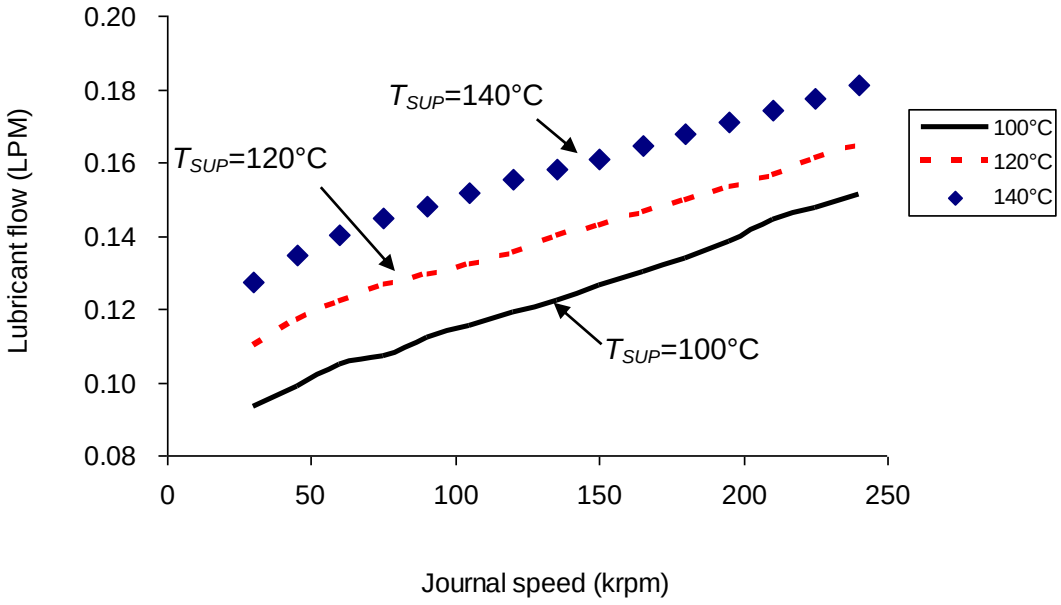


(a) Inner film

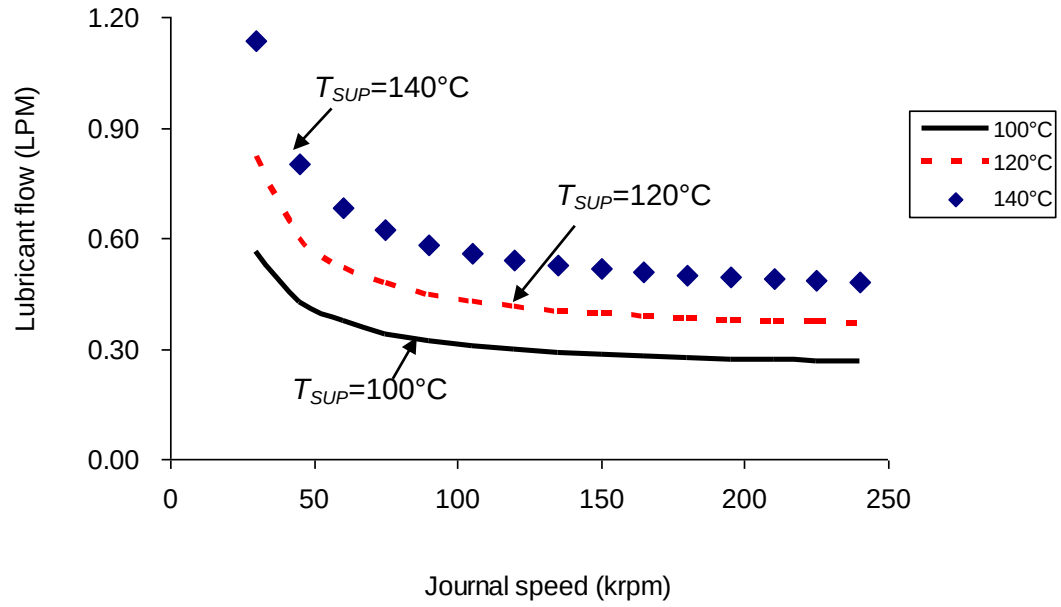


(b) Outer film

**Figure 42. Influence of oil inlet temperature ($T_{SUP}$) on the flow rates through the inner and outer film clearances vs. journal speed. $T_{SUP}$ = 100~140 °C, $P_{SUP}$ = 4 bar, static load = 0.9 N.**

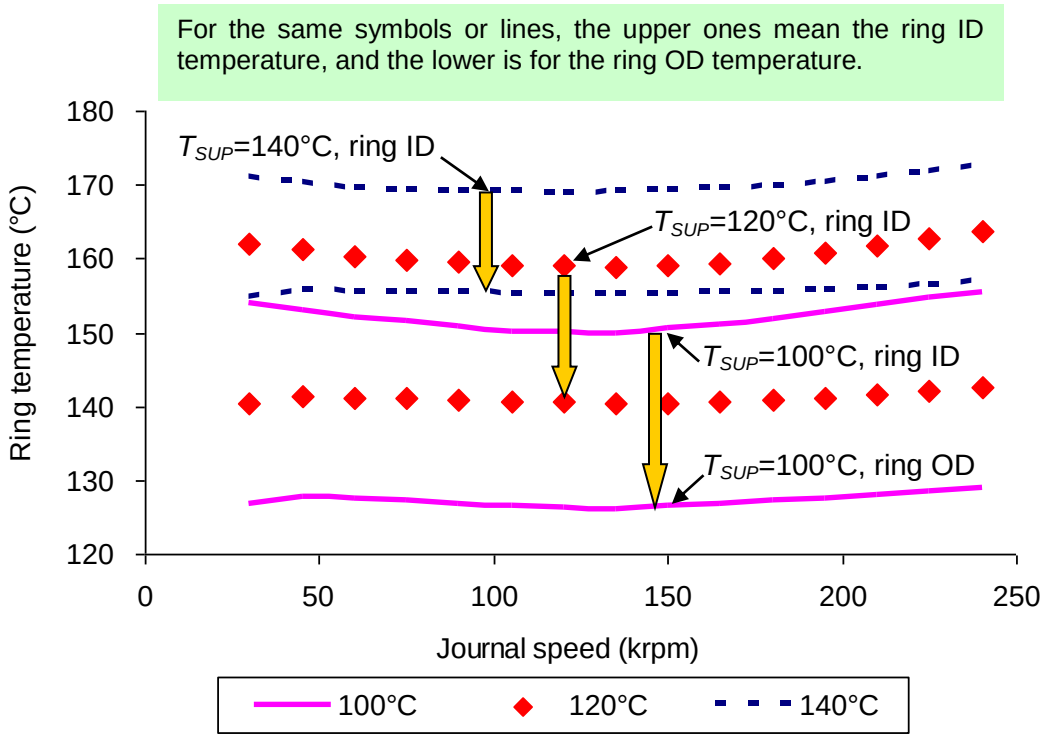


**Figure 43. Influence of oil inlet temperature ($T_{SUP}$) on the average temperatures of the ring inner and outer surfaces vs. journal speed. $T_{SUP}$ = 100~140 °C, $P_{SUP}$ = 4 bar. Static load = 0.9 N. $T_{shaft}$ = 213°C.**

In conclusion, lubricating a (S)FRB with oil (SAE 5W-30) at a lower $T_{SUP}$ can result in an increase of the heat flow from the hot journal, but this effect weakens as the journal rotates at high speeds because the inner film temperature becomes higher. However, a lower $T_{SUP}$ cannot effectively reduce the peak temperature in the inner film and has a negligible effect on the drag power loss. The results occur because the shaft temperature is held constant at 213 ℃. The oil heats too quickly along the axial direction.

For the most part temperature and viscosity fields in the inner film (away from the oil inlet) are not influenced by the oil inlet temperature ($T_{SUP}$).

**Influence of Lubricant Supply Pressure**

An increase of the lubricant supply pressure will increase the flow rates through the films and probably reduce the films temperatures as well as their peak magnitude. However, supplying a larger flow rate into the films requires of a larger size pump and storage volume, which both increases the cost of the product and reduce its efficiency.

Figure 44 presents the influence of the oil supply pressure, $P_{SUP}$ = 3, 4, and 5 bar, on the flow rates of the inner film and outer film versus journal speed for operation with oil inlet temperature ($T_{SUP}$) at 120 ℃. The predictions show, as expected, that a larger $P_{SUP}$ increases the flow rates through both the inner and outer films. Additionally, as the journal speed increases the ratio between the flow rates in the inner film and the outer film narrows, i.e., for $P_{SUP}$ = 4 bar, $Q_o/Q_i \approx$ 8 at 30 krpm decreases to $Q_o/Q_i \approx$ 2 at 240 krpm.

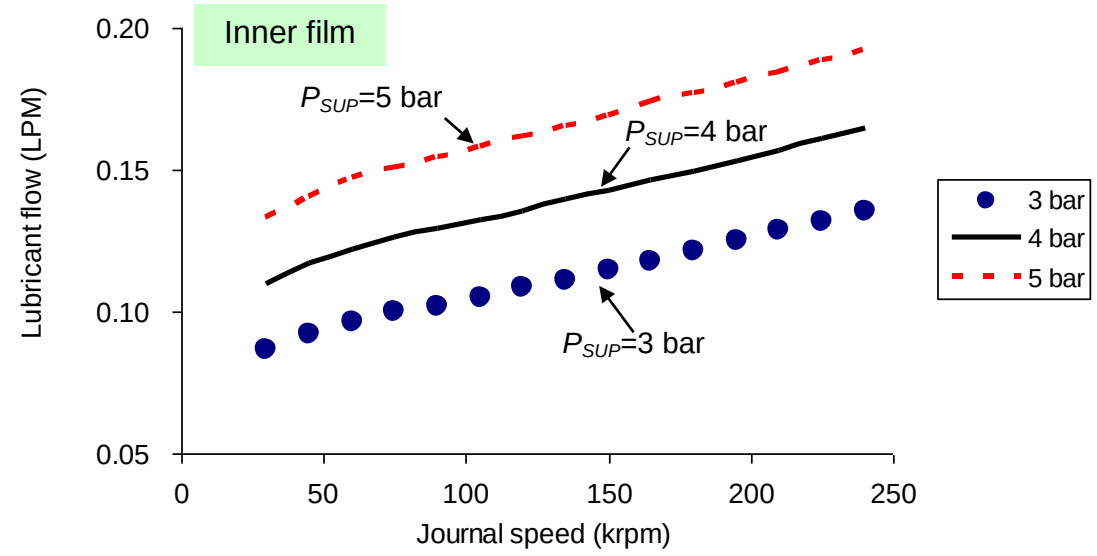


(a) Inner film

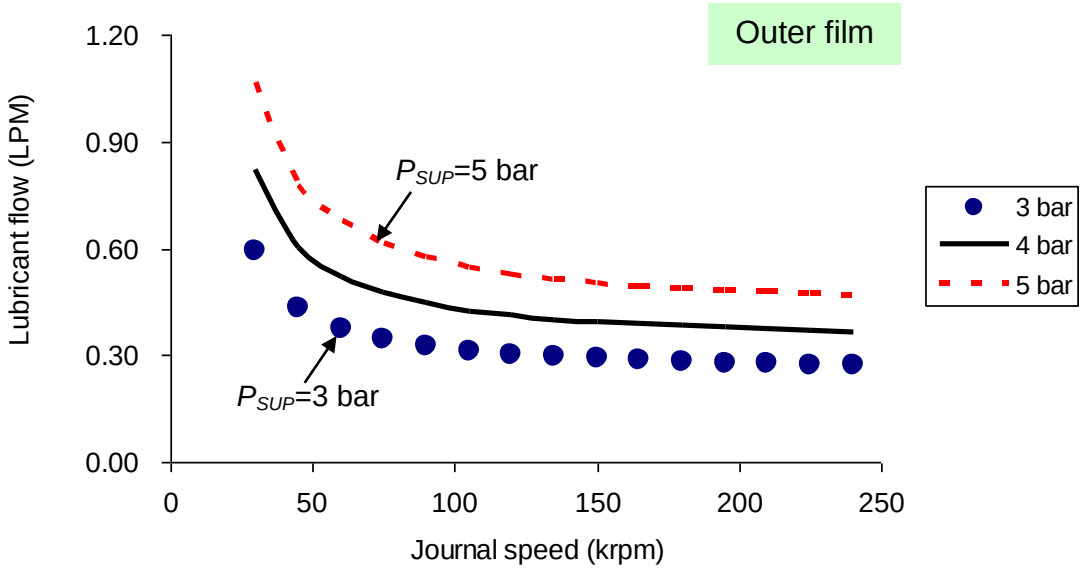


(b) Outer film

**Figure 44. Influence of oil inlet pressure ($P_{SUP}$) on the flow rates through the inner and outer film clearances vs. journal speed. $T_{SUP}$ = 120°C, $P_{SUP}$ = 3~5 bar, static load = 0.9 N.**

Figure 45 presents the influence of the oil supply pressure ($P_{SUP}$) on the total energy into the (S)FRB system versus journal speed when the oil inlet temperature $T_{SUP}$ = 120 ℃. The total energy into the (S)FRB includes the heat flow from the hot journal and the drag power loss generated in the inner film. The graph (a) shows that feeding lubricant at a high $P_{SUP}$ increases the heat flow from the hot journal since the flow rates through the inner film increases. A larger flow rate carries away more thermal energy, causing the inner film temperature to decline (see Figure 49), so that the heat flow from the hot journal (shaft)[32] will accordingly increase for a higher $P_{SUP}$. Incidentally, the maximum heat flow from the journal takes place as the journal spins at around 90 krpm. This occurs because for operation at 90 krpm the temperature difference between the shaft and the average film temperature is greatest (see Figure 46). Above 90 krpm, the heat flow removed from the journal drops due to the increase in the drag power loss. The increased drag power loss is converted into the thermal energy with the journal speed, and then the inner film temperature rises, causing to heat flow from the journal (213 ℃) to decrease.

On the other hand, Figure 45 (b) shows the influence of oil inlet pressure ($P_{SUP}$) on the drag power loss in the inner film versus journal speed (30 krpm ~ 240 krpm). A higher $P_{SUP}$ leads to a larger drag power loss, particularly at high speeds (>150 krpm). For example, when the journal spins at the maximum speed (240 krpm), as $P_{SUP}$ increases from 3 bar to 5 bar, the drag power loss increases by approximately 30%, thus indicating an extra energy (~45 W) is added to the total energy carried by the films. Note

[32] In the presently over-simplified heat flow model, the shaft temperature is assumed constant at 213 ℃.

that this increase is lower than the increase in heat flow (~80 W) from the hot journal for the same operating condition, as shown in Figure 45(a). As a result, the total thermal energy carried away by the films will increase for a higher oil inlet pressure ($P_{SUP}$).

Figure 46 depicts the influence of the oil inlet pressure ($P_{SUP}$) on the average temperature of the inner film versus journal speed. The curve of the average film temperature with journal speed for a given oil inlet pressure explains the change of heat flow from the journal with journal speed as shown in Figure 45(a).

Recall the influence of the oil supply temperature ($T_{SUP}$) on the heat flow from the journal (Figure 40). Hence, Figure 45(a) shows a similar trend of the heat flow versus journal speed for each $P_{SUP}$. The heat flowing from the journal for both various $T_{SUP}$ and $P_{SUP}$ usually begins to increase until the journal speed approaches around 90 krpm and then starts to drop as the journal speed increases. The drag power loss, which increases with the journal speed, is converted to the thermal energy and then raises the (average) inner film temperature, leading to the drop of the heat flow from the journal.

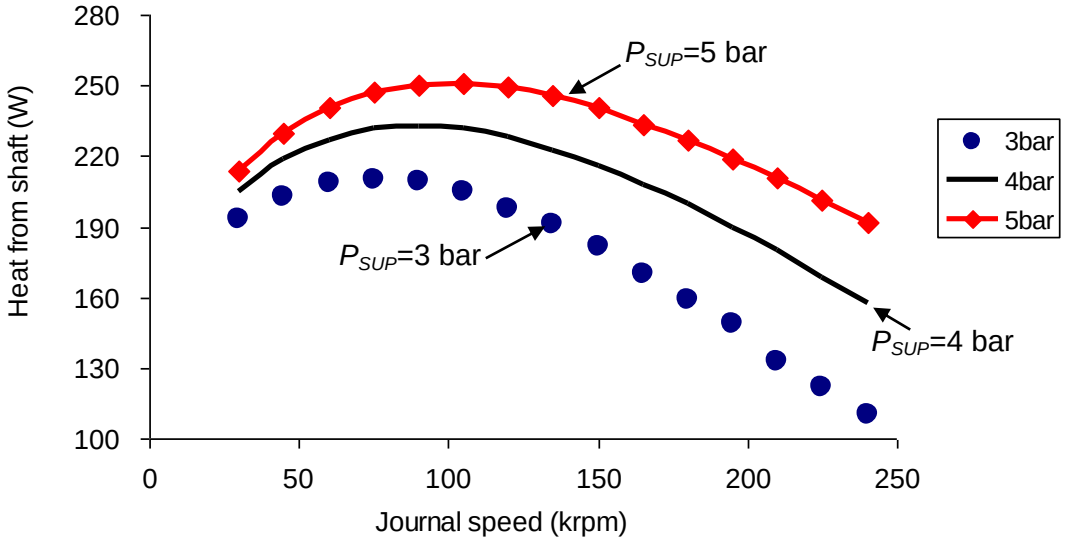


(a) Heat from the journal

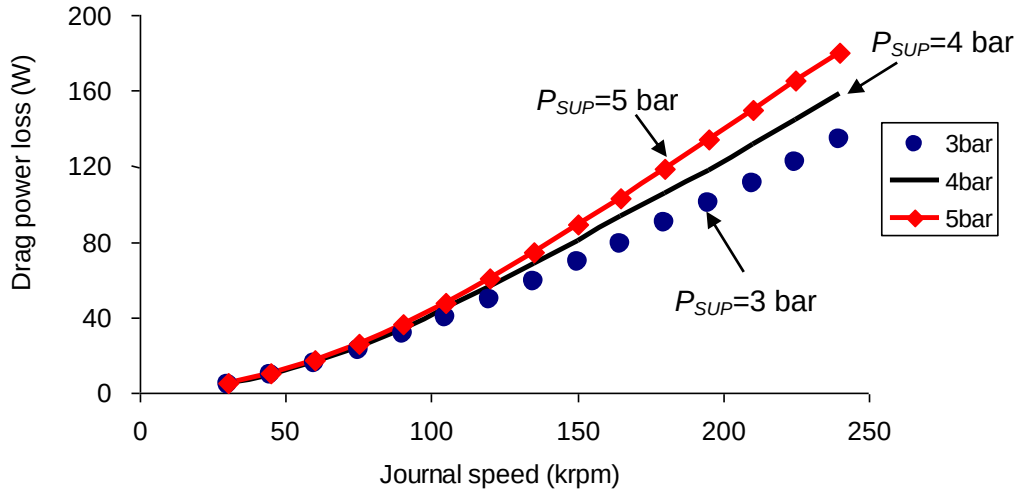


(b) Drag power loss (inner film)

**Figure 45. Influence of oil inlet pressure ($P_{SUP}$) on the total energy into the bearing (heat from the journal and the drag power loss) vs. journal speed. $P_{SUP}$ = 3~5 bar, $T_{SUP}$ = 120°C. Static load = 0.9 N. $T_{shaft}$ = 213°C.**

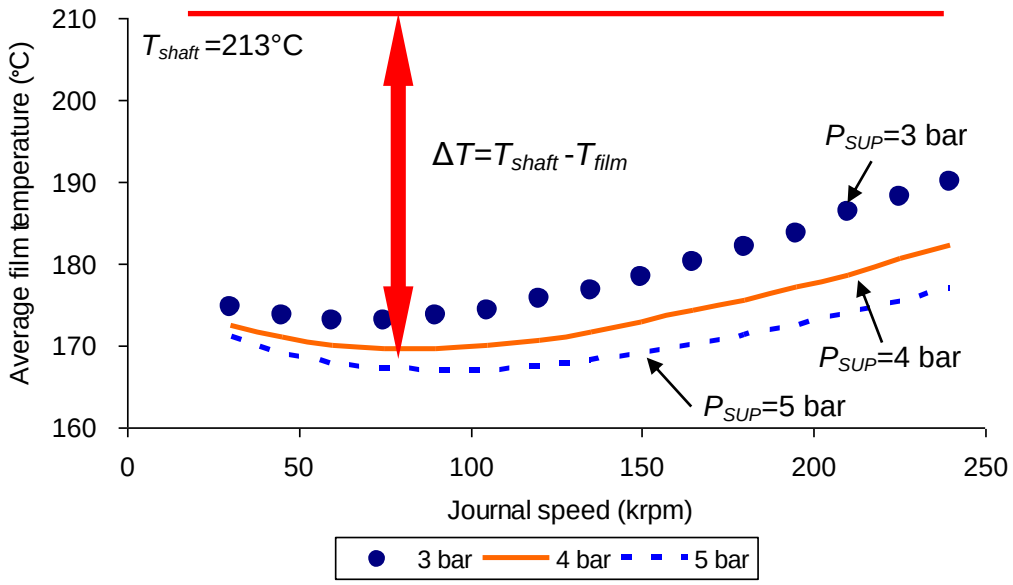


**Figure 46. Influence of oil inlet pressure ($P_{SUP}$) on the average temperature of the inner film vs. journal speed. $P_{SUP}$ = 3~5 bar, $T_{SUP}$ = 120°C. Static load = 0.9 N. $T_{shaft}$ = 213°C.**

Figure 47 depicts the influence of oil inlet pressure (PSUP) on the power loss, represented as a fraction of the power input,[33] for operation at four journal speeds (30 krpm ~ 240 krpm) with a $T_{SUP}$ = 120 ℃. The results show that $P_{SUP}$ has a negligible effect on the drag power loss, whereas journal speed generating the drag power loss has a greater effect. Specifically, the power loss is about 15% of the input energy at 90 krpm. Recall this speed is the threshold speed when the heat flow from the journal starts to decline (see Figures 40 and 45). Note that the oil inlet temperature ($T_{SUP}$) also has a

[33] The fraction of energy is defined as $\frac{Power\ loss}{Power\ input} = \frac{Power\ loss}{Power\ loss + Heat\ from\ journal}$.

negligible effect on the drag power loss, which is ~15% of the total input energy for various $T_{SUP}$ as the journal spins at 90 krpm. At the highest speed, however, the drag power loss is ~60% of the energy available. This fraction is nearly invariant with oil inlet pressure or temperature.

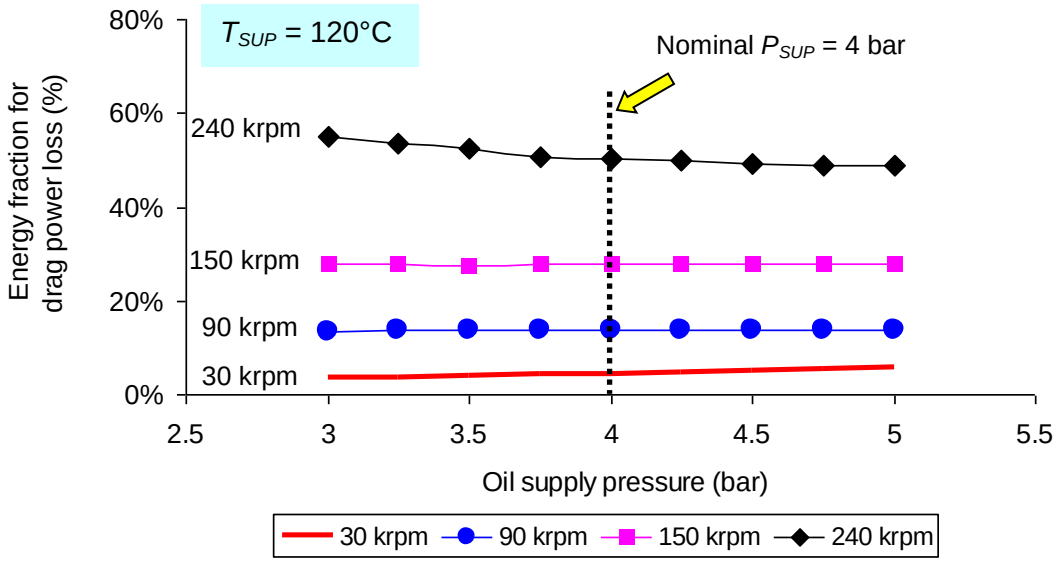


**Figure 47. Influence of oil inlet pressure ($P_{SUP}$) on power loss as a fraction of the total power input (power loss + heat from shaft). Journal speed = 30 krpm, 90 krpm and 240 krpm. $P_{SUP}$ = 3~5 bar, $T_{SUP}$ = 120°C. Static load = 0.9 N.**

Figure 48 presents the influence of the oil supply pressure ($P_{SUP}$) on the total energy out of the (S)FRB system versus journal speed when the oil inlet temperature is equal to 120 ℃. Part of the total thermal energy in the (S)FRB is advected by the inner

and outer films, and the remaining energy is conducted into the casing, which is assumed at the same temperature as the oil inlet temperature (120 ℃). The predictions show that the inner film carries away most of the thermal energy into the bearing system, particularly at high journal speeds, and a higher $P_{SUP}$ causes the inner film to carry more energy since both the heat from the journal and the drag power loss in the inner film increase with $P_{SUP}$. Additionally, the oil inlet pressure has little effect on the heat advected by the outer film and the heat conducted into the casing.

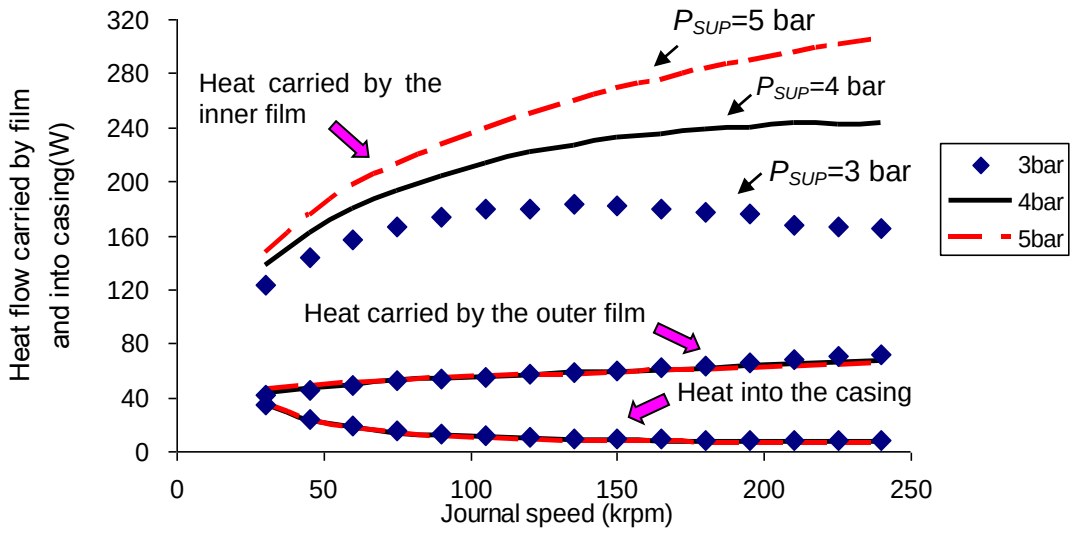


**Figure 48. Influence of oil inlet pressure ($P_{SUP}$) on heat flows carried by the films and into the casing vs. journal speed. $P_{SUP}$ = 3~5 bar, $T_{SUP}$ = 120°C. Static load = 0.9 N.**

Figure 49 shows the influence of oil inlet pressure ($P_{SUP}$) on the average temperatures and the peak temperatures of the inner and outer films for operation at the maximum journal speed (240 krpm). Recall the inlet oil with $T_{SUP}$ = 120 ℃. An increase in $P_{SUP}$ reduces monotonically both the average and the peak temperatures of the inner film, and the decrease of the average film temperature is larger than that of the peak film temperature. The decrease in the inner film temperature is due to a larger flow rate caused by a higher $P_{SUP}$. On the other hand, $P_{SUP}$ has a negligible effect on the peak film temperature and the average film temperature in the outer film (not shown in Figure 49). The outer film temperature is a little higher than the oil supply temperature, indicating that the thermal energy advected by the outer film is small. This occurs because the inner film carries away most of the thermal energy from the hot journal and also generated by the shear drag torque.

To sum, raising the oil inlet pressure ($P_{SUP}$) effectively increases the flow rates through the films, and thus increases both the heat flow from the journal and to a minor extent the drag power loss, leading to a larger thermal energy carried by the inner film. The maximum heat flow from the journal occurs at a journal speed of 90 krpm. When the journal speed exceeds 90 krpm, more drag power loss is converted into thermal energy and raises the (average) film temperature, thus causing the heat from the journal to decline.

In addition, an increase in oil inlet pressure reduces the average temperature of the inner film steadily, but a higher $P_{SUP}$ cannot effectively lower the peak temperature

of the inner film. Note that a higher $P_{SUP}$ also requires of more energy to deliver a larger oil flow rate, thus resulting in a higher cost of operation.

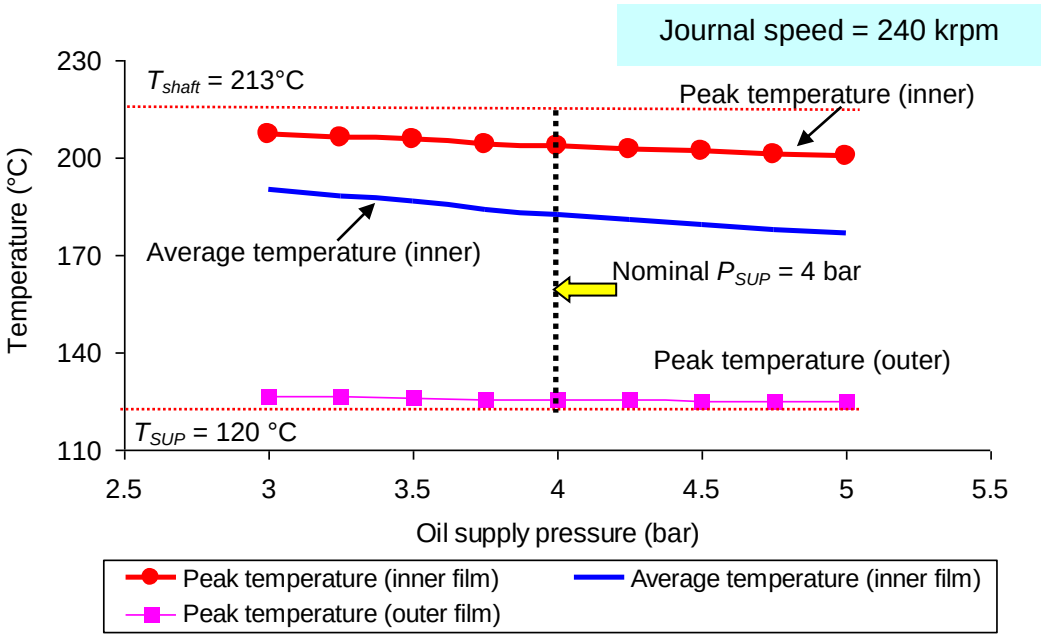


**Figure 49. Influence of oil inlet pressure ($P_{SUP}$) on the average and the peak film temperatures. Journal speed = 240 krpm, $P_{SUP}$ = 3~5 bar, $T_{SUP}$ = 120 °C, static load = 0.9 N. $T_{shaft}$ = 213°C.**

**Influence of Film Clearances (Inner and Outer)**

The size of the film clearances directly affects the flow rates and drag power loss in the film. If a film clearance is too tight, parts are costlier and more difficult to

manufacture and install. Also, the thermal energy in the bearing system cannot be effectively removed by sufficient lubricant flow because of a larger flow resistance which could also cause oil burning. If the film clearance is too large, it not only brings about too large a flow rate that would require of a larger oil pump, but also negatively influences the load support and bearing damping[34][37].

Figure 50 presents the influence of the inner and outer film clearances ($c_i$, $c_o$) on the heat flowing from the journal for operation at the oil inlet pressure $P_{SUP}$ = 4 bar and temperature $T_{SUP}$ = 120 ℃. Three clearances (lower, original or nominal, higher) for each film compose to nine combinations. The nominal clearance of the inner film and outer film at 20 ℃ is $c_i$ = 7.5 μm and $c_o$ = 35 μm, respectively. A larger inner film clearance ($c_i$) leads to a larger flow rate through the inner film, facilitating the removal of more heat from the hot shaft. In addition, the drop of heat flow from the journal at higher journals (> 100 krpm) for a larger $c_i$ is much smaller than that of a smaller $c_i$. This occurs because a larger $c_i$ effectively decreases the accumulation rate of the inner film temperature along the axial direction (see Figure 51), and this change of film temperature directly influences the heat flow from the shaft, whose temperature states constantly at 213 ℃.

Figure 51 depicts the evolution of the inner film temperature along the axial direction at $\theta$=240 ° for three inner film clearances as the journal spins at 240 krpm. The graph shows that the film temperature steadily increases at different rates for the various inner film clearances. For the small inner film clearance (5 μm), the film temperature

[34] The study of the effect of film clearances on the bearing force coefficients is beyond the scope of the current research. The following investigation focuses on the main bearing performance parameters such as heat flows, drag power loss, and peak film temperature, to name a few.

rises so quickly and reaches the peak (maximum) temperature in a very short distance from the oil inlet plane. The peak temperature is close to the shaft temperature. An increase in the inner film clearance increases the flow rate (see Figure 52), which carries away more thermal energy and thus causes the inner film temperature to increase at a lower rate.

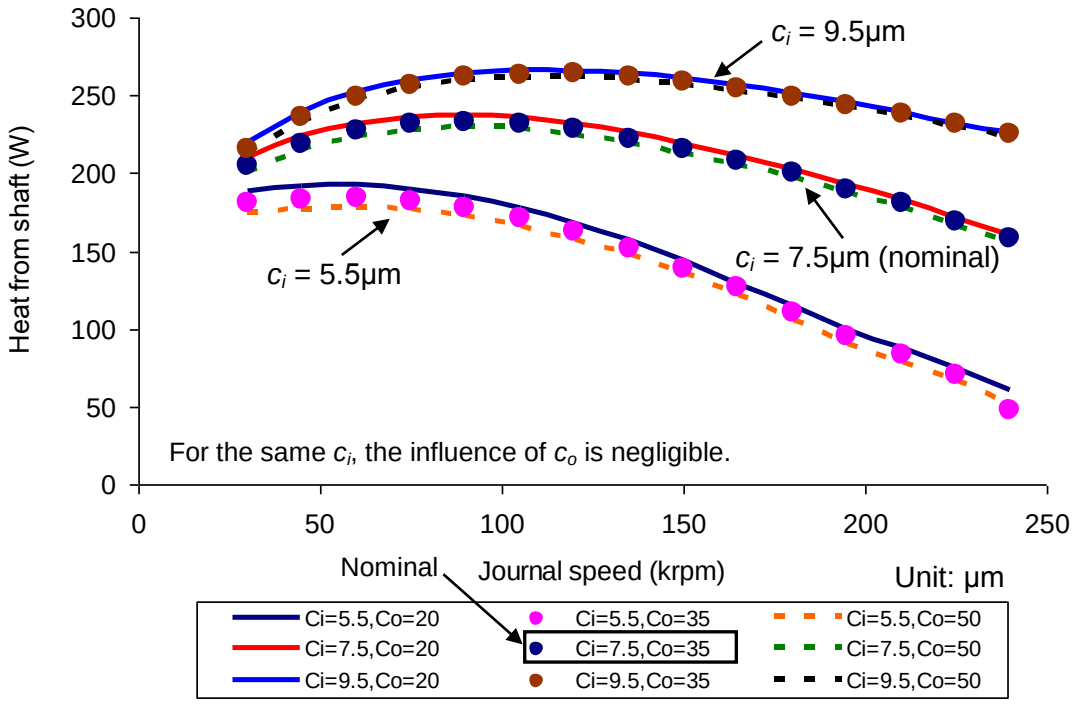


**Figure 50. Influence of inner and outer film clearances ($c_i$,$c_o$) on the heat flowing from the journal vs. journal speed. $P_{SUP}$ = 4.0 bar, $T_{SUP}$ = 120 °C, $T_{shaft}$ = 213°C. Static load = 0.9 N. Nominal $c_i$ = 7.5 μm and $c_o$ = 35 μm.**

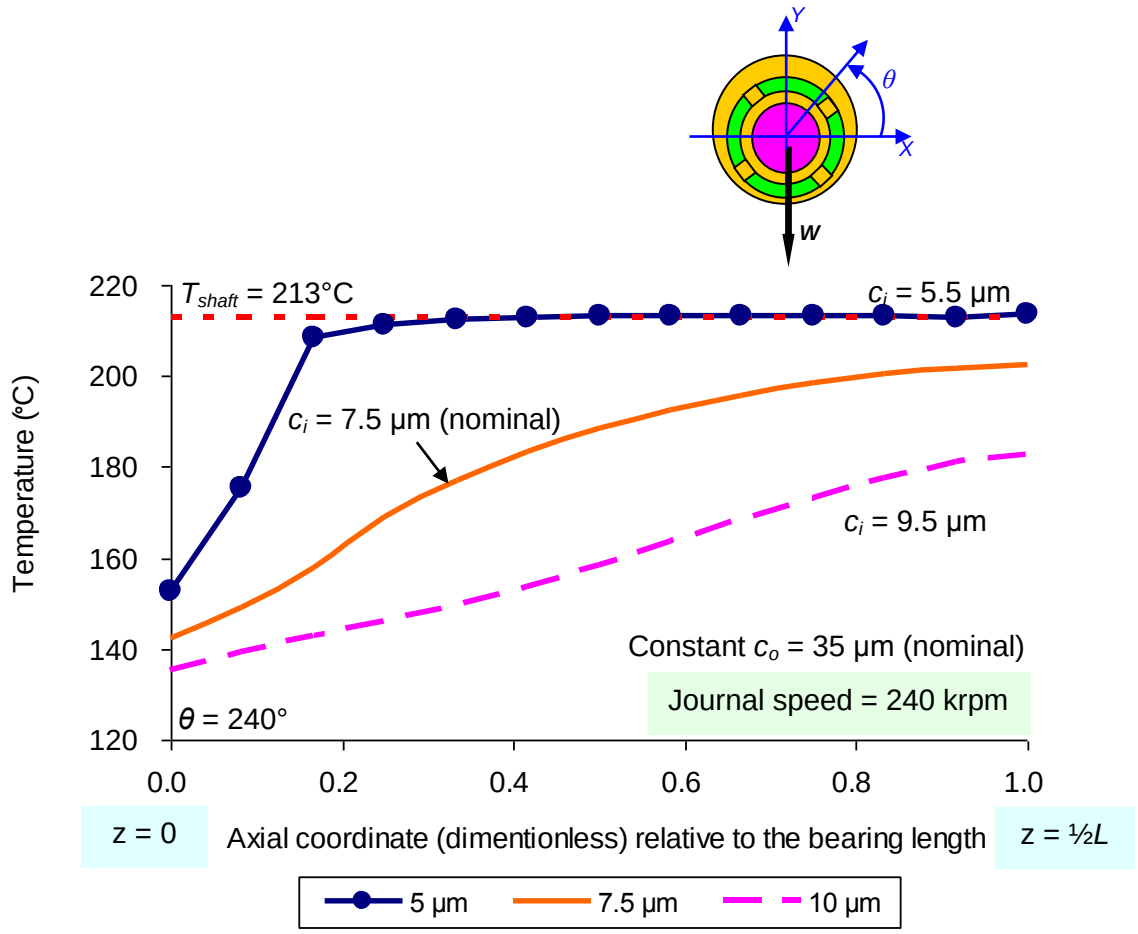


**Figure 51. Evolution of axial temperature in the inner film at $\theta$ = 240° for $c_i$ = 5 µm, 7.5 µm(nominal) and 10 µm. $c_o$ = 35 µm (nominal). Shaft speed = 240 krpm, $T_{SUP}$ = 120°C. $P_{SUP}$ = 4 bar, static load = 0.9 N. $T_{shaft}$ = 213°C.**

Figure 52 presents the influence of inner film clearance ($c_i$) on the flow rate through the inner film for operation at two journal speeds, 90 krpm and 240 krpm. The predictions show that a larger $c_i$ leads to a steady increase in the flow rate through the inner film clearance.

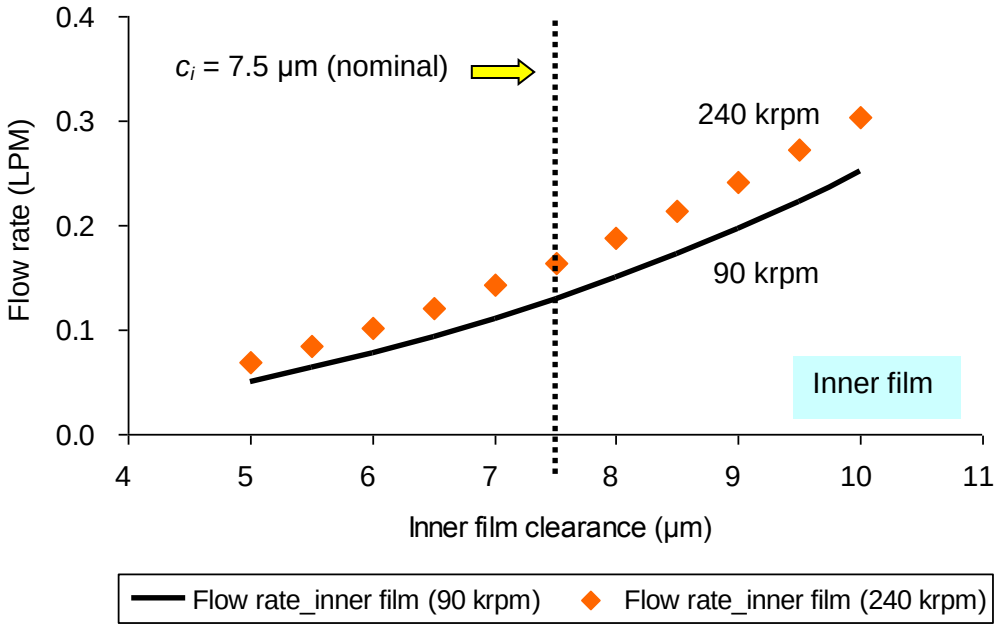


**Figure 52. Influence of inner film clearance ($c_i$) on the flow rates through the inner film region. Journal speed = 90 krpm and 240 krpm. Static load = 0.9 N. $P_{SUP}$ = 4.0 bar, $T_{SUP}$ = 120 °C. Nominal $c_i$ = 7.5 μm and $c_o$ = 35 μm.**

Figure 53 presents the influence of inner film clearance ($c_i$) on the heat flow from the journal for operation over the journal speed range (30 krpm ~ 240 krpm). Recall that the oil inlet pressure $P_{SUP}$ = 4 bar and temperature $T_{SUP}$ = 120 ℃. The predictions show that the heat flow from the journal increases steadily with clearance ($c_i$) for any speed. The increase in the heat flow is more evident at high journal speeds. This occurs since a larger $c_i$ leads to a larger flow rate through the inner film clearance, which can carry away more energy and thus lowers the film temperature (see Figure 57). Note that the

heat flow from the journal drops for an increasing $c_i$ since the film temperature increases because of more drag power loss generated in the film.

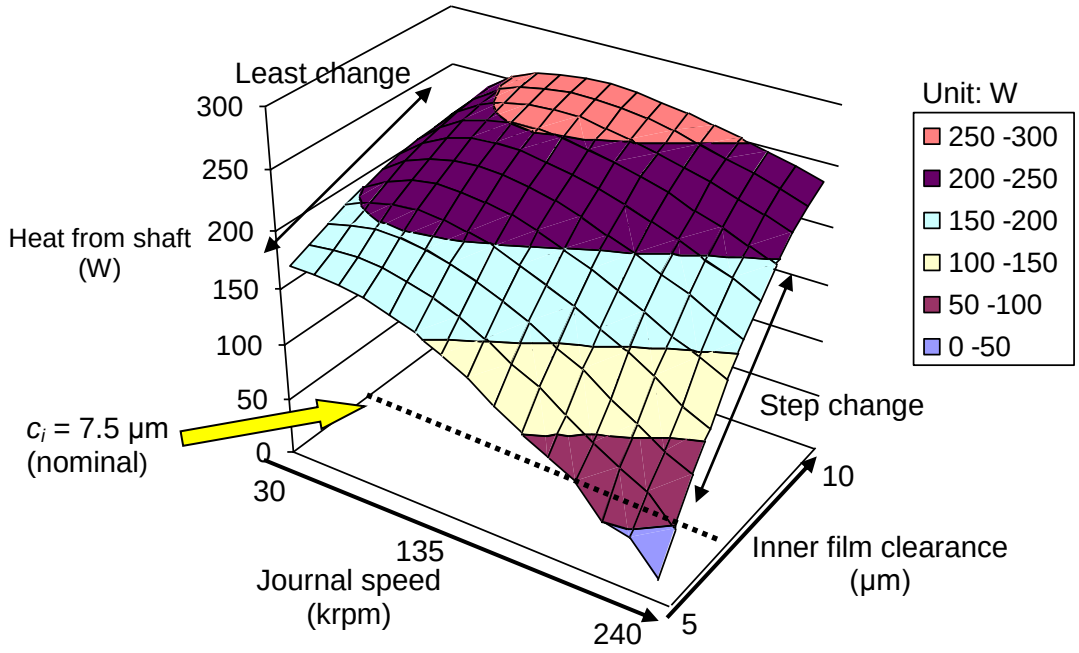


**Figure 53. Influence of inner film clearance ($c_i$) on the heat flow from the journal. $c_o$ = 35 µm (nominal). Shaft speed = 90 krpm and 240 krpm, static load = 0.9 N. $P_{SUP}$ = 4.0 bar, $T_{SUP}$ = 120 °C.**

Under the same operating condition, Figure 54 presents the influence of inner film clearance ($c_i$) on the drag power loss generated in the inner film over the journal speed range (30 krpm ~ 240 krpm). At low journal speeds (< 90 krpm), the drag power loss always remains low for increasing $c_i$ compared with the heat flow from the journal.

However, at high journal speeds, the drag power loss steadily increases with $c_i$, because of the high oil viscosity (induced by a lower film temperature). For example, for operation at 240 krpm, as $c_i$ changes from 5 μm to 10 μm, the drag power loss increases by 30%, (~ 40 W). As a result, it is reasonable to conclude that the total energy advected by the films will increase with a larger inner film clearance ($c_i$).

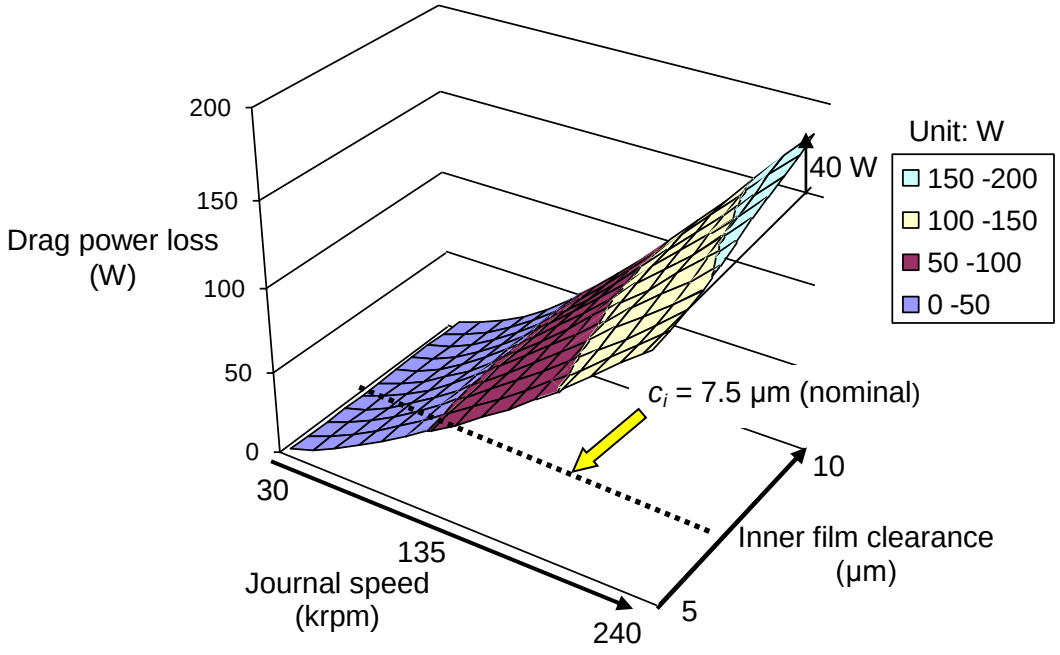


**Figure 54. Influence of inner film clearance ($c_i$) on the drag power loss. $c_o$ = 35 μm (nominal). Shaft speed = 90 krpm and 240 krpm, static load = 0.9 N. $P_{SUP}$ = 4.0 bar, $T_{SUP}$ = 120 °C.**

Figure 55 presents the influence of inner film clearance ($c_i$) on the heat flow conducted through the ring over the journal speed range (30 krpm ~ 240 krpm). The predictions show that the heat flow through the ring decreases for an increasing $c_i$. This occurs because the energy advected by the inner film increases with $c_i$, and the remaining energy that is conducted through the ring decreases correspondingly. Recall that the inner film carries away most of the energy that is from the hot journal plus the drag power loss generated in the inner film.

In addition, the journal speed has a minor effect on the heat flow through the ring, i.e., for the inner film clearance of 5 μm, the maximum difference of the heat flow through the ring, from one valley to the next crest, can be just 10 W, less than 10% of the heat flow at the maximum journal speed.

Figure 56 presents the influence of inner film clearance ($c_i$) on the heat flow conducted into the casing as the journal speed increases from 30 krpm to 240 krpm. The predictions show that an increase in $c_i$ results in a small decrease in the heat flow into the casing. This is because the total energy into the outer film, which equals to the heat flow through the ring, decreases with an increasing $c_i$. As the journal speed increases, the heat flow conducted into the casing starts with a sharp decrease and then remains almost invariant. Note that the variation of the heat flow into the casing with journal speed is much smaller than the total energy input into the (S)FRB system (~ 400 W).

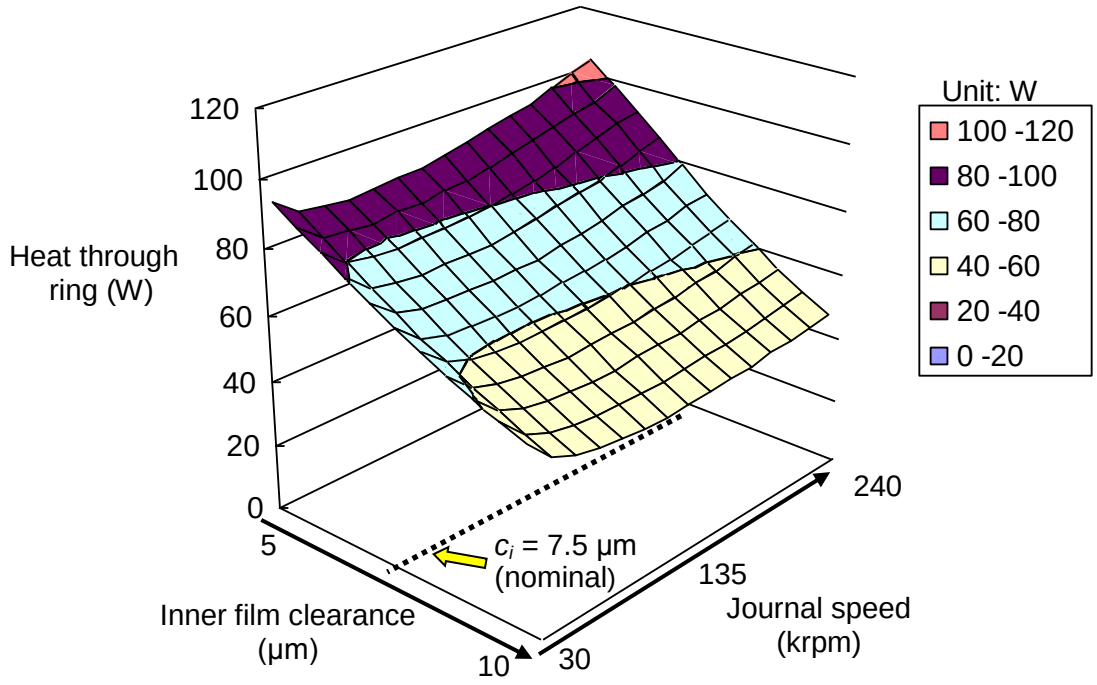


**Figure 55. Influence of inner film clearance ($c_i$) on the heat flow through the ring. $c_o$ = 35 μm (nominal). Shaft speed = 90 krpm and 240 krpm, static load = 0.9 N. $P_{SUP}$ = 4.0 bar, $T_{SUP}$ = 120 °C.**

Figure 57 presents the effect of the inner film clearance ($c_i$) on both the average inner film temperature and the peak film temperature for operation at 240 krpm and at $T_{SUP}$ = 120 ℃. The predictions show that as $c_i$ increases, both the average temperature and the peak temperature of the inner film decrease steadily. This happens due to the larger flow rate through the inner film region. Furthermore, it deserves attention to note that when $c_i$ is less than 6 μm the peak temperature of the inner film is higher than the shaft temperature (213 ℃), indicating the hottest part of the film region convects heat

into the journal instead of carrying heat from it. Note that the outer film temperature is influenced only slightly by the inner film clearance.

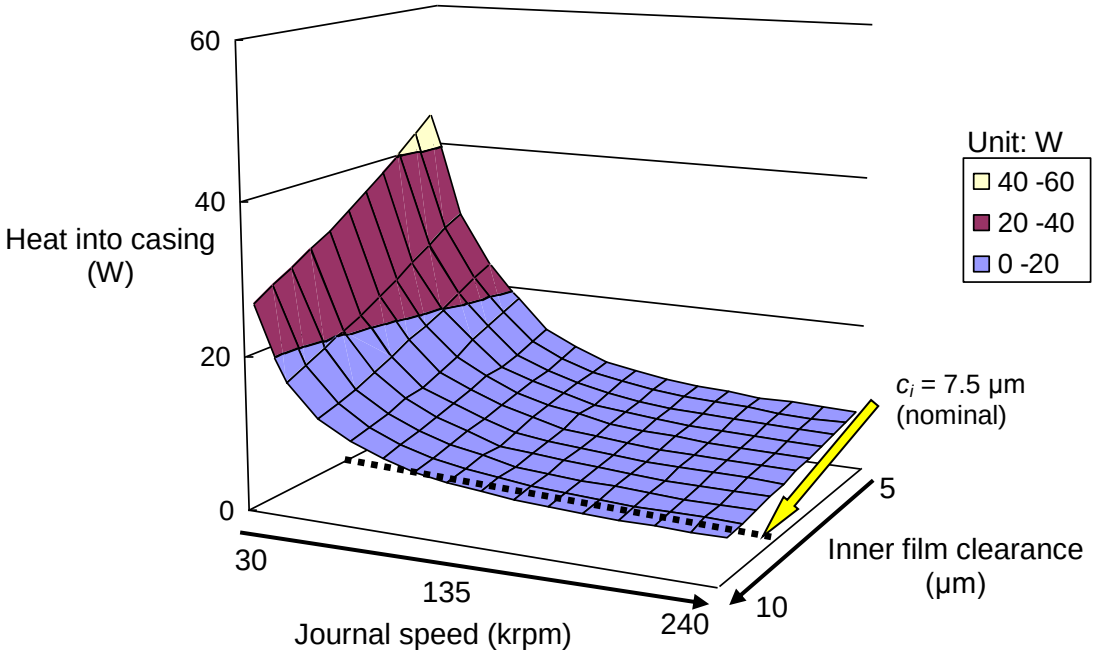


**Figure 56. Influence of inner film clearance ($c_i$) on the heat flow into the casing. $c_o$ = 35 µm (nominal). Shaft speed = 90 krpm and 240 krpm, static load = 0.9 N. $P_{SUP}$ = 4.0 bar, $T_{SUP}$ = 120 °C.**

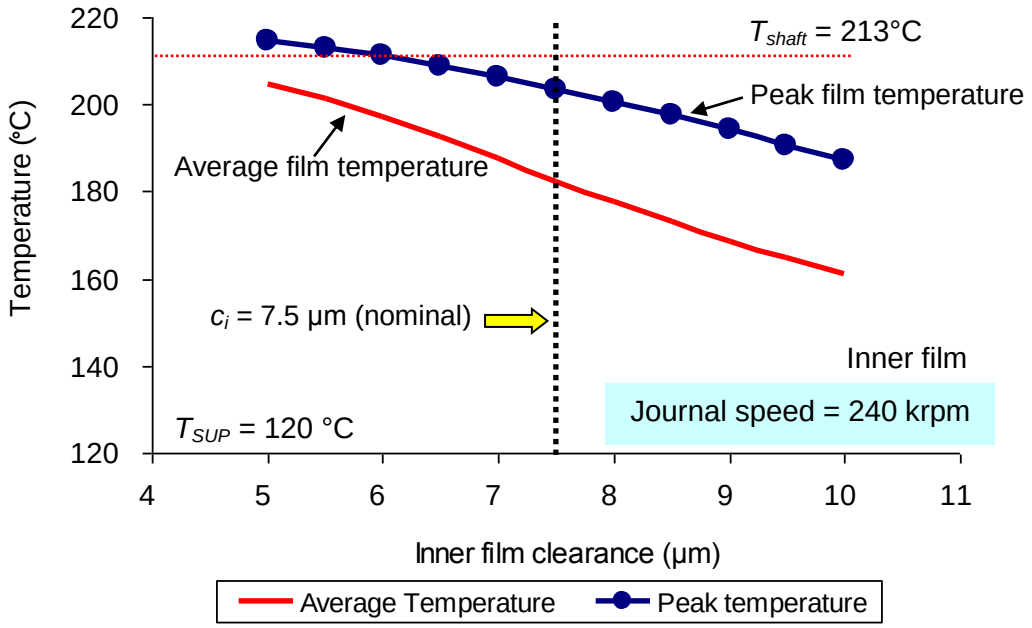


**Figure 57. Influence of inner film clearance ($c_i$) on the average and the maximum film temperatures of the inner film. Nominal $c_o$ = 35 µm. Shaft speed = 240 krpm, $P_{SUP}$ = 4.0 bar, $T_{SUP}$ = 120 °C. Static load = 0.9 N. $T_{shaft}$ = 213°C.**

In conclusion, as the inner film clearance[35] (nominal value = 7.5 µm) increases from 5 µm to 10 µm, the flow rate through the inner film region increases nearly by 5 times. This larger flow rate increases both the heat flow from the journal and the drag power loss in the inner film, thus increasing the thermal energy carried by the inner film. Additionally, a larger $c_i$ steadily reduces the peak temperature and the average temperature of the inner film.

[35] The bearing operating temperature influences the film clearance. The inner film clearance stated here refers to the one at room temperature (~20 ℃).

**Influence of the Number of Axial Grooves**

Figure 58 presents the influence of the number of axial grooves on the average and peak temperatures of the inner film with oil supplied at pressure $P_{SUP}$ = 4 bar and at temperature $T_{SUP}$ = 120 ℃. The graph shows that additional axial grooves[36] (more than the nominal four) on the ring inner surface can steadily lower both the average temperature and the peak film temperature in the inner film for operation at the highest journal speed (240 krpm), since additional supply holes deliver a larger flow rate into the inner film. Note that the outer film temperature is influenced slightly by the number of axial grooves, and not shown in Figure 58 for brevity.

Figure 59 shows the effect of the number of axial grooves on the flow rate through the inner film region for operation at two journal speeds, 90 krpm and 240 krpm. The predictions show that the flow rate is almost linearly proportional to the number of axial grooves on the inner surface of the ring. This occurs since each axial groove has its own supply hole, whose diameter is equal to the groove width.

[36] Machining more grooves increases the product cost. The regular number of axial grooves for an axisymmetric configuration ranges from 3 to 6. For this study, the range expands from 2 to 7.

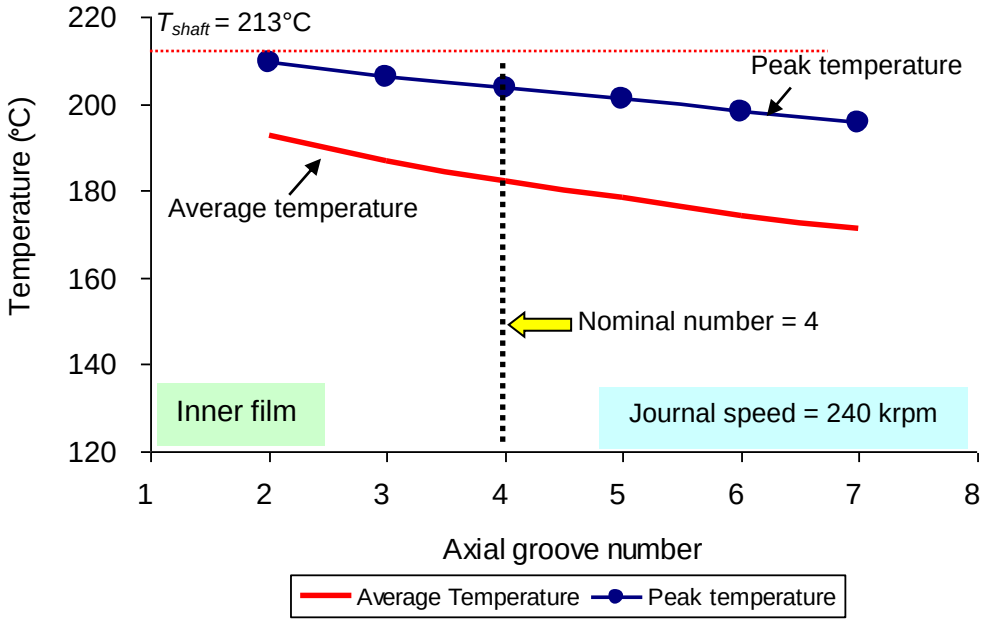


**Figure 58. Influence of number of axial grooves on the average and maximum temperatures of the inner film. Shaft speed = 240 krpm, static load = 0.9 N. $P_{SUP}$ = 4.0 bar, $T_{SUP}$ = 120 °C. Nominal $c_i$ = 7.5 µm, $c_o$ = 35 µm. $T_{shaft}$ = 213°C.**

Figure 60 shows the effect of the number of axial grooves on the drag power loss as the journal speed increases from 30 krpm to 240 krpm with oil inlet pressure $P_{SUP}$ = 4 bar and temperature $T_{SUP}$ = 120 ℃. At high journal speeds, the drag power loss steadily increases with the number of axial grooves. This occurs because the oil viscosity increases for a decreasing film temperature (see Figure 58). Note that adding axial grooves reduces the film area where the drag power loss takes place. Nevertheless, the effect of an increasing oil viscosity overweighs the effect of a decreasing film area.

For the same operating condition, Figure 61 presents the influence of the number of axial grooves on the heat flowing from the journal over the journal speed range (30 krpm ~ 240 krpm). Additional axial grooves can considerably increase the heat flow from the hot shaft. This occurs due to the larger flow rate, which facilitates the removal of more thermal energy. Note that although the lubricant flow rate through the inner film region for operation at 90 krpm is lower than that for operation at 240 krpm (see Figure 59), the heat flowing from the journal at 90 kprm is larger. This occurs because more drag power loss is generated at the high journal speed (240 krpm), causing the inner film temperature to increase, and then the heat flow from the journal (213 ℃) decreases.

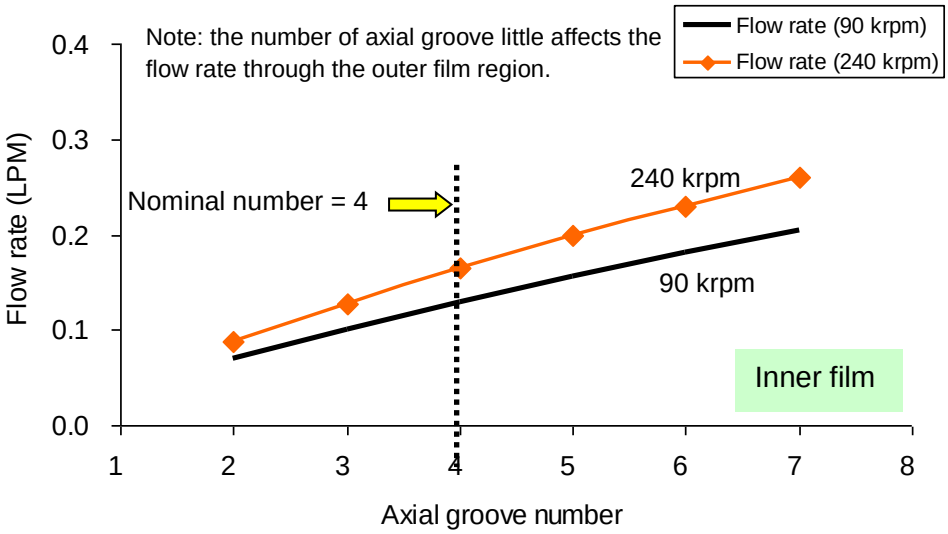


**Figure 59. Influence of number of axial grooves on the flow rate through the inner film clearance. Shaft speed = 90 krpm and 240 krpm, static load = 0.9 N. $P_{SUP}$ = 4.0 bar, $T_{SUP}$ = 120 °C. Nominal $c_i$ = 7.5 μm, $c_o$ = 35 μm. $T_{shaft}$ = 213°C.**

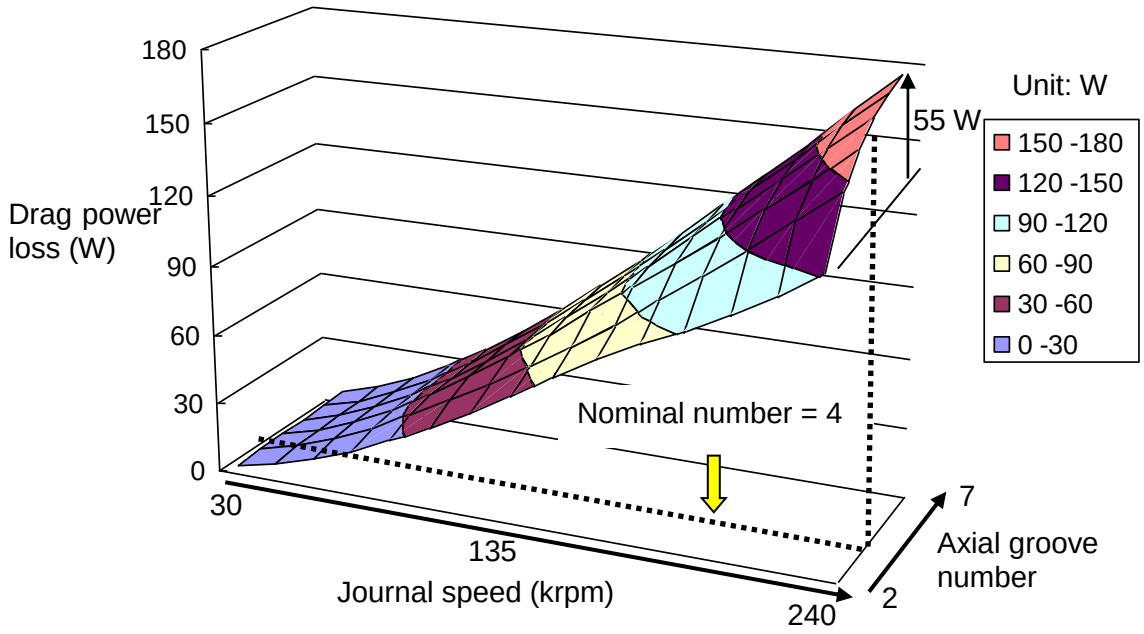


**Figure 60. Influence of number of axial grooves on the drag power loss. Shaft speed = 30 krpm ~ 240 krpm, static load = 0.9 N. $P_{SUP}$ = 4.0 bar, $T_{SUP}$ = 120 °C.**

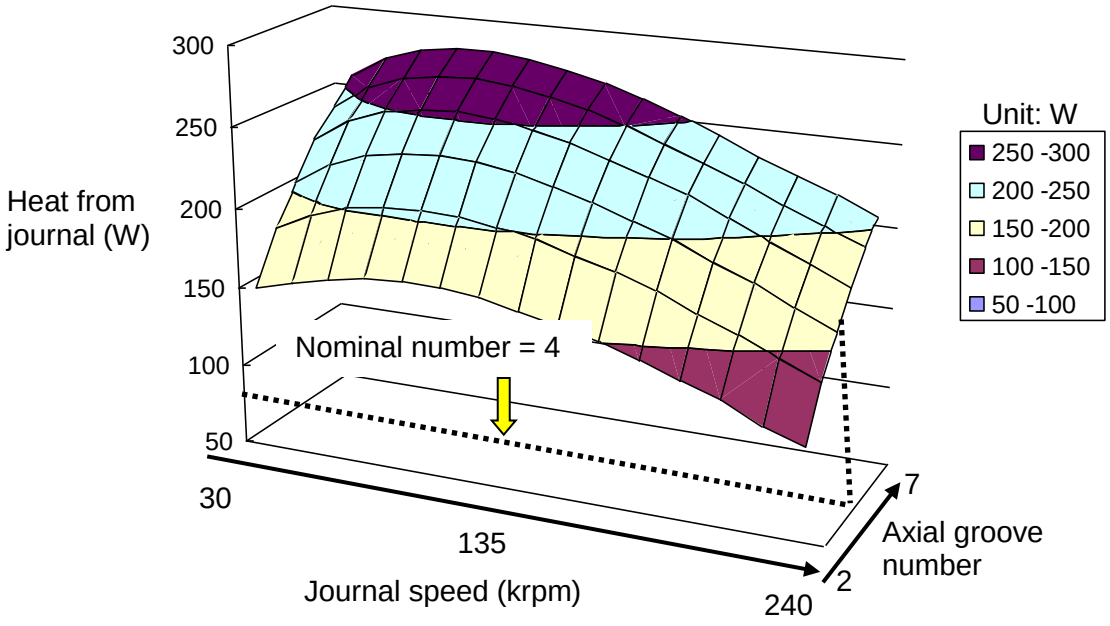


**Figure 61. Influence of number of axial grooves on the heat flow from journal. Shaft speed = 30 krpm ~ 240 krpm, static load = 0.9 N. $P_{SUP}$ = 4.0 bar, $T_{SUP}$ = 120 °C.**

Figure 62 presents the total energy (drag power loss plus heat flow) carried by the inner film versus number of axial grooves for a journal speed range (30 kprm ~ 240 krpm). The predictions show that the maximum thermal energy carried by the inner film takes place for operation at the maximum journal speed (240 krpm) and with the seven axial grooves. This occurs because the drag power loss generated in the inner film is the largest and its increase with journal speed is larger than the decrease of heat flowing from the journal for an increasing journal speed. Note that the number of axial grooves slightly affects the heat flow conducted through the ring (~ 60 W), which is much less than the thermal energy carried away by the inner film.

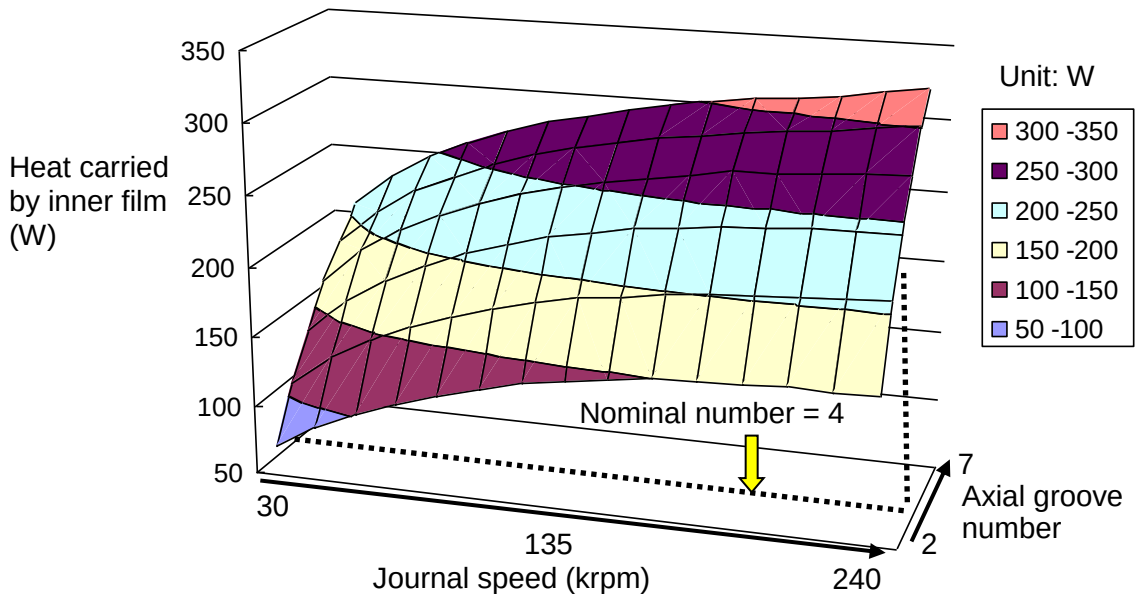


**Figure 62. Influence of number of axial grooves on the heat flow carried by the inner film. Shaft speed = 30 krpm ~ 240 krpm, static load = 0.9 N. $P_{SUP}$ = 4.0 bar, $T_{SUP}$ = 120 °C.**

### Influence of the Size of Axial Grooves

The flow through the inner film region carries away most of the heat generated and also transferred from the shaft. It is reasonable to assume that alterations in the configuration related to the outer film will have small effects not only on the thermal energy advected by the inner film, but also on the drag power loss and the peak temperature in the (S)FRB. Hence, the geometry of the ½ moon groove (on the casing

inner surface) and the circumferential groove (on the ring outer surface) remain the same. The following study focuses on the dimensions of the depth and width of the four axial grooves on the ring inner surface. The four (nominal) axial grooves share the same dimensions.

*Influence of axial groove depth*

Figure 63 presents the influence of the groove depth[37] on the flow rate through the inner film region for operation at two journal speeds (90 krpm and 240 krpm) and with $P_{SUP}$ at 4 bar and $T_{SUP}$ at 120 ℃. The results show that the flow rate through the inner film region increases significantly for an increasing groove depth. This occurs because a deeper groove has a less flow resistance. For instance, if there is no axial groove (groove depth = 0), the film area becomes larger that results in more drag power loss, and the flow rate through the inner film region is too small (~ 0.01 LPM) to effectively remove heat from the hot journal, so that the peak temperature of the inner film is higher than the shaft temperature (see Figure 64). Note that the flow rate shown in Figure 63 refers to the sum of the oil flow rate through the film land[38] region and the amount directly evacuated through the axial groove.

[37] The groove depth changes according to the operating temperature. The variable "groove depth" discussed here is at 20 ℃.

[38] Film land region refers to the region without grooves, and its film thickness is not related with the groove depth.

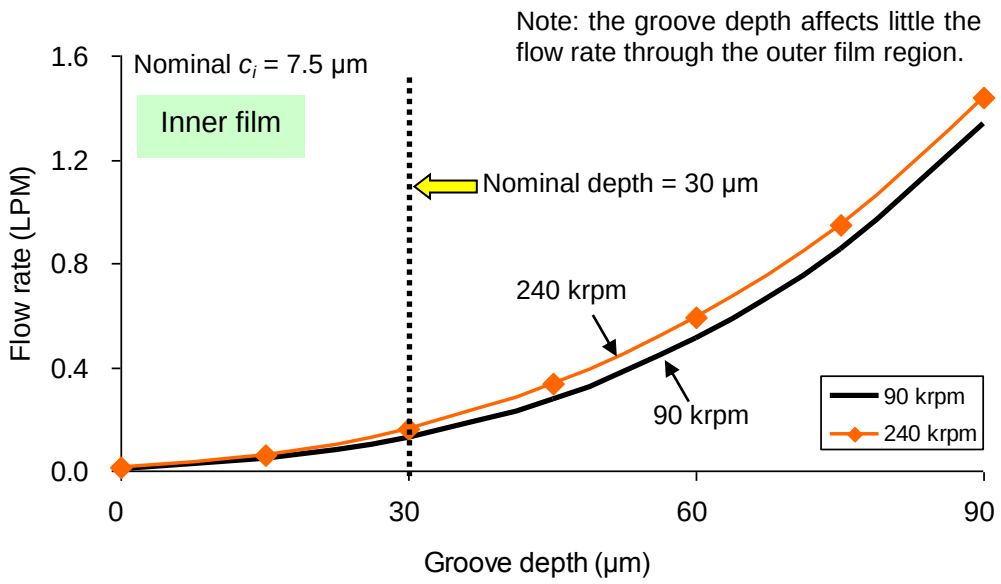


**Figure 63. Influence of groove depth on the flow rate through the inner film clearance. Shaft speed = 90 krpm and 240 krpm, static load = 0.9 N. $P_{SUP}$ = 4.0 bar, $T_{SUP}$ = 120 °C. Nominal $c_i$ = 7.5 μm, $c_o$ = 35 μm. $T_{shaft}$ = 213°C.**

Figure 64 shows the influence of the groove depth on the average and peak temperatures of the inner film for operation at 240 krpm and at $T_{SUP}$ = 120 ℃. The results show that both the average and peak temperatures of the inner film decrease steadily for an increasing groove depth due to the ensuring larger flow rate. The graph also shows that the rate of decrement for the average temperature slows once the groove depth exceeds twice the nominal value. This occurs because the oil viscosity increases as the film temperature decreases for a larger groove depth, thus leading to an increase in the drag power loss. In addition, if there is no axial groove, the peak temperature is

higher than the shaft temperature, indicating the hottest part of film region convects heat into the journal instead of carrying heat from it.

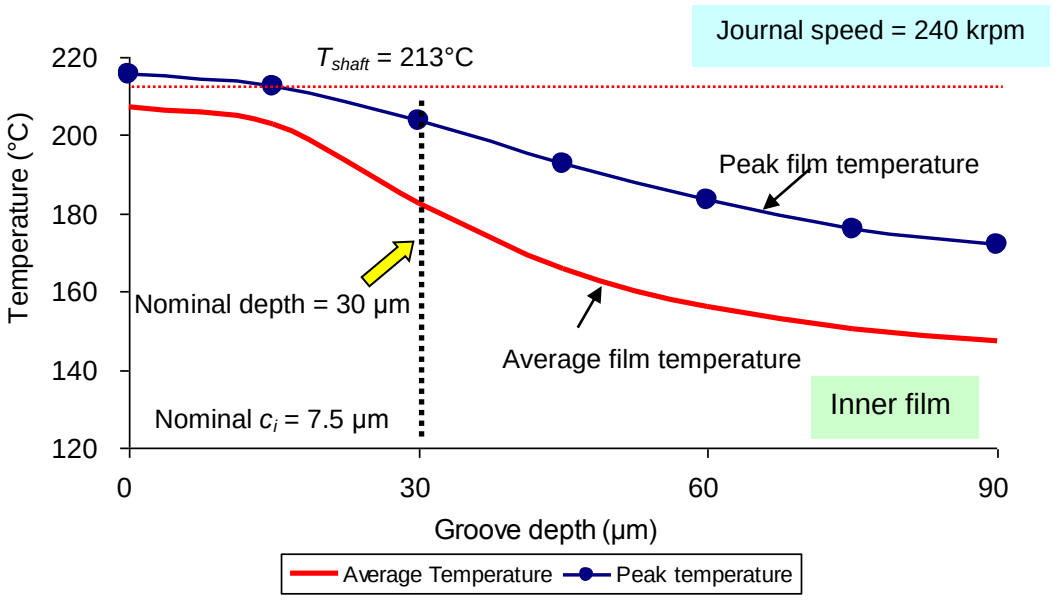


**Figure 64. Influence of axial groove depth on the maximum film temperatures of the inner film. Shaft speed = 240 krpm, static load = 2.0 N. $P_{SUP}$ = 4.0 bar, $T_{SUP}$ = 120 °C. Nominal $c_i$ = 7.5 μm, $c_o$ = 35 μm. $T_{shaft}$ = 213°C. Groove number = 4.**

Figure 65 depicts the effect of the groove depth on the drag power loss for the journal speed range (30 krpm ~ 240 krpm) with oil supplied at $P_{SUP}$ = 4 bar and $T_{SUP}$ = 120 ℃. The predictions show that the drag power loss not only steadily grows for an increasing journal speed, but also dramatically increases as the groove depth becomes larger at high journal speeds. The increase of drag power loss with the groove depth is due to a larger oil viscosity since the film temperature decreases.

For the same operating conditions, Figure 66 shows the influence of groove depth on the drag power drag loss at two journal speeds (90 krpm and 240 krpm). The results show that at the high journal speed, the power loss first declines when the groove depth is shallow (half of the nominal value, at ~15μm). The reduction results from the decrease in the average fluid velocity[39] through the inner film clearance as the groove depth increases because of a larger oil viscosity and a smaller film thickness. The decrease in the flow velocity causes the drag power loss to also decrease. Note that the oil viscosity becomes larger with groove depth, but its effect on increasing the drag power loss is not large enough to overweigh the negative effect of the reduced fluid velocity. Hence, the drag power loss starts to decrease as the groove depth grows, and then increases quickly since the oil viscosity largely increases due to a significant decrease in the oil temperature (see Figure 64). On the other hand, for the low journal speed (90 krpm), the groove depth has no influence on the drag power loss. This power loss is much lesser than that at the high shaft speed (240 krpm).

[39] Recall Eqn. (6) in a prior section, the average fluid velocities along the circumferential and axial directions are $U = -\frac{h_i^2}{12\mu_i}\frac{\partial P_i}{R_J \partial \theta} + \frac{1}{2}(U_S + U_R)$ and $W = -\frac{h_i^2}{12\mu_i}\frac{\partial P_i}{\partial z_i}$, respectively.

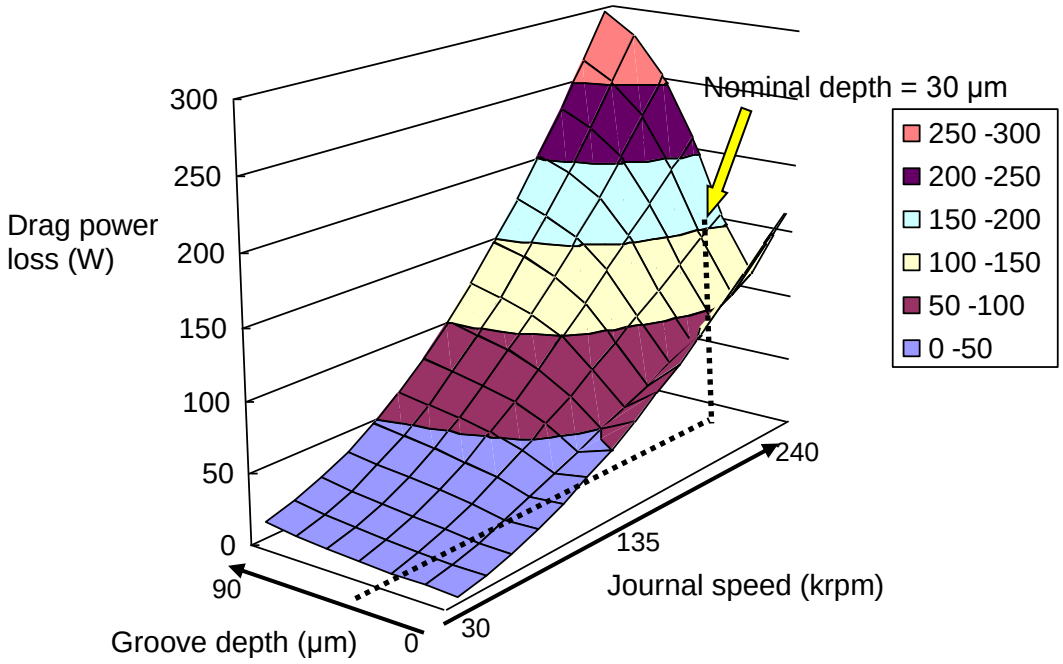


**Figure 65. Influence of axial groove depth on drag power loss. Shaft speed = 30 krpm ~ 240 krpm, static load = 0.9 N. $P_{SUP}$ = 4.0 bar, $T_{SUP}$ = 120 °C. Nominal $c_i$ = 7.5 μm, $c_o$ = 35 μm. Groove number = 4.**

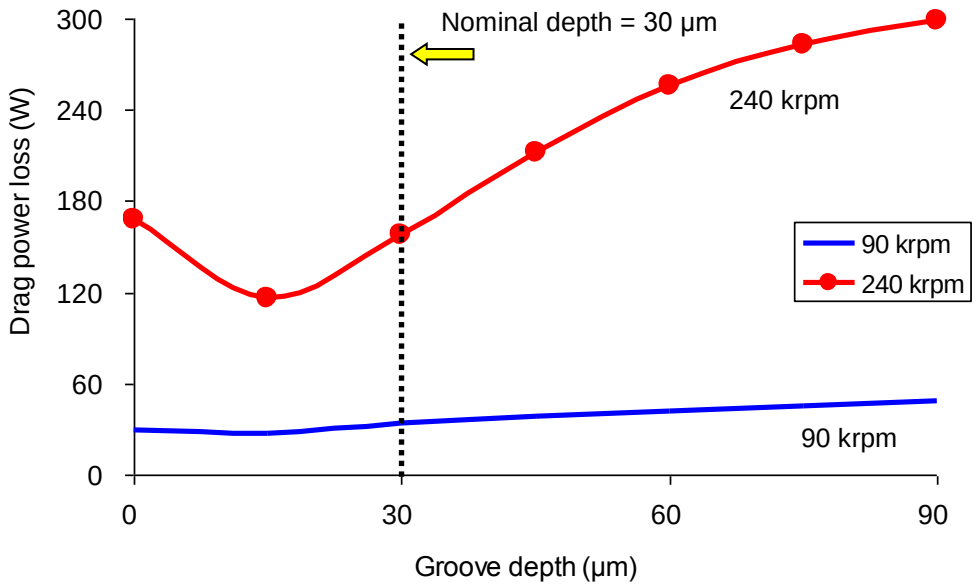


**Figure 66. Influence of axial groove depth on drag power loss. Shaft speed = 90 krpm and 240 krpm, static load = 0.9 N. $P_{SUP}$ = 4.0 bar, $T_{SUP}$ = 120 °C. Nominal $c_i$ = 7.5 μm, $c_o$ = 35 μm. Groove number = 4.**

For the same operating condition ($P_{SUP}$ = 4 bar, $T_{SUP}$ = 120 ℃), Figure 67 shows the effect of the groove depth on the heat flowing from the journal for the journal speed range (30 krpm ~ 240 krpm). The predictions indicate that the heat flowing from the journal steadily increases with the groove depth[40], since the average inner film temperature steadily decreases (see Figure 64). In addition, as the journal speed increases from 30 krpm to 240 krpm, the heat flowing from the journal keeps increasing for large groove depths, but steadily decreases when the groove depth is nil. This occurs

[40] Note that in the oversimplified shaft model, the shaft temperature remains at 213 ℃.

because the flow resistance of the groove declines as its depth increases, so that more oil flows through the groove land and carries away more thermal energy, causing the oil temperature in the groove to decrease. Incidentally, it is reasonable to conclude that the maximum total thermal energy the inner film advects takes place for operation at the maximum journal speed (240 krpm) with the largest groove depth.

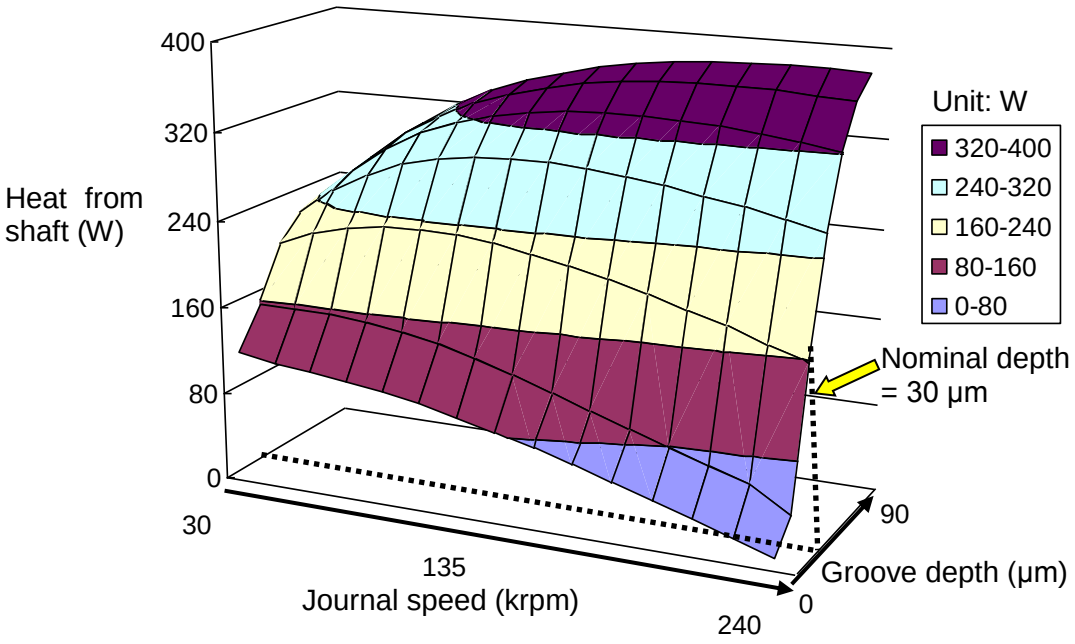


**Figure 67. Influence of axial groove depth on heat flow from the journal. Shaft speed = 30 krpm ~ 240 krpm, static load = 0.9 N. $P_{SUP}$ = 4.0 bar, $T_{SUP}$ = 120 °C. Nominal $c_i$ = 7.5 μm, $c_o$ = 35 μm. Groove number = 4.**

Figure 68 shows the influence of the groove depth on the operating inner film clearance for operation at two journal speeds (90 krpm and 240 krpm) with oil supplied at pressure $P_{SUP}$ = 4 bar and temperature $T_{SUP}$ = 120 ℃. The graph shows the inner film clearance decreases with an increasing groove depth for both journal speeds. This occurs because both the inner film temperature and the temperature of the ring inner surface decrease as the groove depth becomes larger. Since the thermal coefficient of brass ring is higher than that of the iron shaft[41], the ring inner surface experiences a larger thermal shrink than the shaft as the inner film temperature decreases. As a result, the inner film clearance becomes smaller for an increasing groove depth.

Figure 69 shows the effect of the groove depth on the heat flows disposed both through the ring and into the casing for the two journal speeds. The graph shows that the heat flow conducted through the ring decreases steadily as the groove depth grows. This occurs because the larger flow rate through the inner film due to a larger groove depth carries away more heat transferred from the hot shaft. However, the groove depth only influences slightly the heat flow into the casing, so that the heat flow entering the outer film decreases with a deeper axial groove.

[41] The shaft temperature remains constant at 213 ℃.

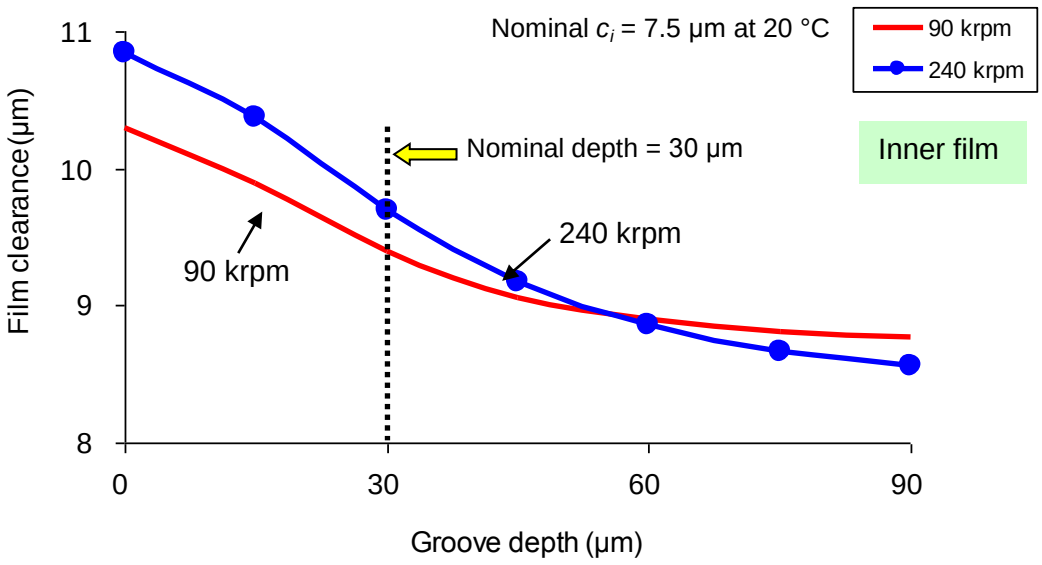


**Figure 68. Influence of axial groove depth on the inner film clearance. Journal speed = 90 krpm and 240 krpm, static load = 0.9 N. $P_{SUP}$ = 4.0 bar, $T_{SUP}$ = 120 °C. Nominal $c_i$ = 7.5 µm, $c_o$ = 35 µm. Groove number = 4.**

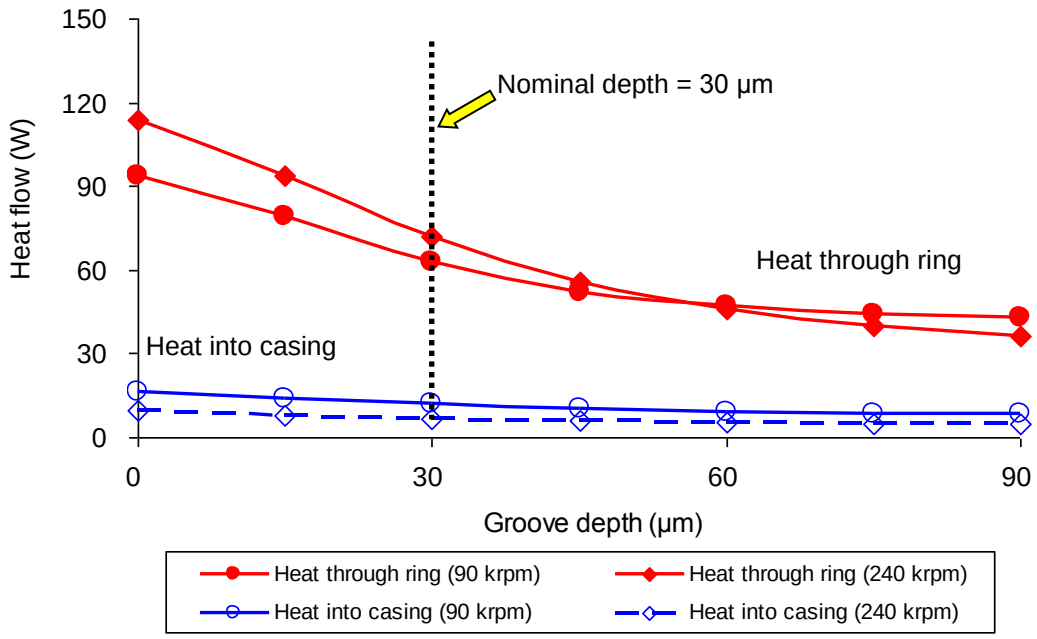


**Figure 69. Influence of axial groove depth on heat flows through the ring and into the casing. Shaft speed = 90 krpm and 240 krpm, static load = 0.9 N. $P_{SUP}$ = 4.0 bar, $T_{SUP}$ = 120 °C. Nominal $c_i$ = 7.5 μm, $c_o$ = 35 μm. Groove number = 4.**

*Influence of axial groove width*

Figure 70 shows the effect of axial groove width on the flow rate through the inner film region for operation at two journal speeds (90 krpm and 240 krpm) with oil inlet pressure $P_{SUP}$ = 4 bar and temperature $T_{SUP}$ = 120 ℃. The graph shows that the total flow rate, which sums the flow rates though both the groove and the land region, steadily increases for a larger groove depth. As the groove width increases, the flow resistance of

the groove decreases, so that the flow rate through the groove increases while the one through the land region declines. This conclusion is supported by the predictions that the film thickness decreases for a larger groove depth (see Figure 74). Note that the diameter of the supply hole is the same with the width of the axial groove.

Figure 71 shows the influence of axial groove width on the average and the peak temperatures in the inner film for operation at the maximum journal speed (240 krpm) with oil supplied at 120 ℃. The graph shows that a larger groove width can lower moderately both the average and peak temperature of the inner film.

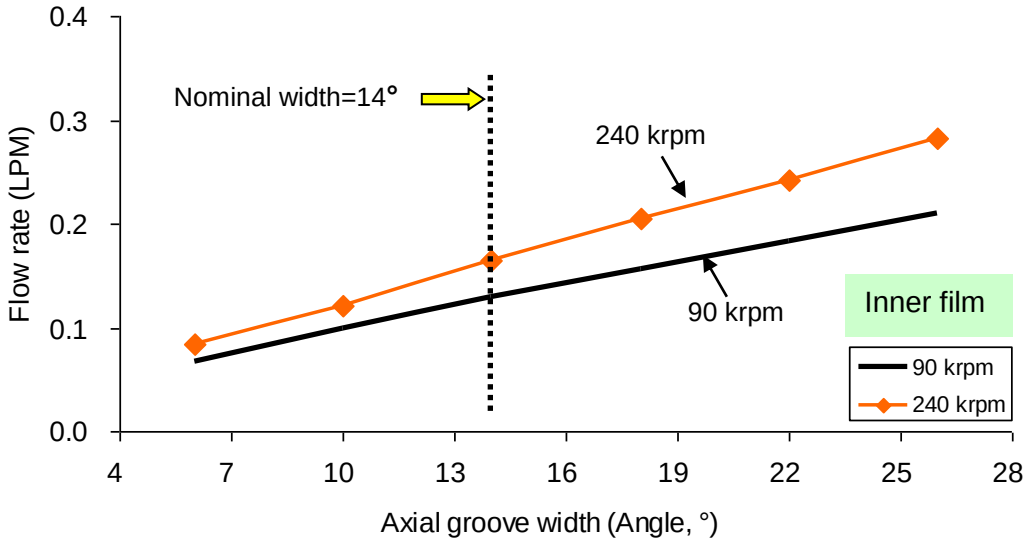


**Figure 70. Influence of groove width on the flow rate through the inner film region. Shaft speed = 90 krpm and 240 krpm, static load = 0.9 N. $P_{SUP}$ = 4.0 bar, $T_{SUP}$ = 120 °C. Nominal $c_i$ = 7.5 μm, $c_o$ = 35 μm. $T_{shaft}$ = 213°C.**

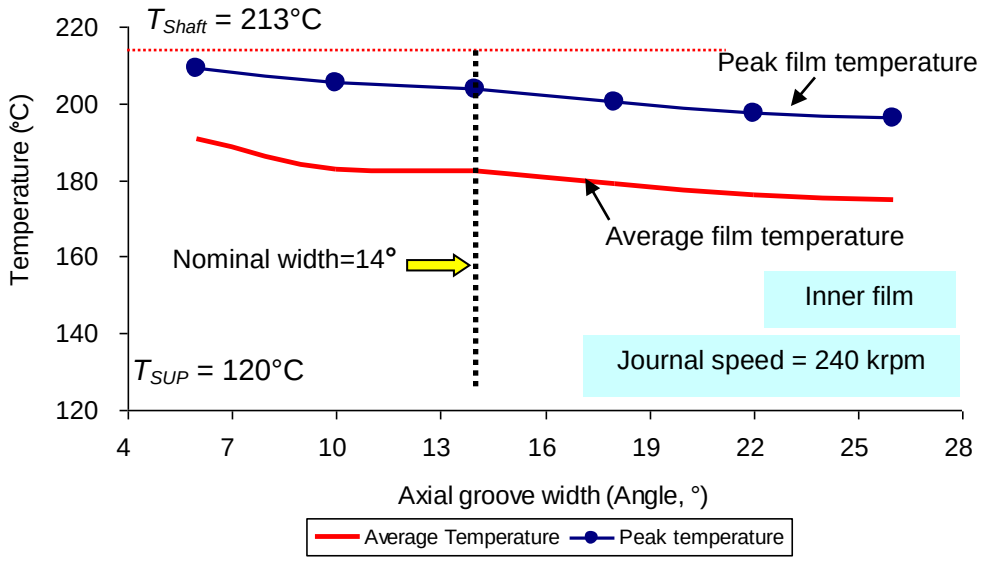


**Figure 71. Influence of axial groove width on the maximum and average film temperatures of the inner film. Shaft speed = 240 krpm, static load = 2.0 N. $P_{SUP}$ = 4.0 bar, $T_{SUP}$ = 120 °C. Nominal $c_i$ = 7.5 μm, $c_o$ = 35 μm. $T_{shaft}$ = 213°C. Groove number = 4.**

Figure 72 shows the influence of (S)FRB inner axial groove width on the drag power loss for the journal speed range (30 krpm ~ 240 krpm) with oil inlet pressure $P_{SUP}$ = 4 bar and temperature $T_{SUP}$ = 120 ℃. The predictions show that the drag power loss decreases as the axial groove becomes larger. This occurs because the growth of the groove width causes the area of film region (where the drag power loss is generated) to decrease. In addition, the decrease in the average flow velocity through the inner film region is another factor that results in less drag power loss, since the film clearance deceases as the groove depth increases. The effects that could reduce the drag power loss

overweigh the effect of the moderate increase in the oil viscosity for the decreasing oil temperature.

Recall that, for the same operating condition, the results in Figure 65 predict that the drag power loss increases for a larger groove depth, while the results in Figure 72 show that the drag power loss decreases for a larger groove width. This discrepancy can be explained by the difference in the influence of the groove depth and width on the oil viscosity. A groove with a larger depth can deliver a larger flow rate into the inner film than a groove with a larger width, so the decrease in the average film temperature for a larger groove depth (~ 60 ℃, see Figure 64) is much larger than that decrease for a larger groove width (~15 ℃, see Figure 71), thus resulting in a larger oil viscosity. Albeit the flow rate flowing into the film land region decreases for either a deeper groove or a wider groove, a much larger oil viscosity for a deeper groove eventually causes the drag power loss to grow.

For the same operating condition ($P_{SUP}$ = 4 bar, $T_{SUP}$ = 120 ℃), Figure 73 shows the influence of axial groove width on the heat flowing from the journal as the journal speed increases from 30 krpm to 240 krpm. Since the average inner film temperature moderately decreases as the axial groove widens (see Figure 71), the heat flowing from the journal whose temperature remains at 213 ℃ decreases.

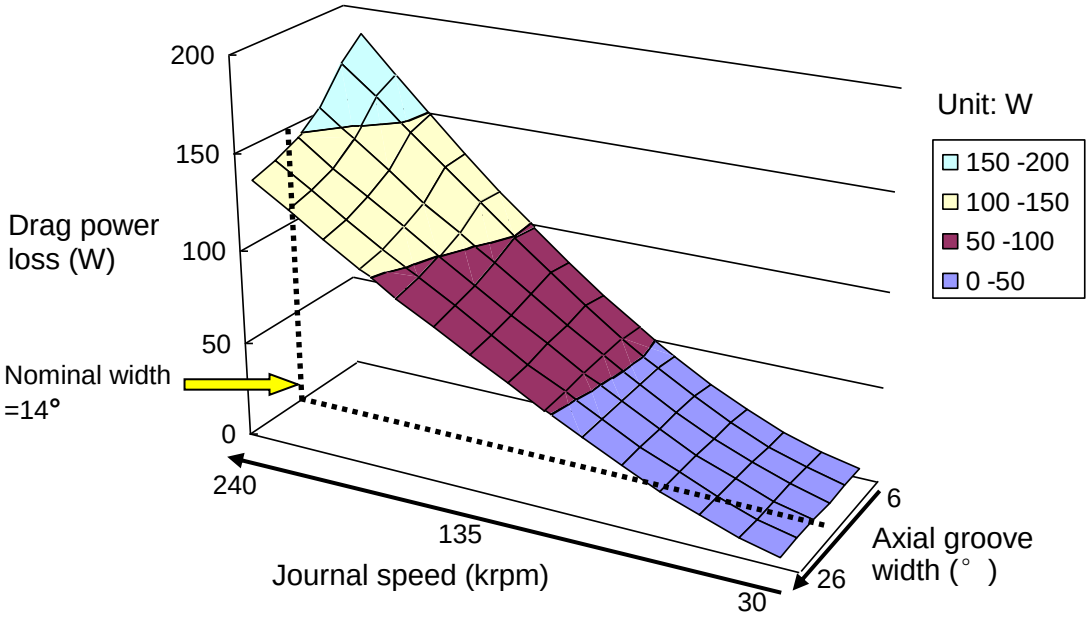


**Figure 72. Influence of axial groove width on drag power loss. Journal speed = 30 krpm ~ 240 krpm, static load = 0.9 N. $P_{SUP}$ = 4.0 bar, $T_{SUP}$ = 120 °C. $c_i$ = 7.5 μm, $c_o$ = 35 μm. Groove number = 4.**

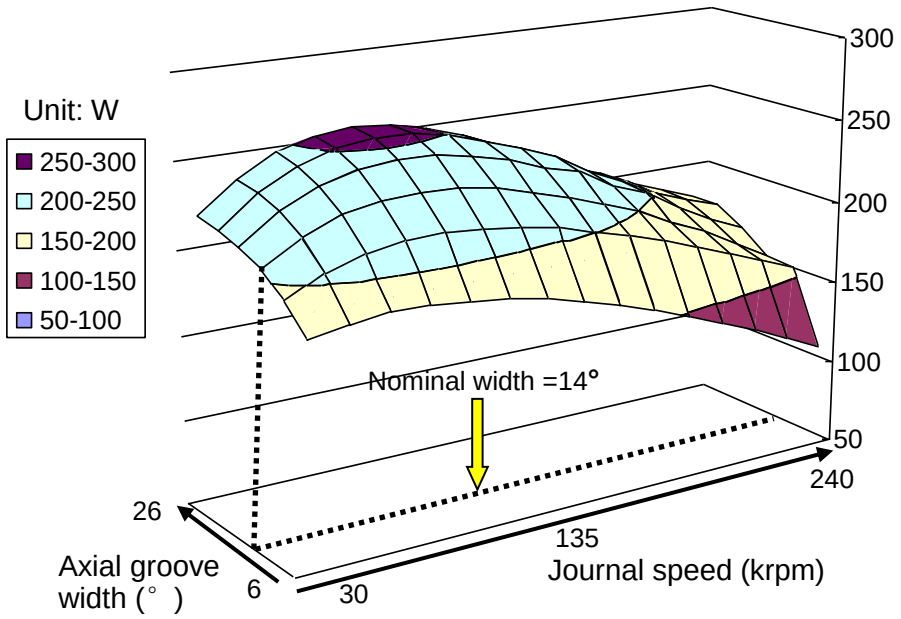


**Figure 73. Influence of axial groove width on heat flow from the journal. Journal speed = 30 krpm ~ 240 krpm, static load = 0.9 N. $P_{SUP}$ = 4.0 bar, $T_{SUP}$ = 120 °C. $c_i$ = 7.5 μm, $c_o$ = 35 μm. Groove number = 4.**

Figure 74 shows the influence of the groove width on the operating inner film clearance for operation at two journal speeds (90 krpm and 240 krpm) when oil is supplied at $P_{SUP}$ equal to 4 bar and at $T_{SUP}$ equal to 120 ℃. The graph shows that the inner film clearance decreases with an increasing groove width for both journal speeds. This occurs because the film temperature and thus the temperature of the ring inner surface decrease for a larger groove width. Since the thermal expansion coefficient of the ring is greater than that of the shaft, the inner film clearance decreases with groove width.

Figure 75 shows the effect of the groove width on the heat flows both through the ring and into the casing for the two journal speeds. The graph shows that the heat through the ring decreases for increasing groove width, but the heat into the casing is slightly influenced by the groove width. As a result, the thermal energy that heats the outer film decreases.

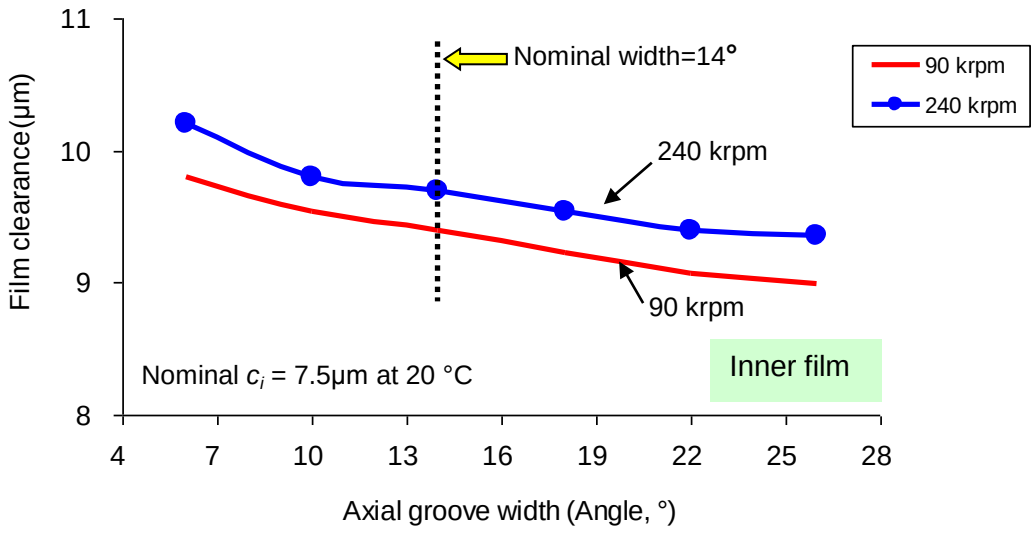


**Figure 74. Influence of axial groove width on the operating inner film clearance. Journal speed = 90 krpm and 240 krpm, static load = 0.9 N. $P_{SUP}$ = 4.0 bar, $T_{SUP}$ = 120 °C. Nominal $c_i$ = 7.5 μm, $c_o$ = 35 μm. Groove number = 4.**

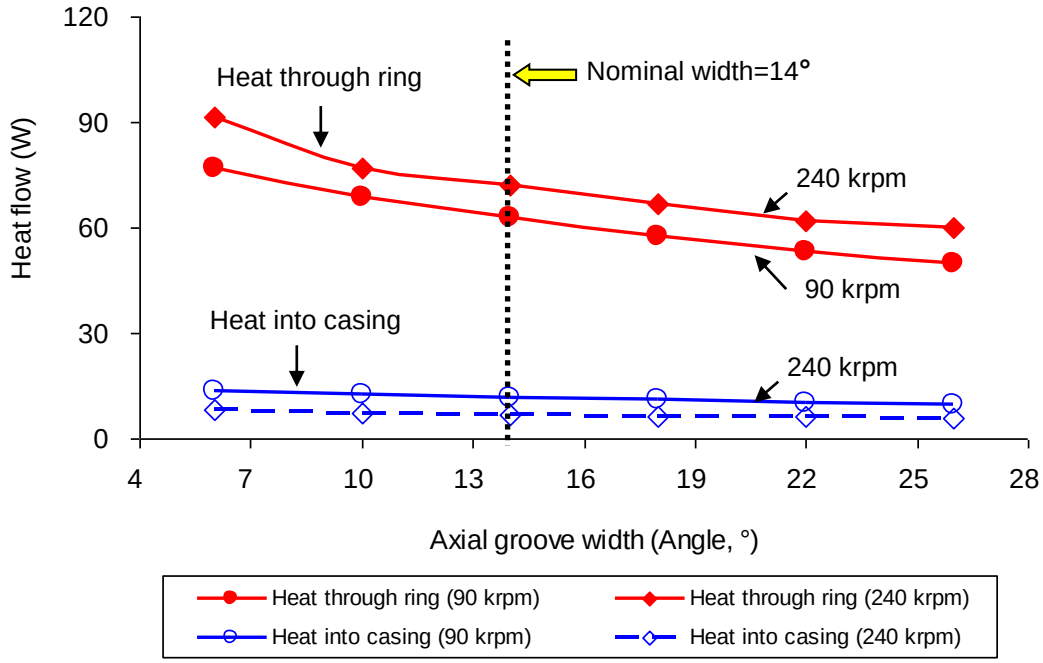


**Figure 75. Influence of axial groove width on heat flows through the ring and into the casing. Journal speed = 90 krpm and 240 krpm, static load = 0.9 N. $P_{SUP}$ = 4.0 bar, $T_{SUP}$ = 120°C. $c_i$ = 7.5 μm, $c_o$ = 35 μm. Groove number = 4.**

To sum, either a deeper groove or a wider groove reduces the flow resistance of the groove, evacuating more oil through the groove but decreasing the flow rate through the film land region. More lubricant flowing out of the bearing aids to remove more thermal energy from it, which results in effectively lowering the average film temperature and thus increasing the oil viscosity. Hence, the drag power loss in the film steadily grows as the groove depth increases. However, as the axial groove widens, the moderate increase of the oil viscosity cannot overweigh the effect of the decreasing film

area, the drag power loss decreases as the groove width becomes larger. Since the decrease in the average film temperature as the groove depth increases larger than that with an increasing groove width, the increase in the heat flowing from the journal for a deeper groove is larger, and thus more thermal energy will be carried by the inner film.

The results indicate that deepening or widening an axial groove does not act beneficially on the (S)FRB, not only raising the cost of manufacturing, but also reducing the lubricant flowing over the film land region. A larger groove depth also dramatically increases the drag power loss, which lowers the TC efficiency.

## Closure

This chapter discusses the influence of lubricant supply conditions ($T_{SUP}$, $P_{SUP}$) and the bearing configurations (film clearances, the number of axial grooves and its dimensions) on the (S)FRB performances, i.e., cooling performance, drag power loss, peak film temperature, etc. The improvement in one performance characteristic usually trades off with another one.

The effects of the lubricant supply condition and the groove dimensions on the (S)FRB performance parameters are summarized below.

1) Lubricating a (S)FRB with a lower inlet temperature ($T_{SUP}$) leads to an increase the heat flow from the journal, particularly at low journal speeds, but it cannot effectively reduce the peak temperature in the inner film since the heat flow from the hot journal, whose temperature is constant at 213 ℃, is

overwhelming. Hence, most of the temperature field in the inner film is strongly influenced by the shaft temperature rather than $T_{SUP}$. $T_{SUP}$ also has a negligible effect on the drag lower loss, because the supply temperature is only felt near the oil inlet as lubricant heats quickly elsewhere in the inner film.

2) Supplying lubricant at a higher oil supply pressure ($P_{SUP}$) effectively promotes the heat flow from the journal and increases the drag power loss to a minor extent. The average and peak temperatures of the inner film decreases for an increasing $P_{SUP}$. The thermal energy entering the outer film decreases.

3) An increase in the inner film clearance increases the heat flow from the journal, but this effect weakens at higher journal speeds. The drag power loss increases as an inner film clearance grows due to an increase in the average velocity of the film flow rate. A larger inner film clearance can significantly reduce the average and peak temperatures of the inner film.

4) Additional (more than four) axial grooves in the ring ID surface deliver more lubricant into the inner film and thus steadily reduce the average and peak temperatures of the inner film, leading to an increase in the heat flowing from the journal. The drag power loss also increases with more axial grooves, since the oil viscosity increases as the average film temperature decreases. Therefore, the total energy carried by the inner film grows. The heat flow through the ring decreases, causing the thermal energy advected by the outer film to decrease.

5) The (S)FRB has an inner film geometry with four radial holes and four axial grooves. An increase in the depth of an axial groove causes the peak and average temperatures of the inner film to quickly drop. At the highest journal speed the drag power loss increases for a larger groove depth due to a larger oil viscosity. The heat flow from the shaft keeps increasing with groove depth. The thermal energy carried away the inner film also increases with groove depth, but the heat flow through the ring decreases.

6) An increase in the axial groove width moderately reduces the peak and average temperatures of the inner film. A larger groove width also causes the drag power loss to decrease at high journal speeds as the area of film land region decreases. However, the heat flow from the journal and the thermal energy advected by the inner film increases with an increasing groove width.

# 8. CONCLUSIONS

An effective thermal management is paramount to ensure reliable turbocharger (TC) operation. Significant sources for thermal energy include heat flowing from a hot shaft and the drag power dissipations in the fluid films. A thermo hydrodynamic (THD) model for a (semi) floating ring bearing is developed to predict the hydrodynamic pressure and temperature fields and the distribution of thermal energy flows occurring in the bearing system. The lubricant flows must carry away most of the thermal energy.

The THD model not only predicts the pressure field in each fluid film along the circumferential and axial directions, but also produces the temperature fields in both films. A finite element heat conduction model of the floating ring predicts its temperature distribution along the circumferential and radial directions and produces the heat flow conducted through the ring. Temperature-dependent oil viscosity and film clearances are both updated during the iterative process.

The thermohydrodynamic model for a (semi) floating ring bearing is adapted to simulate the thermal energy transport in a plain (industrial) journal bearing. The predictions for the pressure and temperature fields of the inner film agree well with published test data in Ref. [5].

Next, the numerical program is used to analyze the performance characteristics of a (semi) floating ring bearing with an actual configuration in a passenger vehicle TC. Predictions of performance reveal the following conclusions:

(1) The inner film temperature dramatically increases by around 90℃ as the oil

flows from the inlet to the exit plane, because the axial flow rate is not large enough to remove the heat from the hot shaft and the local power dissipation due to the shear drag.

(2) The heat flow from the hot shaft is overwhelming, e.g. it contributes almost 95% of total energy that enters into the (S)FRB at a low speed of 30 krpm. As the journal speed increases, the fluid heats and the heat flow from the shaft decreases, but the drag power loss grows considerably.

(3) The inner film flow carries away the majority (>70%) of the total energy available (heat from the hot shaft plus drag power loss), so that that heat through the ring and the heat conducted into the casing is relatively small and remains almost invariant as shaft speed increases.

(4) The peak temperature of the inner film increases with journal speed, varying by just 10 ℃ as the journal speed grows from 30 krpm to 240 krpm. This occurs because the heat flow from the hot shaft is overwhelming and the drag power loss increases with journal speed. Note that the *hot* shaft temperature affects the film peak temperature, which happens immediately after the oil cavitation region ends.

(5) The floating ring develops a considerable temperature variation along its radial and circumferential directions. For operation at 240 krpm, the temperature difference between the ring ID and OD surfaces is as high as 25 ℃, and for the ring ID surface, the temperature changes by 15 ℃ around its circumference.

In addition, the research quantifies the impact of the lubricant supply conditions (pressure and temperature), the bearing film clearances, the number and the size of the supply grooves on the ring ID surface on the bearing performance. The conclusions are summarized as:

(1) Lubricating a (S)FRB with a lower oil supply temperature or a higher supply pressure increases the heat flow from the journal, since the flow rate through the inner film region increases. However, the peak and average temperatures of the inner film are strongly determined by the shaft temperature instead of the oil supply temperature. The simple model assumes the shaft temperature is fixed at 213 ℃. In all instances, the heat flow from the hot shaft is overwhelming.

(2) As the inner film clearance increases from 5 μm to 10 μm, the flow rate through the inner film region grows by five times, leading an increase in the heat flowing from the hot journal. The drag power loss also increases with the inner film clearance, since the oil viscosity increases as the oil average temperature decreases.

(3) Additional axial grooves placed in the inner surface of the floating ring deliver more lubricant into the inner film. An increase in flow rate follows, and is proportional to the number of axial grooves. A larger flow rate steadily reduces the average and peak temperatures of the inner film, causing both the heat flowing from the journal and the drag lower loss to increase because of the increase in the average oil viscosity.

(4) A deeper axial groove reduces the flow resistance of the groove, evacuating more oil through the groove but decreasing the flow rate through the film land region. The oil viscosity largely increases as the average temperature of the inner film decreases by almost 40 ℃, so that the drag power loss grows considerably.

(5) A wider axial groove moderately decreases the average inner film temperature by around 10 ℃, and the effect of the decrease in the flow velocity through the film land region overweighs the effect of the small increase in the oil viscosity. The film land region also decreases as the axial groove width increases. Therefore, as the groove width increases (6 ° to 26 °, with nominal width = 14 °), the drag power loss decreases by 50 W, while the heat flowing from the hot shaft increases by about 70 W for operation at the top speed of 240 krpm.

Since the present thesis focuses on the analysis of (semi) floating ring bearings, i.e. with a non-rotating ring, future work on the thermal flow pattern of a FRB is necessary. Note, however, that San Andrés demonstrates [38] that for most PV/CV turbochargers, the ring rotational speed is large enough to produce a uniform ring temperature in the circumferential direction. In addition, an accurate heat flow model must be systemic and incorporate the shaft, which means the temperatures of the shaft and the inner film are coupled, and hence the current model with invariant shaft temperature needs improvement.

# REFERENCES


[1] San Andrés, L., Barbarie, V., Bhattacharya, A., and Gjika, K., 2012, "On the Effect of Thermal Energy Transport to the Performance of (Semi)Floating Ring Bearing Systems for Turbocharger," ASME J. Eng. Gas Turb. Power, **134**(10), p.102507.

[2] Cormerais, M., Hetet, J.F., Chesse, P., and Maiboom, A., 2006, "Heat Transfer Analysis in a Turbocharger Compressor: Modeling and Experiments," SAE Paper 2006-01-0023.

[3] Baines, N., Wygant, K.D., Dris, A., 2010, "The Analysis of Heat Transfer in Automotive Turbocharger," ASME J. Eng. Gas Turb. Power, **132**(4), p.042301.

[4] Shaaban, S., 2004, "Experimental Investigation and Extended Simulation of Turbocharger Non-adiabatic Performance," Ph.D. thesis, Mechanical Power Engineering Department, Helwan University, Egypt.

[5] Tonnesen, J., Hansen, P. K., 1981, "Some Experiments on the Steady State Characteristics of a Cylindrical Fluid-Film Bearing Considering Thermal Effects," ASME J. Lub. Tech., **103**, pp. 107-114.

[6] Rautenberg, M., Mobarak, A., and Malobabic, M., 1983, "Influence of Heat Transfer between Turbine and Compressor on the Performance of Small Turbocharger," Proc. 1983 Tokyo Int. Gas Turb. Cong., **2**, pp. 567-574.

[7] Bohn, D., Heuer, T., and Kusterer, K., 2005, "Conjugate Flow and Heat Transfer Investigation of a Turbo Charger," ASME J. Eng. Gas Turb. Power, **127**(3), pp.663-669.

[8] Heuer, T., Engels, B., Klein, A., and Heger, H., 2006, "Numerical and Experimental Analysis of the Thermo-Mechanical Load on Turbine Wheels of Turbochargers," ASME Paper GT2006-90526. Proc. of ASME Turbo Expo 2006 Conference, Barcelona, Spain, May 8-11.

[9] Malobabic, M., and Rautenberg, M., 1987, "Adiabatic and Non-Adiabatic Efficiencies of Small Turbocharger Turbines," Tokyo Int. Gas Turb. Cong., **I**, pp.57- 64.

[10] Bohn, D., Moritz, N., and Wolff, M., 2003, "Conjugate Flow and Heat Transfer Investigation of a Turbo Charger: Part II- Experimental Results," ASME Paper GT2003-38449, Proc. of ASME Turbo Expo 2003 Conference, Atlanta, Georgia, June 16-19.

[11] Cormerais, M., Chesse, P., and Hetet, J., 2009, "Turbocharger Heat Transfer Modeling under Steady and Transient Conditions," Int. J. Thermodynam., **12**(4), pp.193-202.

[12] Nguru, R. M., 1999, "Simplified Methodology to Correct Turbocharger Field Measurement for Heat Transfer and other Effects," M.S. thesis, Department of Mechanical and Nuclear, Kansas State University, USA.

[13] Lamquin, T., and Gjika, K., 2009, "Power Losses on a Turbocharger Hydrodynamic Bearing System: Test and Prediction," ASME Paper GT2009-59599, Proc. of ASME Turbo Expo 2009 Conference, Orlando, Florida, June 8-12.

[14] Deligant, M., Povedin, P., and Descombes, G., 2011, "CFD Model for Turbocharger Journal Bearing Performances," Appl. Therm. Eng., **31**(5), pp. 811-819.

[15] San Andrés, L., and Kerth, J., 2004, "Thermal Effects on the Performance of Floating Ring Bearing for Turbocharger," Proc. IMechE, Part J: J. Eng. Trib., **218**(5), pp. 437-450.

[16] Chun, S.M., 2008, "Aeration Effects on the Performance of a Turbocharger Journal Bearing," Trib. Int., **41**(4), pp. 296-306

[17] Heuer, T., Engels, B., and Wollscheid, P., 2005, "Thermomechanical Analysis of a Turbocharger Based on Conjugate Heat Transfer," ASME Paper GT2005-68059, Proc. of ASME Turbo Expo 2005 Conference, Reno-Tahoe, Nevada, June 6-9.

[18] Tanaka, M. and Hori, Y., 1972, "Stability Characteristics of Floating Bush Bearings," ASME J. Lub. Tech., **94**(3), pp. 248-259.

[19] Cross, M. M., 1965, "Rheology of Non-Newtonian Fluids: a New Flow Equation for Pseudo Plastic System," J. Colloid Sci., **20**(5), pp. 417-437.

[20] San Andrés, L., 2010, *Modern Lubricant Theory*, "Thermohydrodynamic Bulk-Flow Model In Thin Film Lubrication" Notes 10, Texas A&M University Digital Libraries. Retrieved September, 2012 from http://repository.tamu.edu/handle/1969.1/93197.

[21] Kays, W.M., and Crawford, M.E., 1980, *Convective Heat and Mass Transfer*, 2nd ed., McGraw-Hill, inc., NY, Chap. 8.

[22] Lee, P., Garimella, S.V., and Liu D., 2005, "Investigation of Heat Transfer in Rectangular Microchannels," Int. J. Heat and Mass Transfer, **48**, pp. 1688-1704.

[23] San Andrés, L., 2010, *Modern Lubricant Theory*, "Liquid Cavitation in Fluid Film Bearings" Notes 6, Texas A&M University Digital Libraries. Retrieved September, 2012 from http://repository.tamu.edu/handle/1969.1/93197.

[24] San Andrés, L., 2012, "Modeling of Heat Flow and Temperature in a Floating Ring," Quarterly Report No.5 to Honeywell Turbo Technologies, November, Texas A&M University, Proprietary.

[25] San Andrés, L., 2010, "Analysis for Numerical Solution of Hydrodynamic Pressure and Mean Lubricant Temperature in Laminar Flow Thin Film," Quarter Report No. 1 to Honeywell Turbocharging Technologies, December, Texas A&M University, Proprietary.

[26] Mitsui, J., Hori, Y., and Tanaka, M., 1986, "An Experimental Investigation on the Temperature Distribution in Circular Journal Bearings," ASME J. Trib., **108**(4), pp. 621-626.

[27] Costa, L., Fillon, M., Miranda, A.S., and Claro, J.C.P., 2000, "An Experimental Investigation of the Effect of Groove Location and Supply Pressure on the THD Performance of a Steadily Loaded Journal Bearing," ASME J. Trib., **122**(1), pp. 227-232.

[28] Singh, U., Roy, L., and Sahu, M., 2008, "Steady-state Thermo-hydrodynamic Analysis of Cylindrical Fluid Film Journal Bearing with an Axial Groove," Trib. Int., **41**(12), pp. 1135-1144.

[29] Massoud, M., 2005, Engineering Thermofluids: Thermodynamics, Fluid Mechanics, and heat Transfer, Springer Berlin Heidelberg, New York, Chap. IV.

[30] Cristea, A., Bouyer, J., Fillon, M., and Pascovici, M.D., 2011, "Pressure and Temperature Field Measurements of Lightly Loaded Circumferential Groove Journal Bearing," Trib. Trans., **54**(5), pp. 806-823.

[31] Dowson, D., Hudson, J.D., Hunter, B., and March, C.N., 1966, "An Experimental Investigation of the Thermal Equilibrium of Steadily Loaded Journal Bearings," Proc Instn Mech Engrs, **131**(3B), pp. 70-80.

[32] Brito, F. P., Bouyer, J, Fillon, M., and Miranda, A.S., 2006, "Thermal Behavior and Performance Characteristics of a Twin Axial Groove Journal Bearing as a Function of Applied Load and Rotational Speed," Paper No. A0735.0708, 5th Int. Cong. on Mech. and Mater. in Design, Porto-Portugal, July 24-26.

[33] Taylor, R. I., 1999, "The Inclusion of Lubricant Shear Thinning in Journal Bearing Models," Proc. Istn Mech, Part J: J. Eng. Trib., **213**(35), pp. 35-46.

[34] Burton, R. A., 1964, "Thermal Aspect of Bearing Seizure," WEAR, **8** (I), pp. 57-72.

[35] International Lubricant Standardization and Approval Committee, 2004, "ILSAC GF-4 Standard for Passenger Car Engine Oils".

[36] Mobile 1 (5W-30) Product Specification Sheet. Retrieved January, 2013 from http://www.mobil.com/USA-English/Lubes/PDS/GLXXENPVLMOMobil1_5W-30.aspx.

[37] Gjika, K., San Andrés, L., and Larue, G. D., 2010, "Nonlinear Dynamic Behavior of Turbocharger Rotor-Bearing Systems with Hydrodynamic Oil Film and Squeeze Film Damper in Series: Prediction and Experiment," ASME J. Comput. and Nonlinear Dyn., **5**(4), p. 041006.

[38] San Andrés, L., 2012, "Finite Element Model for Heat Flow and Temperature in a Rotating Floating Ring," Quarterly Report No.6 to Honeywell Turbo Technologies, February, Texas A&M University, Proprietary.

# APPENDIX A

## Influence of shaft temperature on the (S)FRB performance

In the main body of this thesis, the study on the influence of various lubrication supply conditions is based on a simply model, which takes, regardless of operating conditions, the shaft temperature as constant at 213 ℃. However, in practice, the heat flow model must be systemic and incorporate the shaft and casing. There is an interaction between the shaft temperature and the oil film temperature. The study thus further reveals that the heat flowing from the *hot* shaft constitutes a large fraction of the total thermal energy. The shaft temperature directly influences the average inner film temperature as well as its peak temperature.

This appendix discusses the influence of the shaft temperature on the main bearing performance characteristics, such as the average and peak film temperatures, the film flow rate, and the drag power loss as well as the thermal energy carried away by the films, etc. The shaft temperature deviates by $\pm$ 20 ℃ from the assumed shaft temperature (213 ℃).

Figure A1 shows the influence of the shaft temperature on the average and peak temperatures of the inner film as well as the outlet temperature for operation at the maximum journal speed (240 krpm). Recall that the oil is supplied at temperature $T_{SUP}$ = 120 ℃ and pressure $P_{SUP}$ = 4 bar. The outlet temperature results from the mixing of the inner and outer flow streams leaving the bearing. The prediction shows that the shaft temperature has a minor effect on the film outlet temperature, which indicates that

recording the temperature of the outlet lubricant cannot reflect the change of the shaft temperature. This occurs because the oil flow rate through the outer film region is much larger than that through the inner film region, and thus the outer film flow influences most the outlet mixing temperature. Note that the outer film temperature is close to the oil supply temperature.

In addition, both the average and the peak temperatures of the inner film grow steadily for an increasing shaft temperature, since the heat flowing from the hot journal is a major source of heating the inner film.

Figure A2 shows, $\frac{T_{film} - T_{SUP}}{T_{shaft} - T_{SUP}}$, the ratio of the temperature differences of the inner film average temperature and the shaft temperature both relative to the oil inlet temperature ($T_{SUP}$) versus the shaft temperature. The results show that the shaft temperature has a minor effect on the ratio of the temperature differences relative to the oil inlet temperature. The ratio is a little less than 0.7, indicating that the shaft temperature has a greater influence on the inner film temperature than the oil inlet temperature ($T_{SUP}$).

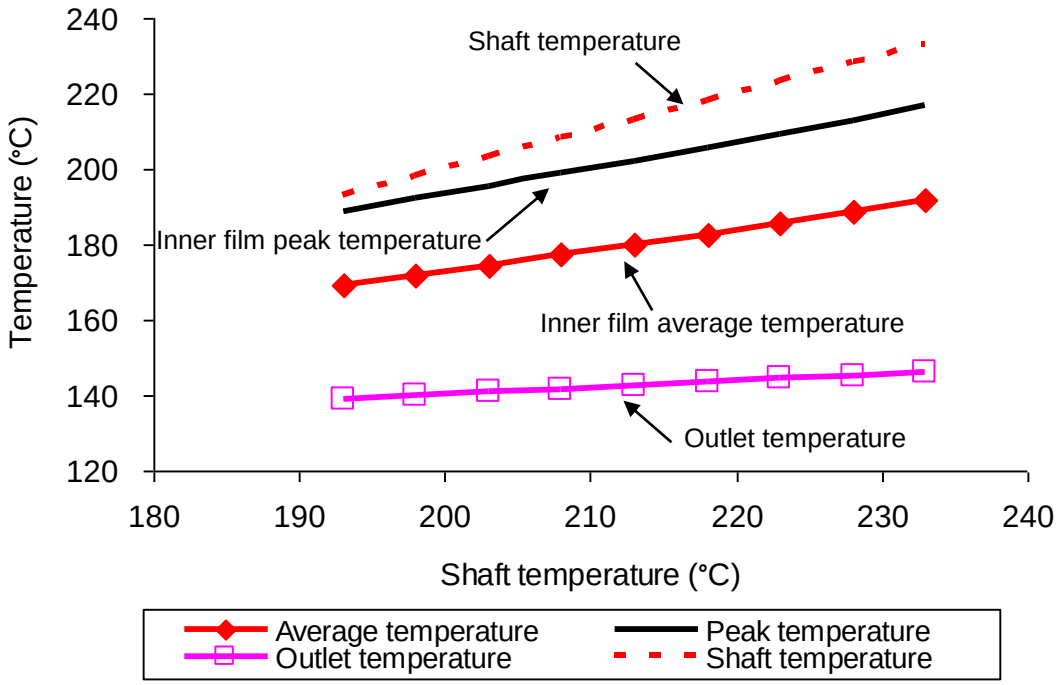


**Figure A1. Influence of shaft temperature ($T_{shaft}$) on the average and peak temperatures of the inner film and the mixing film temperature. $T_{SUP}$ = 120°C, $P_{SUP}$ = 4 bar. Static load = 0.9 N. Journal speed = 240 krpm.**

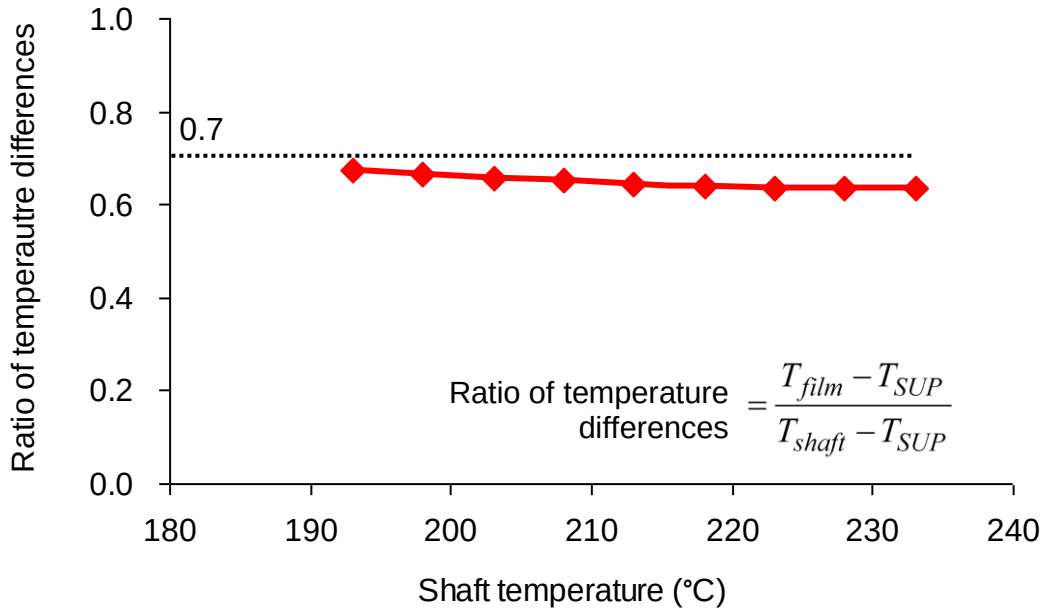


**Figure A2. Influence of shaft temperature ($T_{shaft}$) on ratio of temperature differences. $T_{SUP}$ = 120°C, $P_{SUP}$ = 4 bar. Static load = 0.9 N. Journal speed = 240 krpm.**

Figure A3 shows the influence of the shaft temperature on the flow rate through the inner film region as the journal speed increases from 30 kprm to 240 krpm for operation with oil supply temperature $T_{SUP}$ = 120 ℃ and pressure $P_{SUP}$ = 4 bar. The results show that the flow rate of the inner film steadily increases with journal speed but slightly decreases with a higher shaft temperature. This occurs because an increasing shaft temperature causes a larger thermal growth and leads to a smaller film thickness. This effect overweighs the effect of the decreasing oil viscosity which could increase the

flow rate. Therefore, the flow rate through the inner film region slightly decreases.

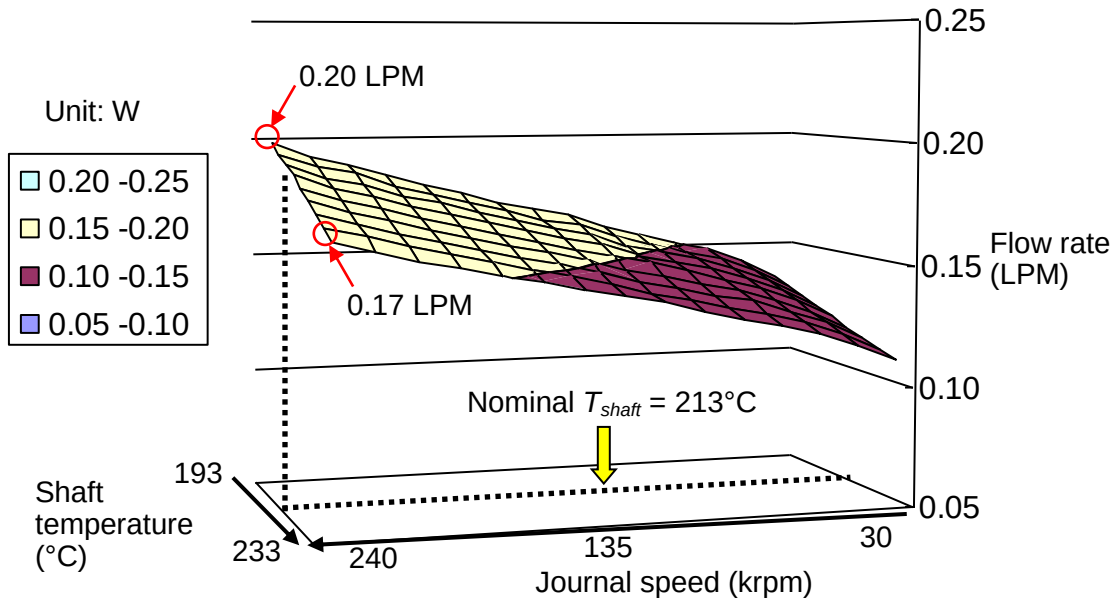


**Figure A3. Influence of shaft temperature ($T_{shaft}$) on the flow rate through the inner film region. $T_{SUP}$ = 120°C, $P_{SUP}$ = 4 bar. Journal speed = 30 krpm ~ 240 krpm. Static load = 0.9 N.**

Figure A4 shows the influence of the shaft temperature on the drag power loss in the inner film as the journal speed increases from 30 kprm to 240 krpm for operation with oil supply temperature $T_{SUP}$ = 120 ℃ and pressure $P_{SUP}$ = 4 bar. The results show that the drag power loss at high journal speeds decreases for an increasing shaft temperature. This occurs because the average oil viscosity decreases as the film

temperature increases for a higher shaft temperature. However, at low journal speeds the drag power loss is not a strong function of the shaft temperature.

For the same operating condition, Figure A5 shows the effect of the shaft temperature on the heat flow from the hot journal and the heat flow conducted through the ring. The predictions show that the heat flow from the journal increases for an increasing shaft temperature. The temperature of the inner film grows with the shaft temperature, but the increase in the average film temperature is lower than the increase in the shaft temperature, i.e., as the shaft temperature increases by 40 ℃, the average temperature of the inner film increases by 20 ℃ (see Figure A1). Note that for a certain shaft temperature, the heat flowing from the shaft begins to increase until the journal speed approaches around 90 krpm and then starts to drop with journal speed as the film temperature increases with journal speed.

On the other hand, a higher shaft temperature leads to a larger heat flow conducted through the floating ring over the journal speed range (30 krpm ~ 240 krpm). This occurs because more thermal energy comes from the hotter journal. Note that compared with the thermal energy flowing from the shaft, the heat conducted through the ring, the only source to heat the outer film, is much smaller.

Figure A6 depicts the influence of the shaft temperature on the total energy carried away by the inner film as the journal speed increases from 30 krpm to 240 krpm. Recall that the oil is supplied at temperature $T_{SUP}$ = 120 ℃ and pressure $P_{SUP}$ = 4 bar. The results show that the maximum thermal energy the inner film could advect takes place at the maximum journal speed and at the highest shaft temperature. Though the

drag power loss decreases a bit for a highest shaft temperature, the heat flowing from the journal largely increases, and thus the total energy carried away by the inner film steadily increases for both a larger journal speed and a higher shaft temperature. Recall that the inner film is responsible for carrying away most of the total thermal energy entering into the (S)FRB.

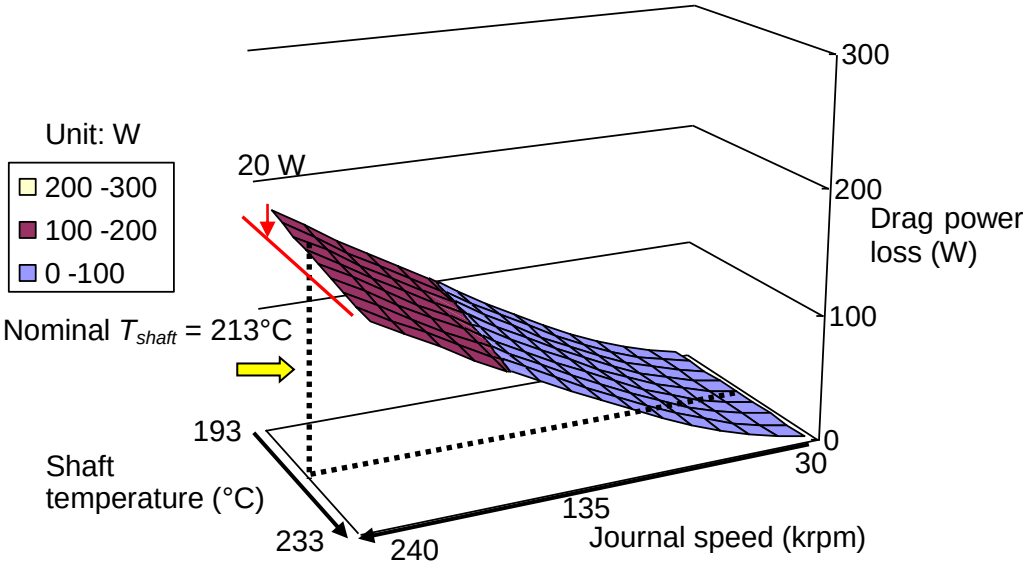


**Figure A4. Influence of shaft temperature ($T_{shaft}$) on the drag power loss. $T_{SUP}$ = 120°C, $P_{SUP}$ = 4 bar. Journal speed = 30 krpm ~ 240 krpm. Static load = 0.9 N.**

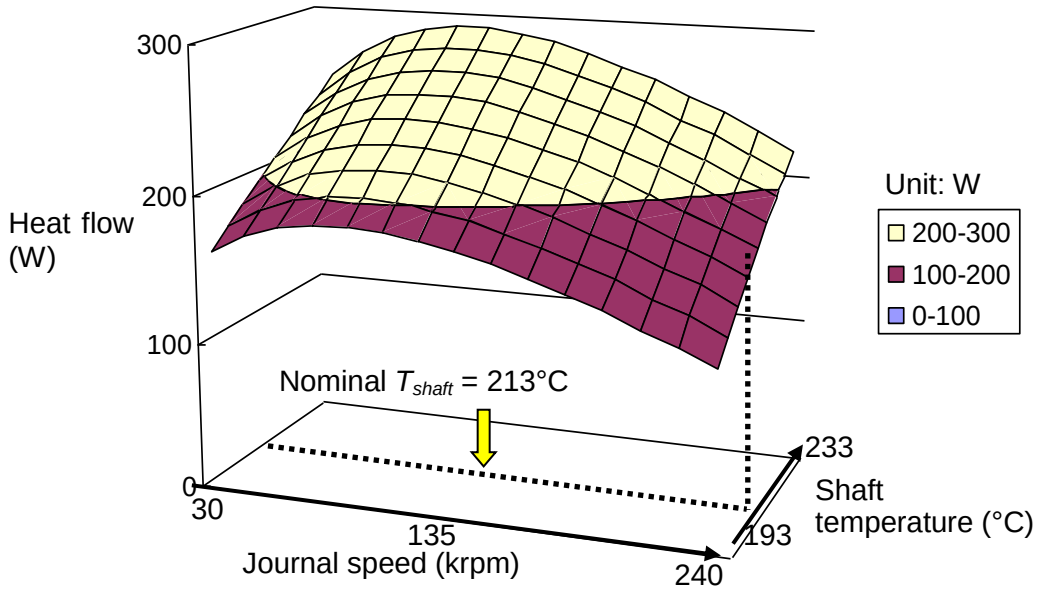


(a) Heat flow from the shaft

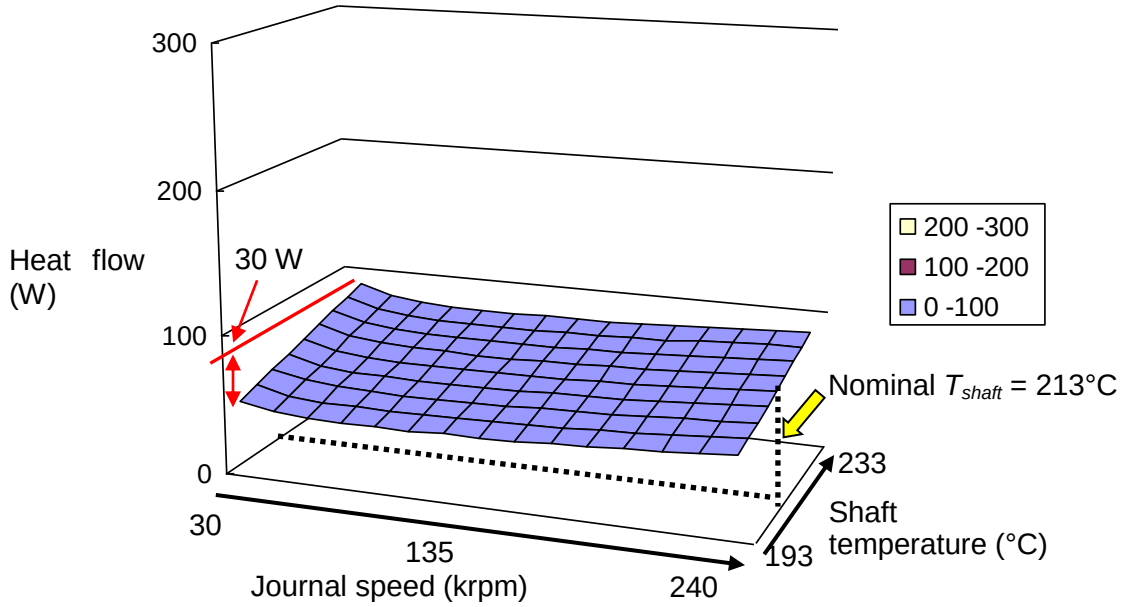


(b) Heat conducted through the ring

**Figure A5. Influence of shaft temperature ($T_{shaft}$) on the heat flows from the shaft and through the ring. $T_{SUP}$ = 120°C, $P_{SUP}$ = 4 bar. Journal speed = 30 krpm ~ 240 krpm. Static load = 0.9 N.**

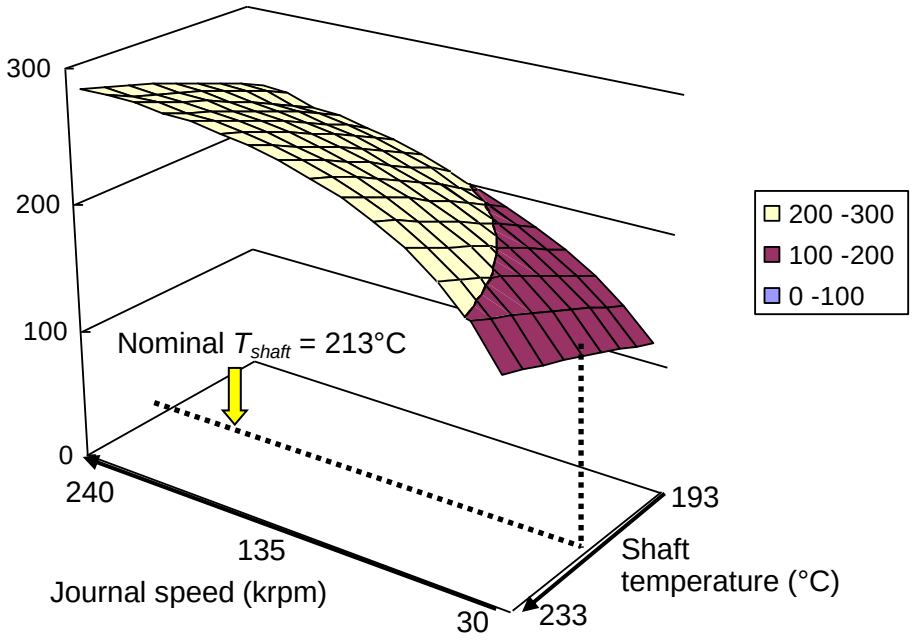


**Figure A6. Influence of shaft temperature ($T_{shaft}$) on the total energy carried away by the inner film. $T_{SUP}$ = 120°C, $P_{SUP}$ = 4 bar. Journal speed = 30 krpm ~ 240 krpm. Static load = 0.9 N.**

In summary, the study on the influence of shaft temperature on the bearing performance of the (S)FRB shows that the shaft temperature has a greater influence on the inner film temperature than the oil inlet temperature ($T_{SUP}$). The inner film temperature increases with a larger shaft temperature, so that the drag power loss in the inner film decreases as the shaft temperature grows because the oil viscosity becomes smaller. However, as expected the heat flow from the shaft increases with shaft temperature. Hence, the total thermal energy carried away by the inner film increases

when the shaft is at a higher temperature. Note that the shaft with a higher temperature leads to a small decrease in the flow rate through the inner film clearance. This occurs due to the larger thermal growth of the inner film clearance when the shaft temperature increases.